ISSN: 3041-0746 (Print)
ISSN: 3029-2573 (Online)

International Journal of AI for Materials and Design

Volume 2 • Issue 3
September 2025

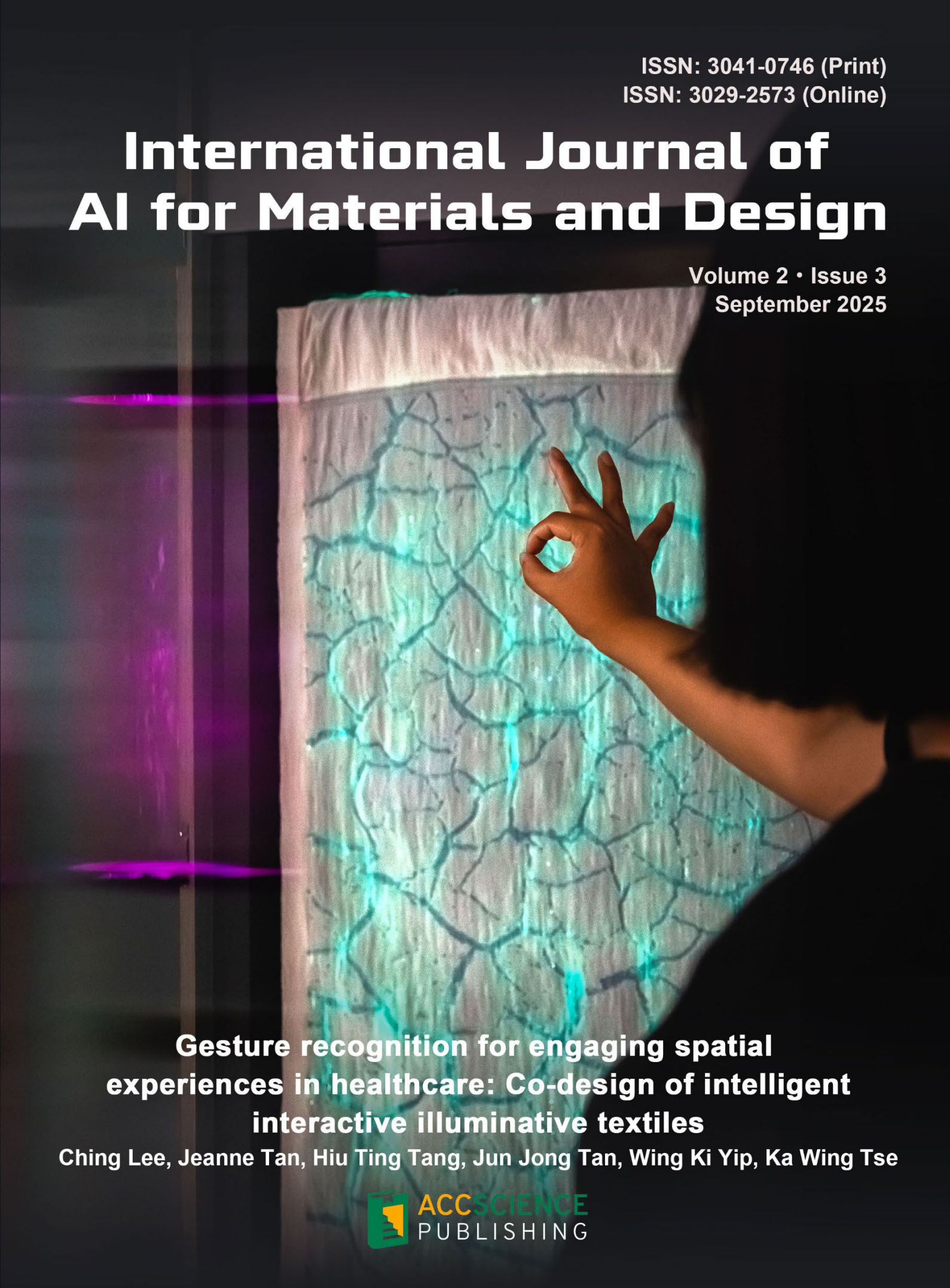

Gesture recognition for engaging spatial experiences in healthcare: Co-design of intelligent interactive illuminative textiles

Ching Lee, Jeanne Tan, Hiu Ting Tang, Jun Jong Tan, Wing Ki Yip, Ka Wing Tse

ACCSCIENCE PUBLISHING

International Journal of AI for Materials and Design

Print ISSN: 3041-0746
Online ISSN: 3029-2573

The International Journal of AI for Material and Design (IJAMD) is a scholarly publication dedicated to advancing the intersection of artificial intelligence (AI), materials science and design. This peer-reviewed journal provides a platform for researchers, academics, and industry professionals to disseminate cutting-edge research, innovative methodologies, and practical applications that leverage AI techniques to enhance the understanding, development, and optimization of aspects related to materials and design processes. IJAMD seeks to contribute to the advancement of technology, innovation, and sustainability in materials design, engineering disciplines, product manufacturing and process technology.

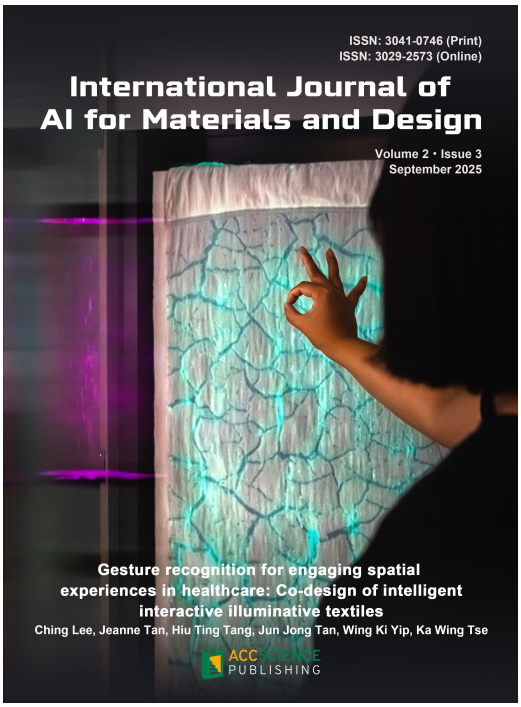

About the Publisher

AccScience Publishing is a publishing company based in Singapore. We publish a range of high-quality, open-access, peer-reviewed journals and books from a broad spectrum of disciplines.

Contact Us

Managing Editor
ijamd.office@accscience.sg

AccScience Publishing
9 Raffles Place, Republic Plaza 1 #06-00 Singapore 048619.

Volume 2 • Issue 3 • September 2025
ISSN 3041-0746 (print) ISSN 3029-2573 (online)

INTERNATIONAL JOURNAL OF AI FOR MATERIALS AND DESIGN

ACCSCIENCE PUBLISHING

Access Science Without Barriers

International Journal of AI for Materials and Design

ISSN: 3041-0746 (print)
ISSN: 3029-2573 (online)

Editorial and Production Credits

Publisher: AccScience Publishing
Managing Editor: Shirley Lu
Production Editor: Sharmila Velapasamy
Article Layout and Typeset: Sinjore Technologies (India)

For all advertising queries, contact ijamd.office@accscience.sg.

Supplementary file

Supplementary files of articles can be obtained at https://accscience.com/journal/IJAMD/2/3.

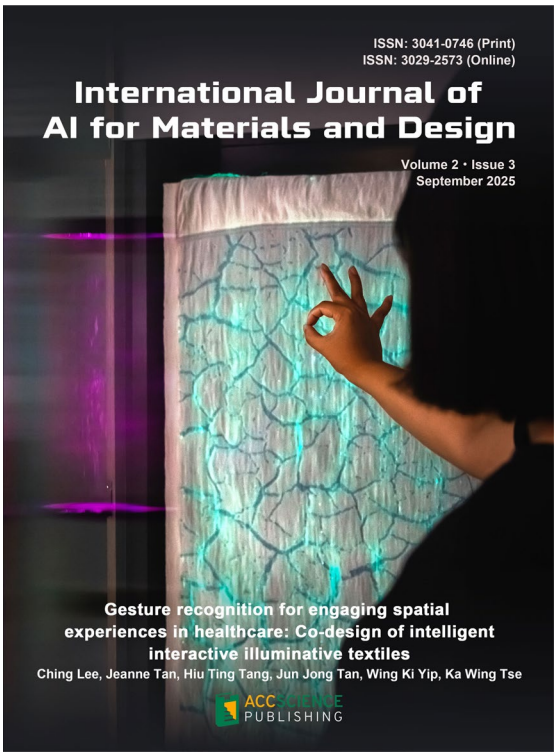

Disclaimer

AccScience Publishing is not liable to the statements, perspectives, and opinions contained in the publications. The appearance of advertisements in the journal shall not be construed as a warranty, endorsement, or approval of the products or services advertised and/or the safety thereof. AccScience Publishing disclaims responsibility for any injury to persons or property resulting from any ideas or products referred to in the publications or advertisements. AccScience Publishing remains neutral with regard to jurisdictional claims in published maps and institutional affiliations.

International Journal of AI for Materials and Design

Editorial Board

*Editorial Board Members as of September 26, 2025

ACCSCIENCE PUBLISHING

Volume 2 | Issue 3 | September 2025 | Page 1 – 87 |

International Journal of AI for Materials and Design

https://accscience.com/journal/IJAMD

CONTENTS

ACCSCIENCE PUBLISHING

International Journal of AI for Materials and Design

REVIEW ARTICLE

A comprehensive review of artificial intelligence applications in composite materials: Predictive, generative, and automation approaches

Hyunsoo Hong†, Samuel Kim†, Jeeeun Lee, and Seong Su Kim*

Department of Mechanical Engineering, College of Engineering, Korea Advanced Institute of Science and Technology, Daejeon, Republic of Korea

Abstract

The rapid advancement of artificial intelligence (AI) has led to its widespread adoption across various engineering fields, including composite materials research. Composite materials, known for their superior mechanical properties and lightweight characteristics, play a crucial role in industries such as aerospace, automotive, and robotics. However, their inherent complexity–such as anisotropic behavior, nonlinear characteristics, and intricate microstructures–poses significant challenges for traditional design and analysis methods. To address these challenges, AI-driven approaches have emerged as powerful tools, offering solutions in prediction, generation, and automation. This review systematically explores applications of machine learning and deep learning in composite materials research, categorized into three major approaches: predictive, generative, and automation models. Predictive models enhance the accuracy of property prediction and microstructure analysis. Generative models facilitate novel material discovery and microstructure design. Automatic models improve quality control and can be used to optimize manufacturing processes through real-time data analysis. By leveraging diverse large-scale datasets, AI provides innovative solutions to the key challenges associated with composite materials and enhances research and design efficiency. This review highlights the transformative potential of AI in composite materials research, providing insights into future research directions and challenges.

Keywords: Composite; Artificial intelligence; Prediction; Generation; Automation; Manufacturing

†*These authors contributed equally to this work.*

***Corresponding author:**
Seong Su Kim
(seongsukim@kaist.ac.kr)

Citation: Hong H, Kim S, Lee J, Kim SS. A comprehensive review of artificial intelligence applications in composite materials: Predictive, generative, and automation approaches. *Int J AI Mater Design.* 2025;2(3):1-30.
doi: 10.36922/IJAMD025210016

Received: May 19, 2025

Revised: July 02, 2025

Accepted: July 15, 2025

Published online: August 4, 2025

1. Introduction

Since the emergence of AlphaGo, artificial intelligence (AI) technology has rapidly advanced over the past decade, alongside the development of graphics processing units (GPUs) for parallel computing.[1,2] AI technology has recently reached a level where it is easily accessible in daily life, as demonstrated by the widespread adoption of generative conversational AI models, such as ChatGPT.[3,4] Furthermore, AI is now a core technology driving innovation across various engineering industries, including autonomous driving, biotechnology, robotics, aerospace, semiconductors, and composite materials.[5-12]

Composite materials are engineered by combining multiple constituent materials to achieve properties superior to those of conventional materials. The exceptional

lightweight characteristics and outstanding mechanical performance of composite materials make them essential in various industries, including aerospace, automotive, energy harvesting, robotics, and construction, as shown in Figure 1.[13-19] The properties of composite materials are influenced by multiple factors, including the types of fiber and resin, as well as the manufacturing process. In addition, their inherent anisotropy, nonlinearity, and complex microstructure make design and analysis significantly more challenging than conventional materials.

Traditionally, the field of composite materials has relied heavily on the expertise of skilled professionals for conducting experiments and developing physics-based models. In addition, simplifying assumptions have often been used to simulate the complex behavior of composite materials. However, these conventional approaches have clear limitations in fully capturing the intricate and diverse characteristics of composite materials. As a result, machine learning (ML) and deep learning (DL) methodologies have recently received significant attention in the field of composite materials. ML is increasingly being explored to overcome the challenges associated with traditional methods, offering new possibilities for improving efficiency and accuracy in the design, analysis, and manufacturing of composite materials.

The applications of ML in the field of composite materials, as illustrated in Figure 2, can be broadly categorized into three aspects:

(i) Prediction: ML enables the analysis of large-scale datasets to uncover complex patterns in areas such as mechanical property and behavior prediction, and design parameter estimations[20,21]
(ii) Generation: ML leverages data-driven learning to construct new information, such as for microstructure design, novel material discovery, and data augmentation[22]
(iii) Automation: ML is applied to optimize composite manufacturing processes, automate defect detection and quality control, and analyze real-time data to enhance manufacturing efficiency.[23]

AI thus serves as a powerful tool for addressing various challenges in the field of composite materials, significantly enhancing research and design efficiency. However, the use of insufficient or unreliable data, as well as the application of unsuitable ML techniques, can lead to suboptimal results or computational inefficiencies.

Therefore, a structured and systematic understanding of ML applications in the field of composite materials is essential. To address this need, this review provides a comprehensive and systematic analysis of ML-driven research on composite materials. The primary contributions of this paper are threefold. First, we propose a clear and structured classification of ML applications for composite materials into three categories: predictive, generative, and automation models. Second, we provide an in-depth review of the state-of-the-art ML techniques within each category, focusing on their practical applications in composite material design, manufacturing, and analysis. Third, we critically discuss the current limitations and challenges of these ML approaches and propose future research directions to address them.

The remainder of this paper is organized as follows: sections 2, 3, and 4 provide detailed discussions on the applications of predictive, generative, and automation models, respectively, in the field of composite materials. Finally, Section 5 presents the key findings, highlights the current limitations, and outlines future research directions for advancing AI-driven developments in this field.

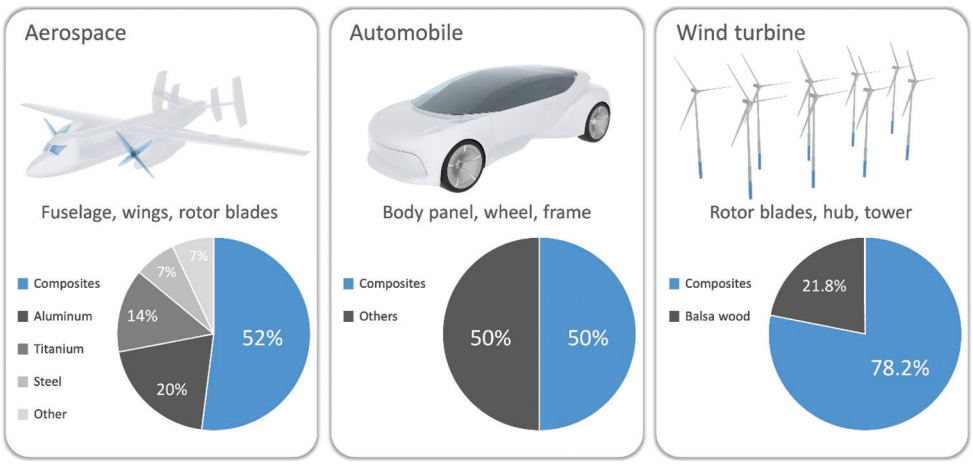

Figure 1. Components made of composite materials and the proportions (by weight) of different materials used in the aerospace, automobile, and wind turbine industries[17-19]

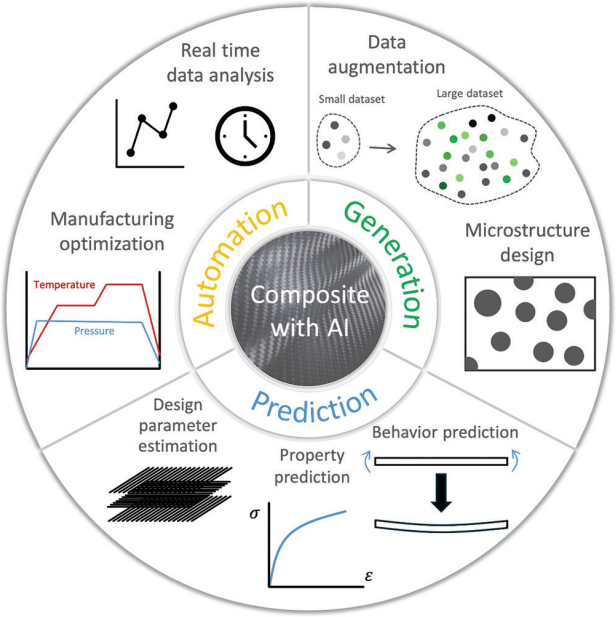

Figure 2. Machine learning applications in composite materials research: prediction, generation, and automation
Abbreviation: AI: Artificial intelligence.

2. Predictive models for composite materials

Predictive ML models are designed to estimate output properties or behaviors based on the given input data by identifying complex patterns and relationships. In the field of composite materials, predictive models play a crucial role as traditional experimental and numerical methods for property prediction can be time-consuming and computationally expensive, especially when dealing with the anisotropic and nonlinear nature of composites. By leveraging ML models trained on extensive datasets, predictive models enable rapid and reliable predictions, significantly enhancing efficiency in material design, performance evaluation, and failure analysis. This section will explore different ML models and techniques used for prediction in composite materials research.

2.1. Deep neural networks (DNNs)

An artificial neural network (ANN) is a type of ML technology inspired by the human nervous system. It serves as a mathematical model for learning information from the given data and recognizing patterns.[24,25] A DNN, as shown in Figure 3A, is a specialized form of ANN that incorporates multiple hidden layers, allowing for the extraction of complex features from data.[26-28] While the concept of ANNs has been around for decades, the advancement of GPU technology has enabled the practical implementation of DNNs, leading to significant breakthroughs in DNN research and applications. Because of their deep architecture, DNNs excel at capturing intricate patterns and relationships, making them particularly effective in handling nonlinear data and solving complex problems. When trained with sufficient, high-quality data, highly accurate predictions can be made for the given inputs, making it a powerful tool for data-driven analysis in various domains.

With the advancement of DNN technology, its applications in the field of composite materials have been steadily expanding. Traditional analytical methods often rely on various assumptions and simplifications that require extensive computational resources and time. However, by learning from large-scale datasets, DNNs can efficiently and accurately predict the behavior and properties of composite materials, overcoming the limitations of traditional methods in terms of speed and precision.

DNNs have been effectively utilized to predict the nonlinear responses and complex characteristics of composite structures, such as composite springs, composite tubes, and bistable composite structures, which are difficult to analyze analytically.[29,30,33] Zhang *et al.*[33] applied a DNN-based surrogate model to analyze the behavior of deployable bistable composite structures with C-cross sections, using finite element analysis (FEA) data for training and subsequently performing structural optimization. Similarly, as shown in Figure 3B, Hong *et al.*[29] utilized DNNs to predict ground reaction forces using self-sensed capacitance data from composite ankle springs, enabling the extraction of running parameters for exo-robot applications. Wang *et al.*[30] developed a DNN-based surrogate model to predict the mechanical properties of braided-textile reinforced tubular structures. Figure 3C shows the performance and error of the predicted results (peak force, mean crushing force, displacement corresponding to peak force, and effective compression stroke). In addition, as shown in Figure 3D, a DNN was utilized to predict the transverse mechanical response of unidirectional fiber-reinforced composites, incorporating the effects of defects, such as matrix voids and fiber-matrix debonding.[31] Their approach used an experimentally validated discrete element method model to generate training data of crack initiation and propagation at the particle-level in representative volume elements (RVEs) of the composite. The trained DNN predicted the initial crack location and the corresponding stress at the onset of cracking with accuracies of 82% and 94%, respectively. DNNs were integrated with the Abaqus FEA code by Tao *et al.*[34] to learn composite constitutive laws, ensuring physical consistency and enabling accurate, data-driven structural predictions. Furthermore, DNNs were used for

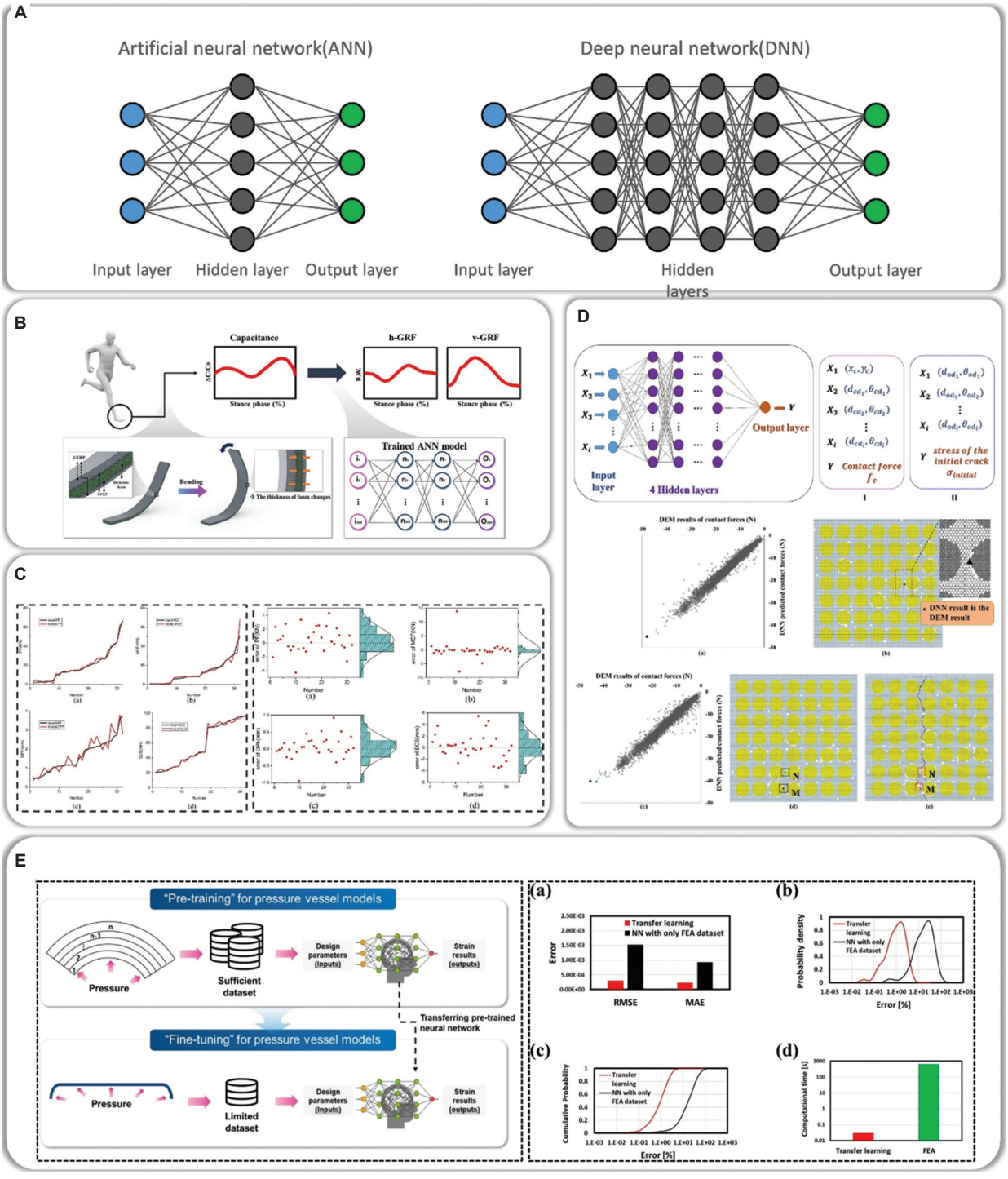

Figure 3. DNNs for composite materials prediction. (A) Structure of ANN and DNN; (B) A schematic illustrating the use of a DNN to predict ground force by applying capacitance-based self-sensing of the foam core in a sandwich composite.[29] Reprinted with permission from Hong *et al.*[29] Copyright © 2022 Elsevier; (C) Prediction results (peak force, mean crushing force, displacement corresponding to peak force, and effective compression stroke) and errors for braided-textile reinforced tubular structures.[30] Reprinted with permission from Wang *et al.*[30] Copyright © 2021 Elsevier; (D) Prediction results of macroscopic stiffness and yield strength of unidirectional fiber composites using DNN;[31] (E) Training process of transfer learning for predicting the behavior of composite pressure vessels and comparison with conventional finite element analysis methods.[32] Reprinted with permission from Hong *et al.*[32] Copyright © 2024 Elsevier.

Abbreviations: ANN: Artificial neural network; DEM: Discrete element method; DNN: Deep neural network; FEA: Finite element analysis; GRF: Generalized random forests; MAE: Mean absolute error; NN: Neural network; RMSE: Root mean squared error.

permeability prediction, in which statistical RVEs with randomized fiber distributions were generated specifically for training DNNs to address the stochastic nature of fibrous microstructures.[35]

These examples highlight the significant impact of DNNs on the research of composite materials. DNNs enable accurate predictions and efficient calculations, capturing complex structural responses that are challenging to model with traditional methods. By learning from large datasets, DNNs provide a reliable alternative or complement to numerical methods, such as FEA, offering data-driven insights and improved speed and precision when optimizing composite materials and structures. However, DNNs face significant limitations when there is insufficient data or when the model encounters conditions different from those in the training dataset. In such cases, transfer learning techniques serve as a powerful tool to overcome these challenges.[36-38] By applying the knowledge (such as network weights and feature representations) obtained from a pre-trained model to a new related problem, transfer learning accelerates training, improves performance, and enables effective learning even with limited data. For example, transfer learning has been applied to predict the behavior of composite pressure vessels by combining analytical and numerical data, significantly enhancing both accuracy and computational efficiency.[32] As presented in Figure 3E, the approach involves pre-training on a large-scale analytical dataset with relatively low fidelity but low cost, and then fine-tuning with a smaller-scale numerical dataset that offers higher fidelity but at a higher cost. This strategy enables the rapid assessment of structural integrity under various loading conditions, reducing the need for time-consuming finite element simulations.

2.2. Convolutional neural networks (CNNs)

A CNN is a type of DL model specifically designed for image processing and analysis.[39-41] Unlike general DNNs, CNNs are highly effective at handling image-based data, making them particularly advantageous for visual data-related problems. As illustrated in Figure 4A, CNNs use convolutional and pooling operations to efficiently extract important features from input data, reducing the need for manual feature engineering. CNNs have demonstrated exceptional performance in various vision tasks, including image classification, object detection, and facial recognition.[42-44]

In the field of composite materials, microstructure analysis and fiber orientation prediction are often difficult to conduct using conventional analytical methods or general DNNs.[48,49] Taking advantage of the superior pattern recognition capabilities of CNNs, image data of composite materials can be utilized to predict microstructures and material behavior, making CNNs essential when considering image-based composite material problems.

CNNs have been successfully applied to various aspects of composite material analysis.[45,46,50-52] Key characteristics, such as the fiber arrangement, fiber diameter, and resin content, can be extracted from microstructure images using CNNs, which can then be used to predict the mechanical behavior and failure mechanisms of composite materials. As shown in Figure 4B, CNN-based models have been employed to predict the stacking angles of fiber-reinforced composites from cross-sectional images.[45] Extracting composite stacking information is particularly valuable for the reverse-engineering of composite material structures, as the performance of fiber-reinforced composites is highly sensitive to stacking angles.

U-Net architectures, which are built on CNNs, have been used to predict stress fields within composite microstructures by using stress maps generated from FEA as training data.[50] U-Net models provide a computationally efficient alternative to traditional simulations, reducing the computational burden of multi-scale modeling while maintaining high levels of predictive accuracy.

In addition to stress field and stacking angle predictions, CNNs have been applied to estimate the mechanical properties of composite materials, such as the transverse modulus, tensile strength, and fracture toughness, based on microstructural images using finite element simulation results as training data.[51] By training on a large dataset of RVEs, these models can capture complex material behaviors and improve the accuracy of property estimation.

Moreover, as shown in Figure 4C, CNN-based approaches have been successfully implemented for efficient prediction of the 3D permeability of fibrous microstructures by integrating 2D image-based learning with circuit analogy models.[46] The permeability is a crucial factor in composite material manufacturing since it affects the ability of the fibrous reinforcement to achieve complete impregnation during the resin infusion process. The use of CNNs not only accelerates the permeability prediction process but also enhances the overall understanding of fluid flow in porous composite media.

These studies highlight the transformative potential of CNNs in composite materials research, offering new possibilities for advanced composite structures through enhanced image-based analysis and prediction. However, despite the effectiveness of CNNs, one limitation is the challenge of acquiring sufficient training data. Specifically, collecting high-quality images of composite materials is difficult, which limits the model's learning process. In addition, CNN-based approaches require extensive pre-processing of image data, increasing the complexity of implementation.

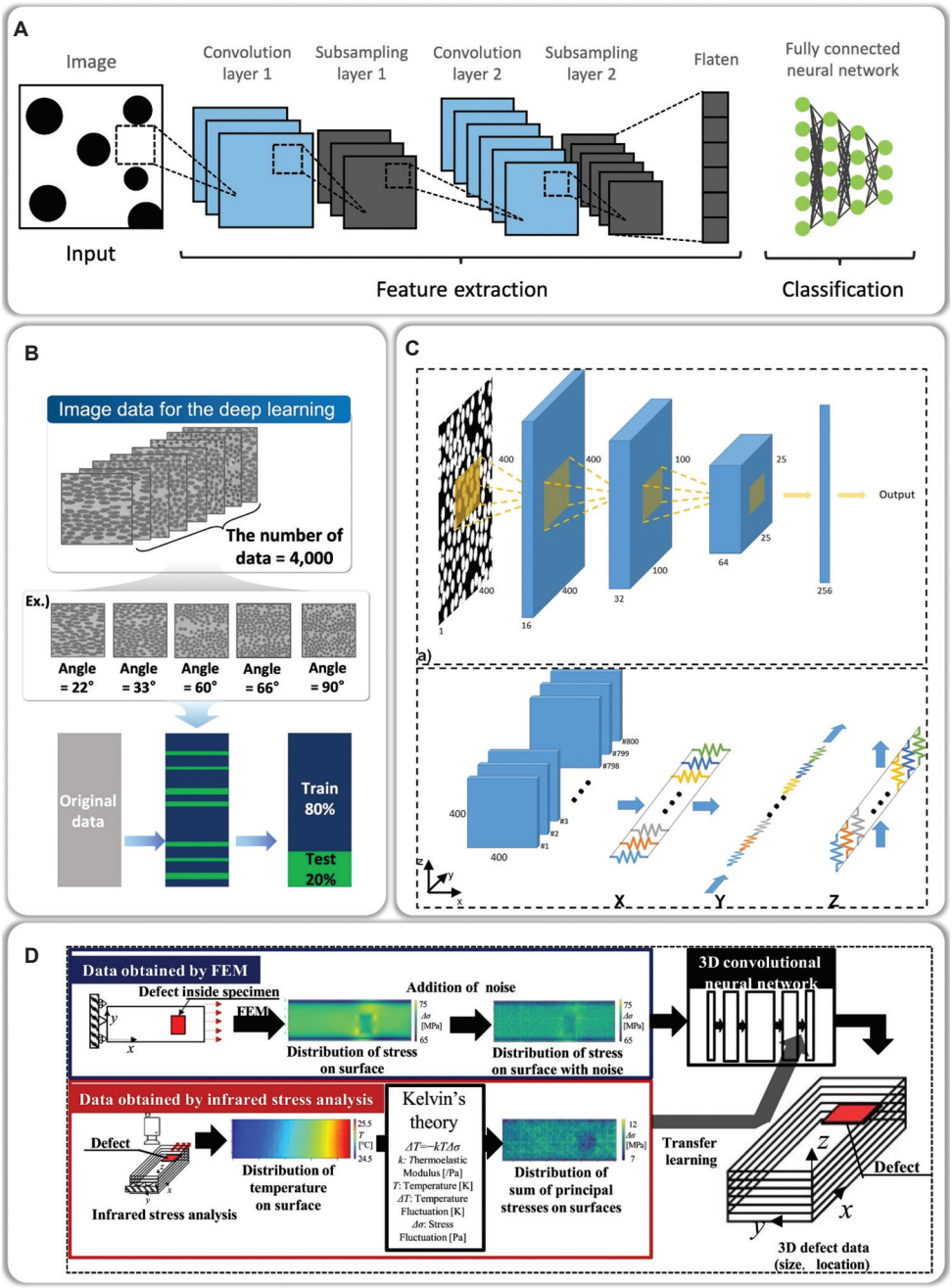

Figure 4. CNN architecture and research utilizing CNN in the field of composite materials. (A) Structure of CNN; (B) Image data and data classification process for predicting stacking angle based on cross-sectional images;[45] (C) CNN architecture and circuit analogy configuration used for estimating the principal permeability values of the considered 3D fibrous structures;[46] (D) Ground truth of defects for each layer of the composite laminate and the predicted results.[47]
Abbreviations: CNN: Convolutional neural network; FEM: Finite element method.

To address these challenges, data augmentation techniques, such as rotation, distortion, and noise addition, can be used to enhance the training dataset.[53,54] For example, Shim *et al.*[55] applied CNN and data augmentation to predict the stress-strain curves of composites fabricated through mechanical recycling, enabling effective learning even with a limited dataset. In this process, each image was rotated by 90°, 180°, and 270°, and then horizontally flipped to generate eight images per single specimen. Generative models, discussed in the next section, can also be used for data augmentation to obtain more diverse images and further enhance training efficiency.[56-58]

Similarly, as with DNNs, many studies have also utilized transfer learning techniques to enhance the training efficiency of CNNs. Kojima *et al.*[47] used transfer learning with CNNs to predict internal defects in carbon fiber-reinforced polymer (CFRP) laminates by combining data generated through FEA with infrared stress distributions obtained from experiments. Figure 4D presents the ground truth of defects for each layer of the composite laminate, together with the predicted results obtained through transfer learning. By fine-tuning these models with a limited set of experimental data, transfer learning improves their generalization capabilities across various composite structures. The results show that as the amount of experimental stress measurement data increases, transfer learning-based defect prediction outperforms traditional FEA-based approaches in terms of efficiency. Moreover, Liu *et al.*[59] aimed to diagnose damage in composite materials using transfer learning with CNNs by leveraging Lamb wave signals generated from numerical simulations and applying them to experimental data. By integrating transfer learning with domain adversarial learning, the model achieved high generalization performance across complex domain discrepancies, leading to highly accurate delamination prediction. In addition to cases of domain adaptation, where only the domains differ while the tasks remain the same as in the aforementioned studies, transfer learning can also be applied when there are differences in the source and target tasks. Xu *et al.*[60] extracted vector representations of the geometric morphology and distribution characteristics of two-phase composites from images to establish similarity between the source and target domains. Their method enabled the use of small datasets through transfer learning, yielding high prediction accuracy for mechanical properties, such as stiffness, strength, and toughness. Techniques such as data augmentation and transfer learning not only enhance the efficiency of predictive models but also enable broad applicability across diverse tasks and DL models.

In addition, developing hybrid models by integrating CNNs with other ML/DL methods holds promise for enhancing their ability to capture and analyze complex composite material structures.[61-64] Among various approaches, attention mechanism-based CNNs have demonstrated strong capabilities in capturing complex failure behaviors. Liu *et al.*[64] incorporated an attention-based loss function into a CNN framework, enabling the model to focus more on high-damage regions in thick composites with wrinkles, thereby achieving effective prediction of failure modes.

2.3. Recurrent neural networks (RNNs)

RNNs are a type of DL model designed to process sequential data, and they excel in handling data that contain temporal or spatial-order relationships. Unlike feedforward neural networks or CNNs, RNNs receive data one step at a time in sequential order, as shown in Figure 5A, and have feedback connections in the hidden layers to recognize the sequential structure of the data. This architecture is advantageous in problems where the order of inputs is important, and it also offers the flexibility to handle variable-length data. However, RNNs have a drawback known as the long-term dependency problem, where the influence of distant inputs diminishes over time despite their relevance. In addition, as weights are multiplied across time steps, the model suffers from vanishing or exploding gradient issues. To address these problems, advanced RNN-based models, such as long short-term memory (LSTM) and gated recurrent unit (GRU), are commonly used (Figure 5A). LSTM utilizes three gates to selectively store, transmit, and discard information, and uses a memory cell to retain long-term data. GRU, a simplified version of LSTM, applies an update gate to determine how much of the previous information to keep, and a reset gate to decide how much of the past information to forget, thereby overcoming the limitations of conventional RNNs.

Since composites exhibit highly nonlinear and time-dependent behavior, RNNs have been actively studied and applied in various research areas.[65,66,70-76] Chen *et al.*[70] predicted the nonlinear behavior of composites, such as the time-dependent nonlinear elastic-plastic response that varies with the strain/loading path, using an LSTM network capable of processing the entire time sequence. As a result, the trained LSTM model accurately predicted stress with a maximum error of <4%, and the model successfully reproduced the stress-strain hysteresis curves even under nonlinear cyclic loading conditions. Yousefi *et al.*[65] also employed an LSTM DL model, as shown in Figure 5B, to predict the long-term water absorption and thickness swelling behavior of a composite composed of hydrophilic cellulose fibers and hydrophobic polypropylene. By training the model with the initial 200 h of data obtained from immersion experiments, they demonstrated that the LSTM can effectively predict the long-term physical behavior of the composite for the subsequent 1300 h. Furthermore, RNN-based models have also been utilized to predict the behavior of composites under dynamic loading conditions. Borkowski *et al.*[71] employed a GRU to predict the response of ceramic matrix composites (CMCs) under non-monotonic loading and microstructural variations, and demonstrated that stable predictions could be achieved without overfitting across 60 test sets. Gao *et al.*[66] applied an LSTM to predict the axial stress of concrete-granite composites under impact conditions, as shown in Figure 5C. The trained model was able to predict stress responses to new impact velocities, joint roughness

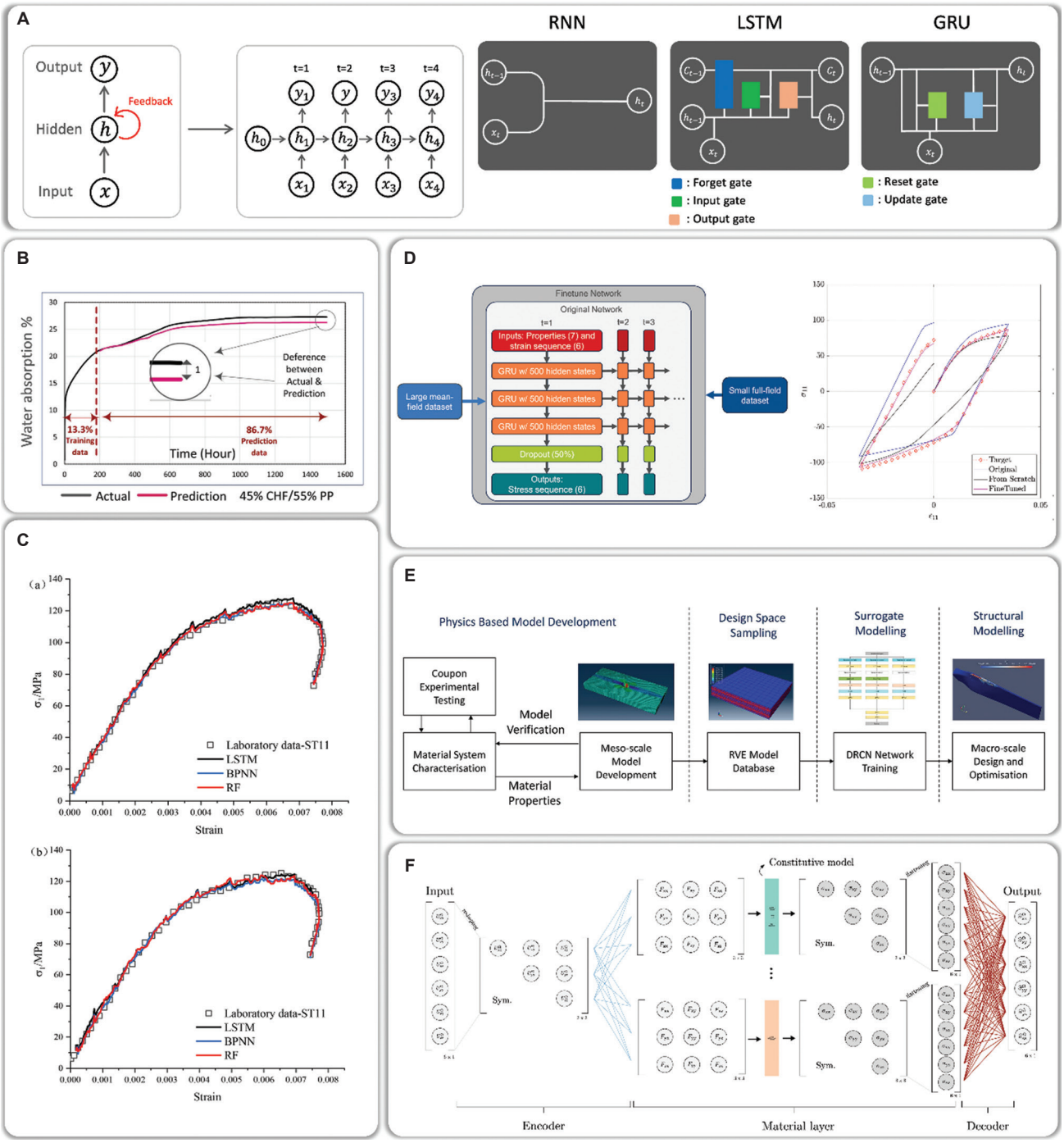

Figure 5. RNN, LSTM, and GRU architectures and research utilizing RNN in the field of composite materials. (A) Structure of RNN, LSTM, and GRU; (B) Comparison of actual and predicted results of water absorption;[65] (C) Comparison between the actual and predicted stress values;[66] (D) Network architecture and the transfer learning approach utilizing a large mean-field and a small full-field data set;[67] (E) Overview of data-driven multiscale framework using DRCN networks;[68] (F) Architecture of PRNN for finite strain framework.[69]

Abbreviations: BPNN: Backpropagation neural network; CHF: Corn husk fiber; DRCN: Decomposing residual convolutional neural; GRU: Gated recurrent unit; LSTM: Long short-term memory; PP: Polypropylene; PRNN: Physically recurrent neural network; RF: Random forest; RNN: Recurrent neural network; RVE: Representative volume element.

coefficients, and strain inputs, and showed improved prediction accuracy compared to backpropagation neural network and random forest models. RNNs have also been employed to predict the shape transformation of 4D-printed active composite structures. Sun *et al.*[73] designed an active composite beam using materials with different coefficients of thermal expansion and treated the material distribution as sequential data. By applying an RNN model, they successfully predicted the resulting shape under a stimulus of a 100°C temperature increase, achieving over 2000 times faster performance compared to conventional finite element simulations. In addition, to enhance the performance of RNNs, bidirectional RNNs – which process input sequences in both forward and backward directions – have been employed in studies to identify the location and size of defects in laminated composites[77] and to efficiently predict the time-dependent damage of composite hydrogen tanks.[78]

However, RNNs require a large amount of data for training and are difficult to capture spatial patterns compared to CNNs. To address these limitations, recent studies have explored combining RNNs with techniques such as transfer learning[67,79-82] and CNNs.[68,83-85] Cheung *et al.*[67] combined transfer learning with a GRU-based DL model to reduce the computational cost of predicting the nonlinear elasto-plastic behavior of short fiber reinforced composites, as shown in Figure 5D. In this approach, a mean-field-based RNN model was used with low-fidelity samples, while high-fidelity full-field simulation data were employed for fine-tuning. As a result, they successfully developed a framework with excellent computational efficiency and generalization performance. Jian *et al.*[80] also employed a combination of bidirectional LSTM and transfer learning to predict the behavior of CFRP composites in the very high cycle fatigue regime. In their approach, transfer learning was applied to predict the fatigue behavior of a new batch by leveraging existing experimental data. An attention mechanism was incorporated to focus on critical segments of the fatigue curve, such as regions with abrupt changes, thereby improving prediction accuracy and convergence speed. However, attention mechanisms, while advantageous for highly complex, imbalanced, or long-dependency data, may lead to overfitting and increased computational time when applied to low-complexity or relatively uniform data.[78] Therefore, careful consideration of the characteristics of the data is essential when applying attention mechanisms. As shown in Figure 5E, El Said[68] employed a deep recurrent CNN that combines CNN and LSTM to predict the nonlinear damage behavior of laminated composite structures. In particular, since features such as layup configuration, wrinkles, and ply gaps exhibit spatial characteristics, a CNN was used to extract spatial information from RVE images, which was then converted into sequences and fed into the LSTM to predict the stress at each time step. CNN-RNN-based models have also been applied to predict the evolution of surface roughness in carbon/carbon composites under thermochemical ablation[83] and to assess damage in composites subjected to low-velocity impacts.[85] According to a study by Truong *et al.*,[84] combining CNN with GRU yielded the highest prediction accuracy compared to using CNN, RNN, GRU, or LSTM individually.

Moreover, traditional RNNs are less robust to new conditions due to the absence of physically derived patterns, which prompted a series of studies to explore physically RNN (PRNN) models that incorporate physical constraints directly into the RNN architecture.[69,86] Maia *et al.*[69] aimed to predict the path- and rate-dependent stress responses of composites by embedding the constitutive models into the material layer of the PRNN, as shown in Figure 5F. This approach enabled them to incorporate the non-linear elasto-viscoplastic, path- and rate-dependent behavior of the matrix, as well as the nonlinear elastic and anisotropic characteristics of the fibers, into the RNN architecture. As a result, the model accurately predicted stresses with a mean absolute error of 5–7 MPa and a relative error within 5–10% under various loading conditions, and was also used to successfully extrapolate to loading conditions not included in the training data.

2.4. Physics-informed neural networks (PINNs)

DNNs accurately represent the relationship between the given inputs and outputs based on large-scale labeled datasets. However, due to their purely data-driven learning approach, the relationship itself remains a black box, which may limit their ability to reflect physical phenomena reliably. In contrast, PINNs integrate physical laws into the neural network learning process, as shown in Figure 6A.[87,88] PINNs do not require any labeled (input-to-output) data for training, and the governing partial differential equation (PDE), as well as initial and boundary conditions that describe the process being modeled, are used to train the neural network.

In the case of composite materials, solving the various PDEs that describe the elastic behavior, heat transfer, and damage or fracture models through FEA is time-consuming, and ML-based predictions often fail to reflect real physical phenomena. In contrast, predictions generated by PINNs can be consistent with the specified physical laws, even outside the training domain, making PINNs a powerful tool for efficiently predicting complex phenomena in composites research, such as plastic deformation, flow through porous media, and heat

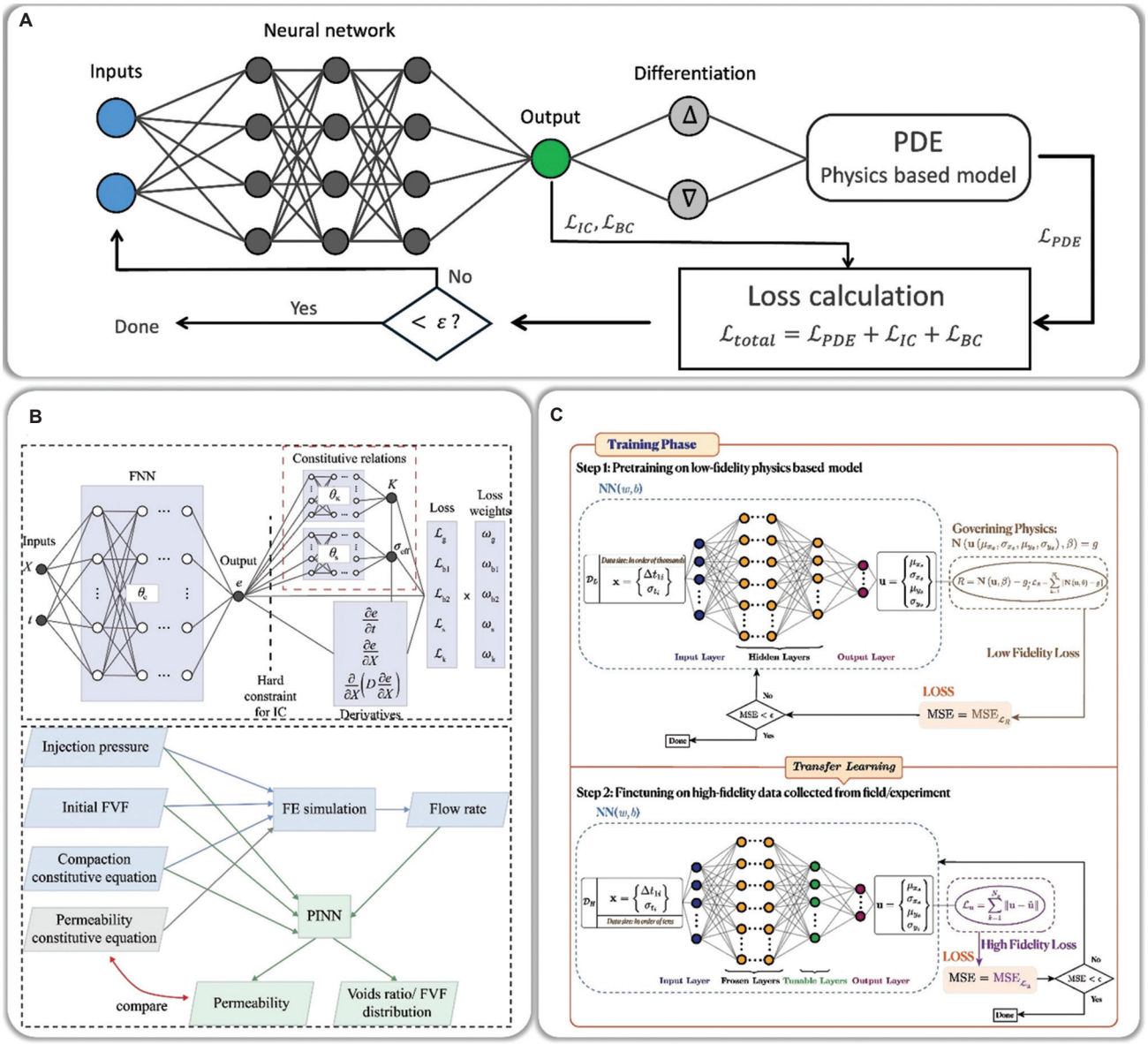

Figure 6. Structure of PINNs and research utilizing PINNs in the field of composite materials. (A) Structure of PINNs; (B) PINN framework and prediction results for estimating FVF distribution and permeability during injection-based measurements;[89] (C) multi-fidelity PINN framework for predicting defect positions in composites.[90]

Abbreviations: FE: Feature engineering; FNN: Forward neural network; FVF: Formation void fraction; MSE: Mean squared error; NN: Neural network; PDE: Partial differential equation; PINN: Physics-informed neural networks.

transfer. In addition, PINNs do not require meshing of the solution domain, and parameterized PDEs can be solved by including the process parameters directly as inputs to the neural network. Thus, PINNs can be utilized as accurate, time-efficient, data-free surrogate models for rapid process optimization.

Several studies have successfully applied PINNs for analyzing composite materials.[89-95] Using PINNs, researchers successfully predicted the composition-property relationships of basalt fibers, which are known for their mechanical and thermal stability.[92] Compared to traditional ANNs, the PINN model exhibited significantly improved predictions of the elastic modulus and tensile strength. This improvement highlights the PINN's advantage in incorporating physical constraints into the learning process to enhance the model's predictive accuracy.

Moreover, PINNs have also been applied to predict property degradation in carbon fiber/epoxy composites exposed to high-intensity radiative environments, such as weapon-induced explosions and solar flux.[95] The model

demonstrated high precision and reliability, with errors in the order of 10^{-5}. Compared to conventional numerical methods, such as the finite element method and finite difference approaches, the PINN framework reduced the computation time by over an order of magnitude.

To better represent the response of real fibrous reinforcements, Lee *et al.*[89] incorporated experimental data of the permeability and compressibility relations into the PINN training process to explain the remaining physics not expressed in the governing equations, as presented in Figure 6B. Real-time simulations of transverse permeability measurements were also conducted to extract the permeability relation using experimental data of the flow rate and injection pressure.

These examples demonstrate how PINNs are transforming composite materials research using more reliable, faster, and data-efficient methods for prediction, design, and analysis. While PINNs offer significant potential in the field of composite materials, conventional PINN models may struggle to fully capture the complex multi-physics and multi-scale issues inherent in composite materials. Obtaining a good balance between physics and data can also be challenging, potentially resulting in slower learning rates or difficulties in convergence. In addition, the training process is sensitive to network hyperparameters and can fall into local minima, and research is ongoing to improve the training performance of PINNs.[96]

To overcome these limitations, it is necessary to enhance model performance by utilizing hybrid models that combine data-driven neural networks with physics-based learning, enabling the simultaneous integration of physical laws and data-based training.[97,98]

A notable advancement in this field is the development of a transfer learning-based multi-fidelity PINN framework (mfPINN) to mitigate the effects of sparse and noisy sensor data, as well as the limited accuracy of idealized governing equations.[90] A low-fidelity PINN model is first trained based on the governing physics. Then, the information learned is transferred to a data-driven DNN, which is trained on a smaller set of high-fidelity data, as shown in Figure 6C. The mfPINN framework is used for acoustic source localization in anisotropic composites and is shown to accurately predict the location of defects or signal sources within composite materials. By integrating high-fidelity and low-fidelity data, the mfPINN enhances localization accuracy while preventing data overfitting and reducing the need for expensive high-resolution data, which is often difficult to obtain in practice.

In addition, Hanna *et al.*[99] used PINNs with CNNs to predict the 2D permeability tensor field of a glass fiber fabric, including localized variations. Alternatively, PINNs can be combined with numerical solvers to enhance training when simulating multi-scale problems, such as the dual-scale permeability of fibrous reinforcements.[100] Furthermore, applying active learning to efficiently select important training data is expected to provide a more effective learning.[101]

2.5. Explainable AI (XAI)

XAI is an approach that aims to provide clear and interpretable explanations for the results generated by DL models.[102,103] Typically, AI functions as a black box, making predictions without offering sufficient insight into the reasoning behind them. However, as illustrated in Figure 7A, the reliability of AI-driven results can be improved by utilizing XAI, which provides a transparent explanation of the decision-making process. This transparency not only enhances the reliability of AI systems but also enables users to better understand and interpret the factors influencing the model's predictions, making AI more accessible in various applications. When using AI for the analysis and design of composite materials, simply obtaining the output values of the results is insufficient. In particular, composite materials exhibit nonlinear properties and are sensitive to numerous factors, requiring careful analysis. While XAI is not a type of DL model, such as DNNs or CNNs, it has been widely used with ML models to predict composite defects, damage, and mechanical properties, explaining the decision-making process and improving the reliability of predictive models.

Several studies have highlighted the potential of XAI in this field.[32,104-109] Hong *et al.*[32] developed a predictive model for the behavior of a composite pressure vessel and utilized XAI to analyze the impact of stacking angle and layer thickness on its performance using permutation feature importance for each design parameter. Daghigh *et al.*[106] developed an XAI-based ML model for predicting defect characteristics (depth, size, and thickness) in composite materials using infrared thermography (IRT) data and evaluated the feature importance of each parameter. Yossef *et al.*[104] predicted the flexural strength of composite laminates using a decision tree-based gradient boosting algorithm as the ML model. They combined the ML model with XAI to analyze how the design parameters influence laminate strength and to provide a visual interpretation of the relationships between these factors (Figure 7B). Azad and Kim[105] developed an XAI-based model with vision transformers to detect damage in CFRP composites, as shown in Figure 7C. Their approach provided visual insights into areas of delamination, enhancing the damage detection process. Similarly, Song *et al.*[107] applied XAI to textile-reinforced mortar beams to predict the bending

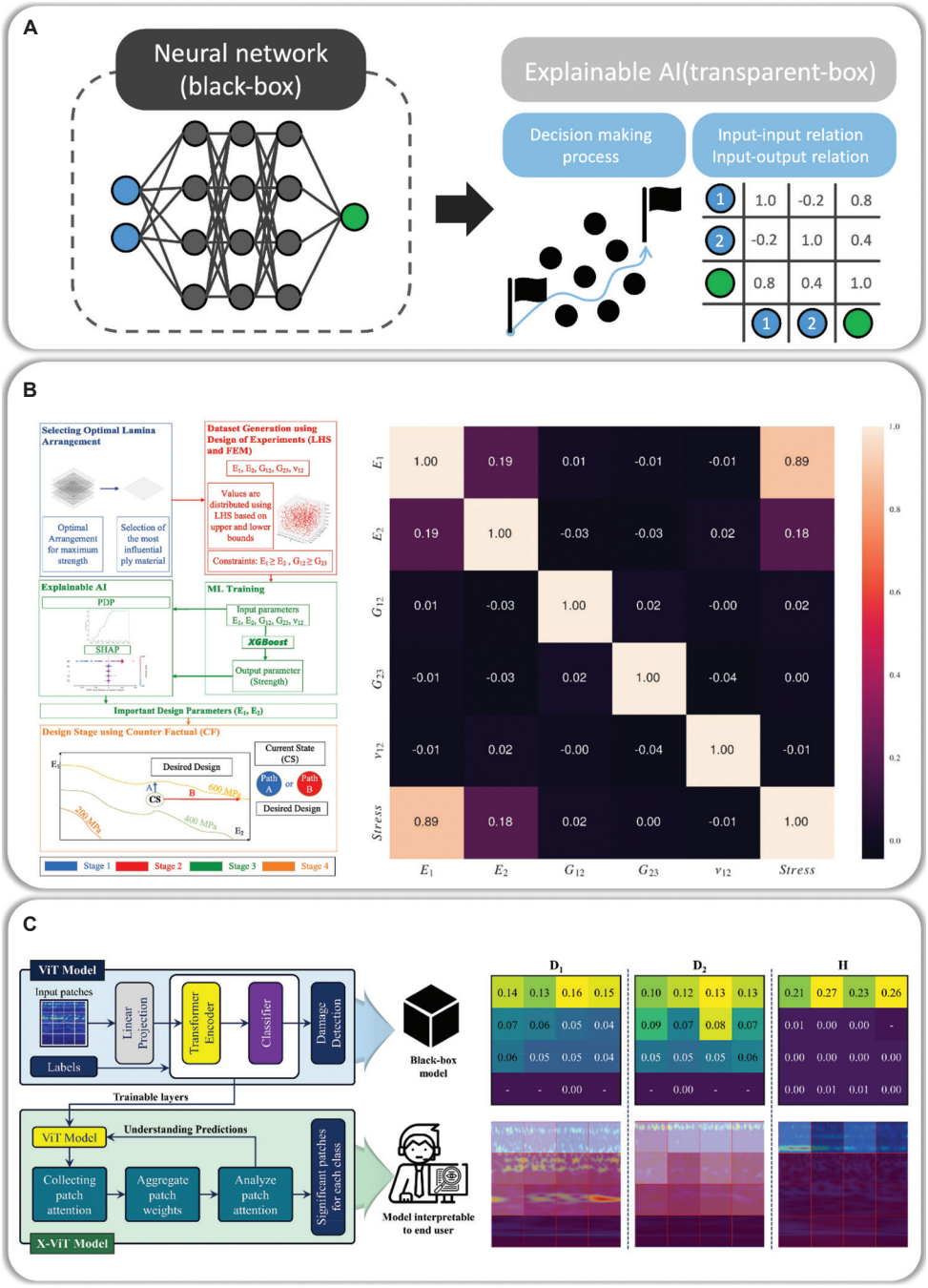

Figure 7. Structure of XAI and research utilizing XAI in the field of composite materials. (A) Structure of XAI; (B) Analysis of the relationships between design parameters of composite laminates and their impact on performance;[104] (C) Methodology and results of utilizing XAI to analyze the delamination mechanisms of composites.[105]

Abbreviations: FEM: Finite element method; LHS: Latin hypercube sampling; PDP: Partial dependence plot; SHAP: Shapley additive explanation; ViT: Vision transformer; XAI: Explainable artificial intelligence.

load capacity, revealing the key factors that influence the material's strength, such as the fiber tensile strength and cross-sectional area.

These studies demonstrate the growing role of XAI in composite materials, providing critical insights for material design, defect detection, and optimization of manufacturing parameters. By combining ML with explainability, XAI is advancing the development of more efficient and transparent processes for the design and manufacture of composite materials.

2.6. Summary of predictive models for composite materials

The applications of predictive ML models in the field of composite materials are summarized in Table 1, along with the advantages and limitations of each type of ML method. The ML approach should be tailored to the target application, as no method is superior to another. The ML framework should be constructed based on the number of variable parameters, the required accuracy of predictions, the type, quantity, and quality of the available data, as well as the knowledge of the governing equations. It is important to understand the characteristics of the problem being modeled to select the most suitable ML method for efficient training and accurate predictions.

3. Generative models for composite materials

Predictive models are designed to predict the output results based on the given input data, whereas generative models learn from existing unlabeled data to generate new data. In other words, generative models can create entirely new images, texts, designs, and structures, making them particularly valuable for various applications, including data augmentation and innovative design exploration.[111,112] One of the most well-known examples of generative models is ChatGPT, which demonstrates the potential of this technology in natural language generation. In the field of composite materials, obtaining experimental and simulation data often demands considerable time and cost. Furthermore, the vast range of material combinations and configurations leads to diverse shapes, properties, and characteristics, making the potential applications of generative models even more promising.

3.1. Variational autoencoders (VAEs)

VAEs are the most common types of generative models designed to generate data in a latent space.[113,114] As depicted in Figure 8A, VAEs primarily consist of an encoder and a decoder, where the encoder maps input data to a latent

Table 1. Applications, advantages, and limitations of predictive models for composite materials

ML method	Applications	Advantages	Limitations
Generic DNNs	-Prediction of nonlinear responses, mechanical properties, structural behaviors of composites,[29-31,33,34] and pressure vessel behavior[32]	-Efficient alternative to traditional numerical simulation	-Dependence on large quantities of high-quality data
CNNs	-Analysis of microstructure[50,110] -Prediction of stacking angle,[45,51] 3D permeability,[46] and microstructural property[60] -Detection of defect from IR stress measurements,[47] damage from lamb wave signals[59]	-Accurate predictions on image-based data	-Difficulties in collecting sufficient high-quality images. -High pre-processing load
RNNs	-Prediction of nonlinear stress-strain response of composites (elasto-plastic, path-dependent),[70] long-term water absorption and swelling,[65] dynamic loading behavior in CMCs and concrete granite composites,[66,71] shape transformation in 4D printed composites,[73] and fatigue behavior of composites[80] -Combination with CNN for spatial-temporal modeling[68,83-85]	-Ability to model sequential, time-dependent data, such as stress history or environmental exposure -Support for variable-length data -Use of advanced variants (LSTM, GRU, and Bi-RNN) to enhance prediction stability, memory retention, and directionality	-Need for large training datasets -Limited capability in spatial pattern extraction compared to CNNs -Susceptibility to vanishing/exploding gradients in generic RNNs
PINNs	-Thermochemical curing process[91] -Predict composition-property relationships of basalt fibers,[92] acoustic source localization in anisotropic composites,[90] and property degradation in carbon fiber/epoxy composites[95]	-No requirement for labelled training data -Physically-consistent predictions beyond the training domain	-Accuracy dependence on the compatibility of governing equations with the modeled process being. -Limitations due to idealized assumptions in governing equations vs. noise and variability in real-world data
XAI	-Analysis of feature importance for composite pressure vessel performance[32] -Prediction of the mechanical strength of the textile-reinforced beam[107] and defects in composite materials[106] -Design of FRP laminate[104] -Detection of visual delamination[105]	-Improved transparency in the decision-making process and prediction reliability -Visualization of influential factors	-Trade-off between explainability and predictive accuracy compared to complex black-box models

Abbreviations: Bi-RNN: Bidirectional recurrent neural network; CMCs: Ceramic matrix composites; CNNs: Convolutional neural network; DNNs: Deep neural networks; FRP: Fiber-reinforced polymer; GRU: Gated recurrent unit; IR: Infrared; LSTM: Long short-term memory; ML: Machine learning; PINNs: Physics-informed neural networks; RNNs: Recurrent neural network; XAI: Explainable artificial intelligence.

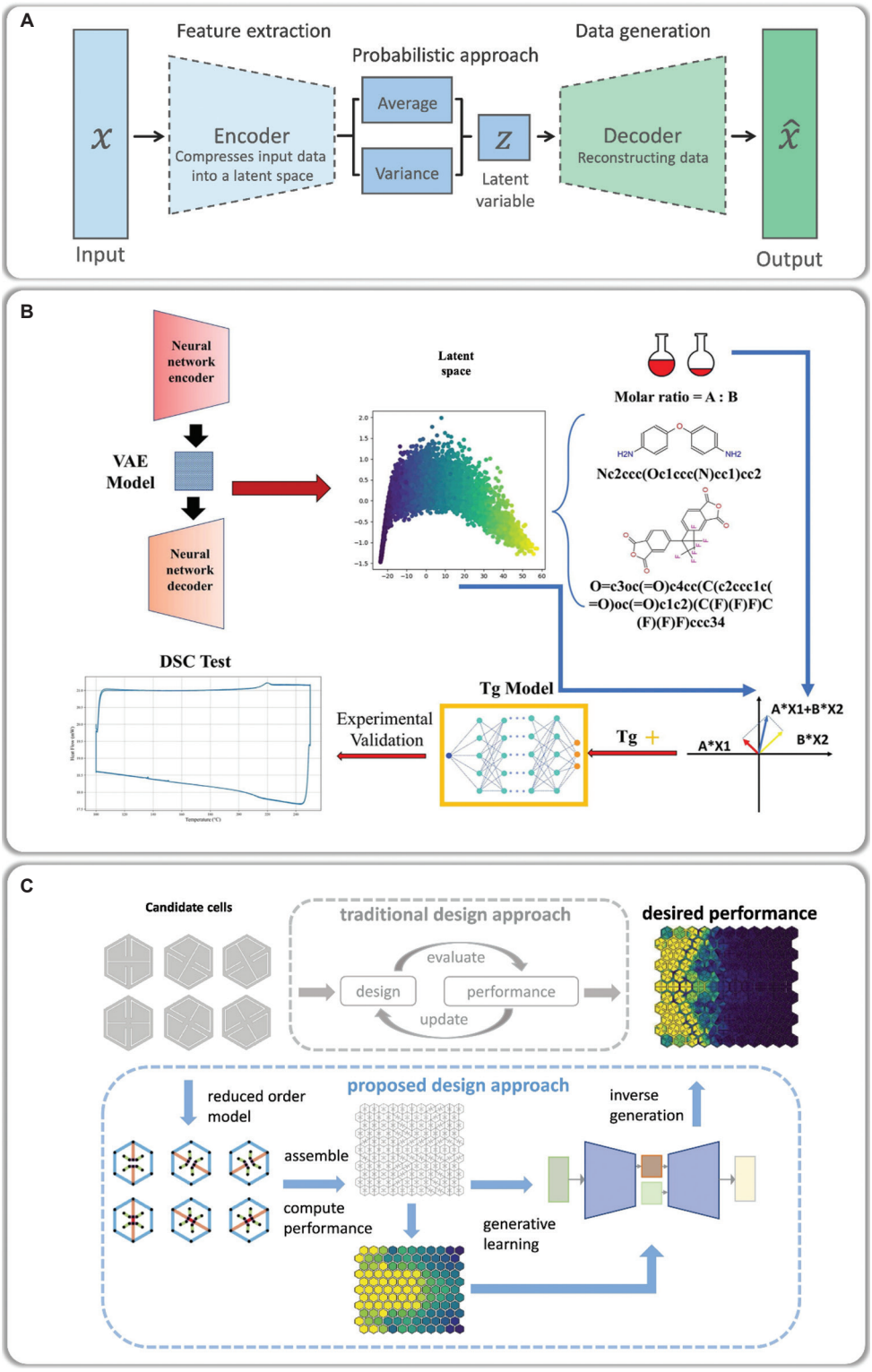

Figure 8. Structure of VAE and research utilizing VAE in the field of composite materials. (A) Structure of VAE; (B) VAE framework for material discovery of SMPs with targeted glass transition temperature.[115] Reprinted with permission from Teimouri and Li.[115] Copyright © 2024 John Wiley and Sons; (C) VAE framework used for designing unit cells and their arrangements to achieve impact mitigation with desired performance in metamaterials.[116] Reprinted with permission from Wang *et al.*[116] Copyright © 2024 Elsevier.
Abbreviations: DSC: Dice similarity coefficient; SMPs: Shape memory polymers; VAE: Variational autoencoders.

space, and the decoder reconstructs the original data from the input data. Specifically, to prevent the model from merely replicating the input, VAEs employ a probabilistic approach by encoding the input into the parameters of a Gaussian distribution (i.e., mean and standard deviation), and reconstructing the data by minimizing a loss function composed of a reconstruction loss and a Kullback-Leibler (KL) divergence term. As a result, VAEs are highly useful for generating, transforming, and compressing data, as well as creating new samples.

VAEs can serve as a powerful tool in the field of composite materials to address data scarcity issues and generate new designs.[115-120] For instance, a VAE-based approach was used for generating and optimizing composite layups with specified properties.[117] This method allows for increased flexibility in designing complex layup structures and outperforms traditional optimization methods, providing faster results and expanding the design space.

Moreover, as shown in Figure 8B, VAEs were applied to the design and material selection process in the development of thermoset shape memory polymers (SMPs) with high glass transition temperatures. Teimouri and Li[115] applied a VAE-based approach coupled with transfer learning to explore the vast chemical design space of SMPs. Their model optimized the glass temperature of SMPs, which was experimentally verified to be highly accurate, thus enhancing the material development process by reducing time and resource consumption.

Furthermore, as presented in Figure 8C, VAEs have also been utilized in the design of metamaterial arrays for impact protection. To address the high computational cost of traditional optimization methods, such as genetic algorithms and Bayesian optimization, Wang *et al.*[116] employed VAEs to generate unit cell designs and graded arrays with desired performance. The generated graded metamaterial demonstrated a 97.25% similarity to the target performance and significantly delayed the transmission of impact energy through the material compared to conventional designs.

However, conventional VAEs rely solely on a continuous Gaussian latent space and focus on learning static distributions, which makes it difficult to represent the complex mechanisms of composite materials and limits their ability to predict dynamic changes. Therefore, research is ongoing to apply extended VAE models to resolve these challenges. For instance, the vector quantized-VAE (VQ-VAE) constructs a discrete latent space, allowing the generation of new data through diverse combinations and thus enabling more reliable results. Using VQ-VAE, Wang *et al.*[119] predicted the 3D damage field of composite laminates under various low-velocity impact conditions and demonstrated high performance even with a small dataset. In addition, in a β-VAE, a hyperparameter β is introduced to adjust the weight of the KL divergence term in the standard VAE, thereby promoting statistical independence among latent variables. Jiang *et al.*[120] predicted the residual stiffness degradation caused by fatigue damage in CMCs with the aid of β-VAE. By combining β-VAE with neural ordinary differential equations, they captured the latent dynamics of fatigue damage progression and reconstructed the full stiffness degradation curves over fatigue cycles. Moreover, their model enabled accurate predictions even under new loading conditions through latent variable interpolation and partial data retraining.

These studies illustrate the versatility of VAEs in enhancing the design and performance of composite materials. By enabling the generation of complex material configurations and reducing the reliance on extensive experimental datasets, VAEs are anticipated to revolutionize the design and optimization of composite structures in various industries, including aerospace, automotive, and civil engineering.

3.2. Generative adversarial networks (GANs)

VAEs are powerful tools for data generation, but the quality of the generated data is relatively low, particularly for applications that require high-resolution images or complex patterns. They also struggle to capture fine details and intricate variations in real-world data, often leading to reconstruction errors, especially with high-dimensional or complex structures. On the other hand, GANs can address these limitations by implicitly estimating the probability distribution, flexibly learning highly complex and nonlinear data distributions in high-dimensional spaces. GANs employ two competing neural networks: a generator, which creates data that mimics real samples, and a discriminator, which distinguishes real data from generated data.[121] The structure of a GAN is depicted in Figure 9A. Through this competitive process, both networks progressively improve, refining the quality of the generated data. Composite material analysis involves capturing details of the intricate microstructures and variations from data consisting of high-resolution images and complex patterns. Consequently, GANs can be a particularly powerful tool in the field of composite materials.

In recent studies, GANs have been used to synthesize realistic 2D microstructures of unidirectional fiber-reinforced composites. Guo *et al.*[123] applied a deep convolutional GAN to generate 2D transverse microstructures of fiber reinforced composites. Their approach captured key microstructural features, such

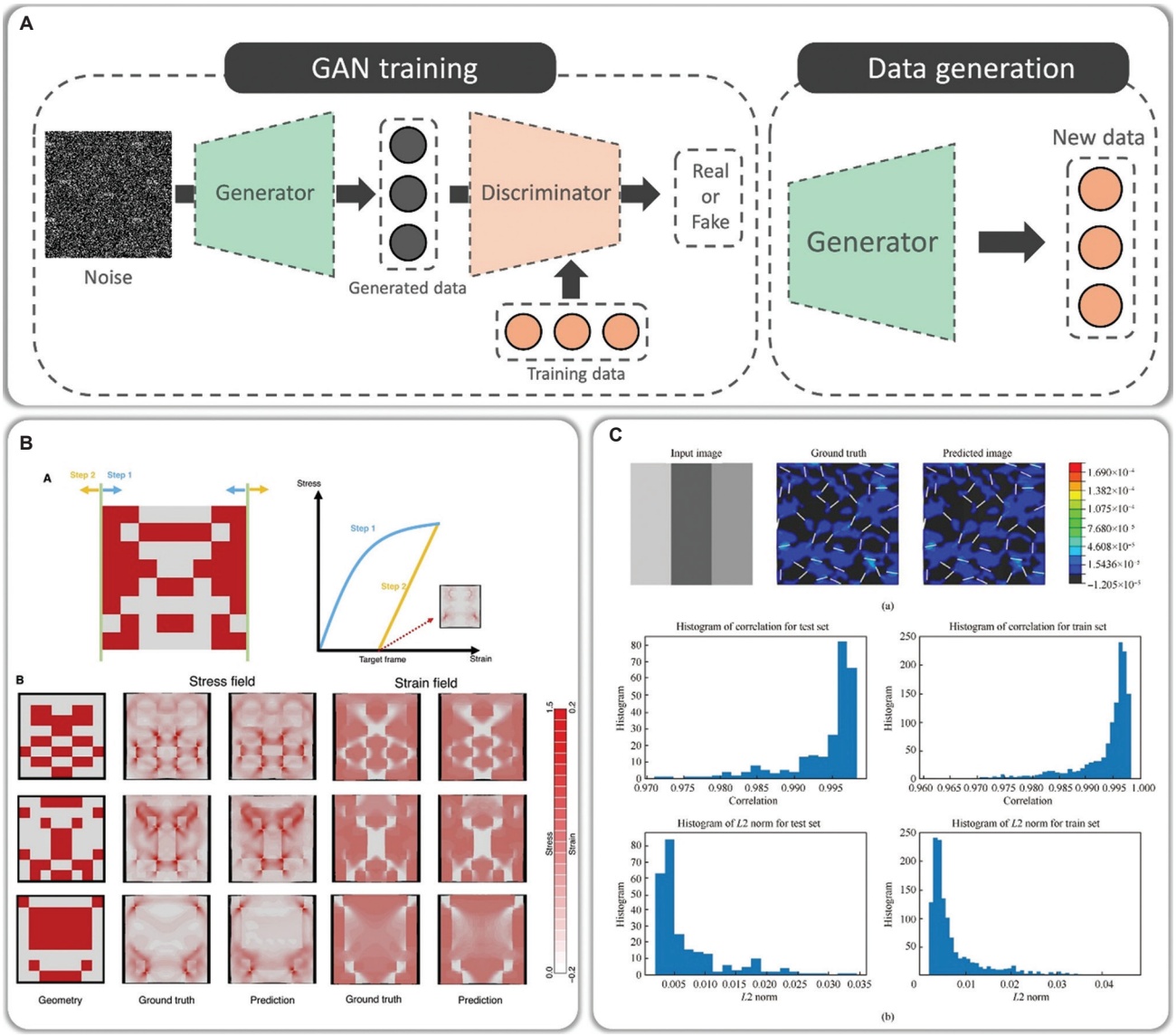

Figure 9. Structure of GAN and research utilizing GAN in the field of composite materials. (A) Structure of GAN; (B) Strain and stress field prediction results using conditional GAN and comparison with FEM (ground truth).[122] Reprinted with permission from Yang *et al.*[122] Copyright © 2021 The American Association for the Advancement of Science; (C) Stress field results derived from the microstructure of chopped fiber composites using conditional GAN.[110] Abbreviations: FEM: Finite element method; GAN: Generative adversarial network.

as the fiber diameter, fiber volume fraction, fiber spatial distribution, and resin-rich regions, which traditional random microstructure generators struggled to represent. Comparisons of the generated microstructures with real data highlighted the accuracy of GANs in modeling the detailed characteristics of composite structures.

In addition, GANs have been utilized for multi-objective optimization in the design of engineered cementitious composites.[124] The tensile stress, strain, and cost are optimized simultaneously for varying mixture proportions and fiber types, demonstrating the potential of GANs for complex multi-variate, multi-objective material design challenges in civil engineering applications.

Another innovative application of GANs is in topology optimization. Li *et al.*[125] integrated GANs with subset simulation to guide the design of periodic structures with desired bandgap properties. This hybrid approach allows for efficient generation of rare samples in high-dimensional design spaces, facilitating the identification of optimal topologies for composite structures. The method has proven to be effective in the topology optimization of

2D periodic structures, offering new avenues for material design with tailored mechanical properties.

Furthermore, a GAN model, referred to as IRT-GAN, was developed for automated defect detection in composite materials using IRT.[126] By utilizing simulated large-scale numerical datasets with various defects, IRT-GAN was trained to generate segmentation images of defects automatically. This method demonstrated improved detection performance for both glass fiber- and CFRPs, highlighting the ability of GANs to enhance quality control in composite manufacturing processes.

Conventional GANs generate data solely based on random noise without control over the output. On the other hand, conditional GANs (cGANs) introduce additional conditions to enable the generation of goal-oriented data tailored to specific conditions. Yang *et al.*[122] utilized cGANs to enhance stress and strain field predictions, as conventional GANs have been shown to generate arbitrary outputs following simple data distributions. As shown in Figure 9B, they accurately predicted both global mechanical properties (e.g., stiffness and resilience) and localized stress concentration phenomena corresponding to specific composite microstructures and loading conditions, achieving computation times of less than one second. Similarly, as shown in Figure 9C, Gupta *et al.*[110] developed a CNN-based GAN model to predict principal stress distributions by incorporating factors such as the microstructure of chopped carbon fiber epoxy composites, material properties, and time-dependent loading conditions. These studies present cGAN models as strong candidates for generating and predicting the physical behavior of composites based on their microstructure.

Overall, the integration of GANs into composite material design, optimization, and defect detection presents numerous advantages, including enhanced accuracy in microstructure modeling, multi-objective material optimization, and quality inspection. As these technologies continue to evolve, they hold the potential to revolutionize the development and manufacture of composite materials, leading to higher performance, reduced costs, and improved efficiency in industries such as automotive, aerospace, and civil engineering.

3.3. Other generative models

In addition to VAEs and GANs, diffusion-based deep generative models are being increasingly explored as generative models in the field of composite material research.[127] Diffusion models consist of a forward phase in which noise is gradually applied to the original image until it resembles Gaussian noise, and the reverse phase in which the model learns the process of progressively eliminating the noise to obtain the original image, as shown in Figure 10A. This process is based on a Markov chain, where each step refers only to the previous one, enabling stable training through the repeated learning of small changes. As a relatively recent and advanced DL approach, diffusion models demonstrate high performance in generating realistic 2D and 3D composite microstructures by learning from large datasets of actual material structures.[128,129] As shown in Figure 10B, Lyu and Ren[128] accurately reconstructed various complex 2D and 3D microstructures of composite materials, such as random textures and chessboard structures, using a diffusion model. The generated images showed distributions highly consistent with the original structures when evaluated using indicators, such as the two-point correlation function, lineal-path function, and Fourier descriptor. Furthermore, conditional generation of 3D structures corresponding to target permeability ranges was also conducted, demonstrating the feasibility of performance-driven inverse material design. As illustrated in Figure 10C, Bastek and Kochmann[130] proposed a diffusion model-based generative framework to design metamaterial structures that satisfy target stress-strain responses with nonlinear mechanical behavior. They employed a pixel-based 2D microstructural representation as the design parameter, enabling the expression of nonlinear physical phenomena, such as buckling, internal contact, and plastic deformation. After training, the model was evaluated on previously unseen target responses, achieving a normalized root mean square error as low as 1.5%, thereby demonstrating its high accuracy and effectiveness for inverse design applications.

A diffusion-based model is also used by Huang *et al.*[131] for data amplification for non-destructive structural health monitoring of CFRP composite plates using Lamb wave damage signals. It is demonstrated that the diffusion model outperformed VAE and GAN methods in terms of the diversity and quality of the generated samples. With ongoing advancements in ML/DL, diffusion models are poised to play a crucial role in the future of composite material design and optimization.

Normalizing flows (NFs) are a type of generative model that consists of a chain of parameterized invertible mappings to obtain the likelihood of a new sample by transforming the input probability distribution into a well-defined probability distribution, such as the normal distribution. NFs perform sampling, reconstruction, and probability density estimation stably through their invertible structure, which leads to fewer unstable training issues compared to GANs and reduces blurry samples often seen in VAEs. Stochastic inverse design of microstructures for woven CMCs with tailored anisotropic

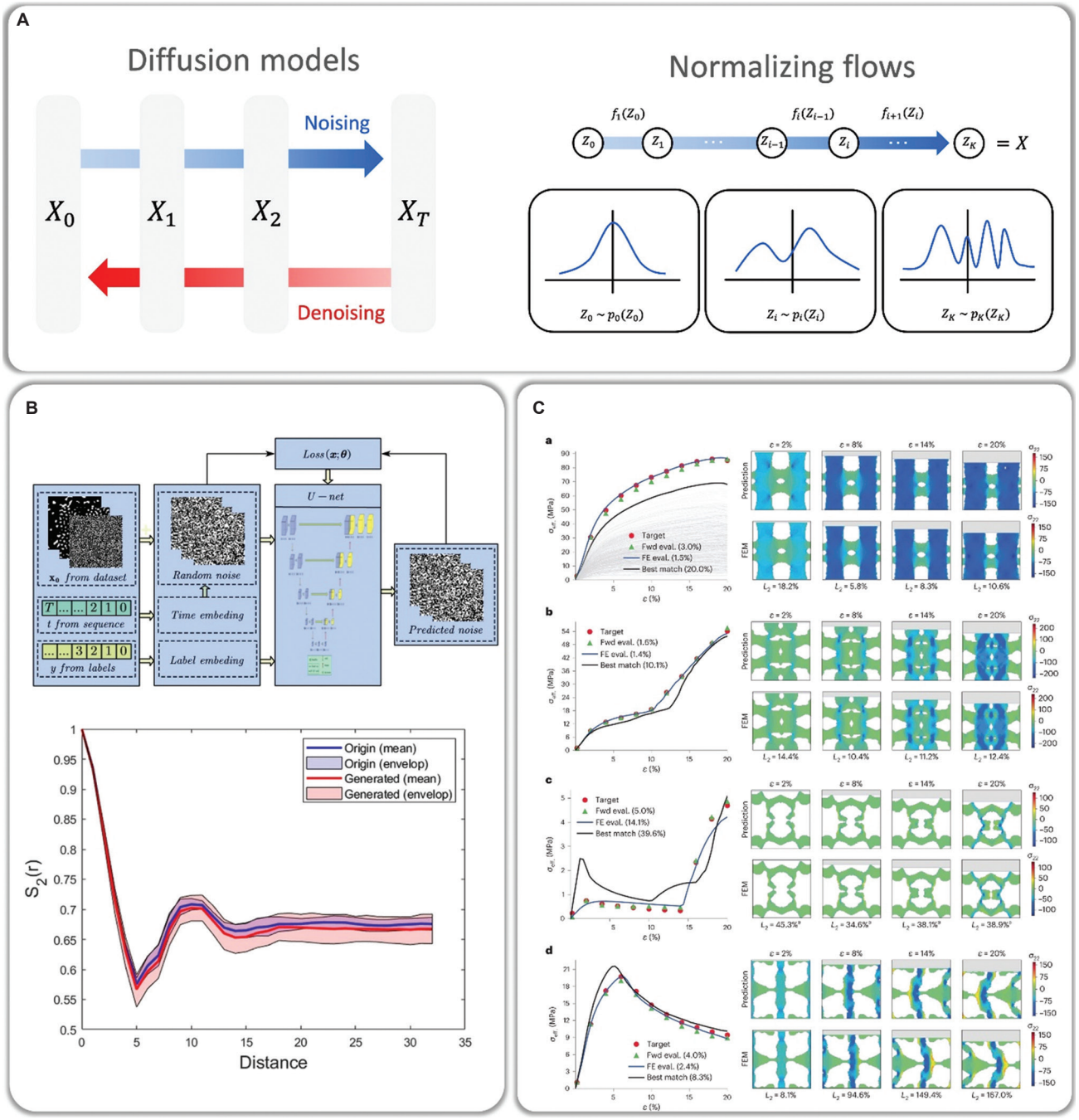

Figure 10. Structures of diffusion models and normalizing flows, as well as research utilizing diffusion models in the field of composite materials. (A) Structure of diffusion models and NFs; (B) The training process of the conditional diffusion model and comparison between the generated microstructures and the original microstructures;[128] (C) Metamaterial synthesis for four stress-strain responses.[130]

thermal conductivities was conducted through Bayesian inference, combining principal component analysis to reduce dimensionality, a VAE for data compression and to learn the prior distribution, and an NF model to generate new samples.[132] The framework was able to identify a range of novel microstructures with a target property, rather than a single optimal sample, including samples beyond the original training set. NFs are also implemented by Mirzaee and Kamrava[133] to generate microstructures of porous materials for a given target property from CNN-encoded 3D images via stochastic inverse design. NF models enable the incorporation of the stochastic nature of composite materials, providing a more realistic approach to design and optimization.

3.4. Summary of generative models for composite materials

The applications of generative models in composite materials research are summarized in Table 2, along with the advantages and limitations of each type of ML method.

Although the use of generative models is appealing for discovering new designs and materials, limitations include the difficulty in manufacturing the optimized microstructures, considering the extremely stochastic nature of composite materials. The design process should be constrained by the manufacturability of the generated composite structure, and additive manufacturing and automated technologies could be used in combination with generative models to create more accurately tailored structures.

Moreover, while transformer-based generative models, such as GPT-like architectures, Image GPT, and vision transformer-based diffusion generators,[134-136] have not yet been widely applied in composite materials research, their potential in the field is promising. The ability of transformer-based generative models to capture complex patterns and long-range dependencies makes them suitable for applications such as microstructure generation and cross-modal composite design. Future research exploring the adaptation of these foundation models could open new directions for AI-driven composite materials research and further enhance the generative design workflow.

4. Automation models for composite materials

Automation models refer to AI technologies that not only analyze data in real time and make automated decisions but also actively control, execute, and optimize manufacturing processes. Unlike predictive or generative models that primarily focus on producing outputs from given inputs or generating new data, automation models are characterized by their ability to autonomously manage dynamic workflows through continuous feedback, control strategies, and real-time optimization. This includes decision-making tasks, such as defect detection, process monitoring, and quality control, as well as direct process control, adaptive manufacturing scheduling, robotic motion planning, and real-time process optimization. These models are particularly used in automated manufacturing processes, robotic control systems, and autonomous driving, playing a critical role in improving both efficiency and quality.[138-140]

Composite materials are manufactured through complex processes that often demand significant time and cost. Moreover, manual production can lead to variations in material properties, making defect detection and quality control crucial to maintaining high standards. In addition, the ability to automatically adjust process parameters in real-time is crucial in accommodating the sensitivity of composites to environmental and operational conditions. Therefore, AI automation – encompassing both decision logic and process execution – is emerging as a key technology for enhancing efficiency, consistency, and quality in the production of composite materials. The manufacturing methods and applications utilizing automation models covered in this review are shown in Figure 11A.

4.1. Machine learning/deep learning-driven quality control

Defect detection and quality control are essential to maintain consistent quality and prevent significant

Table 2. Applications, advantages, and limitations of generative models for composite materials

Machine learning method	Applications	Advantages	Limitations
Variational autoencoders	-Composite layup generation and optimization[117] -Shape memory polymer property optimization[115] -Metamaterial design for impact mitigation[116]	-Generative and inference models	-Low quality of generated data, especially for high-resolution data or complex patterns
Generative adversarial networks	-Microstructure generation for fiber composites[123] -Engineered cementitious composites: multi-objective material optimization[124] -Topology optimization for periodic structures[125] -Defect detection in composites[126]	-High resolution results -Effectiveness for complex multi-modal distributions	-Potential occurrence of mode collapse, resulting in repetitive pattern generations
Diffusion models	-Microstructure generation[128] -Data amplification[131]	-High quality and diversity of generated samples	-High Computational demands and need for large training datasets
Normalizing flows	-Microstructure generation with targeted property[133,137]	-Likelihood estimation for a given sample	-Complex training processes, sensitivity to model architecture, and scalability challenges

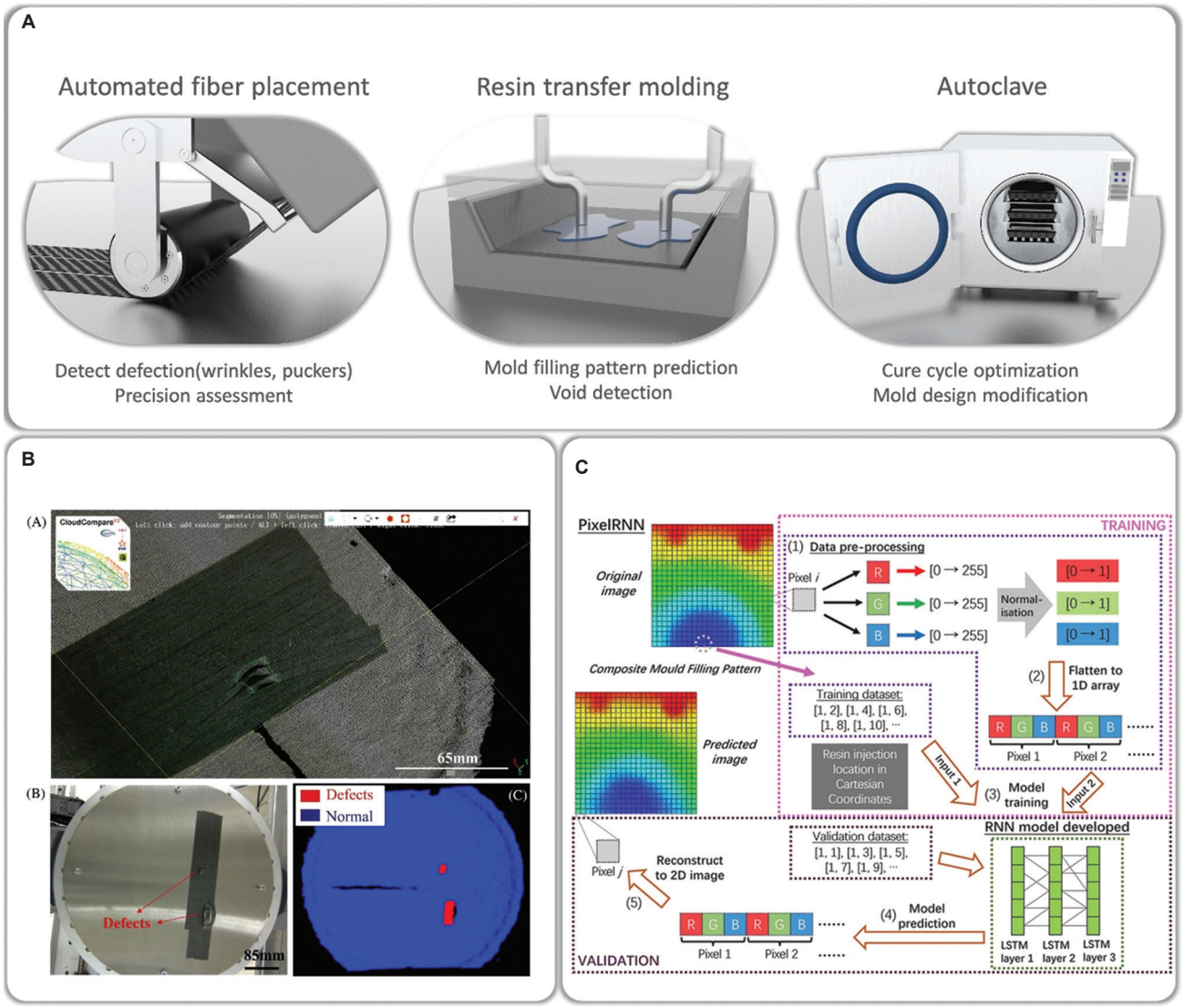

Figure 11. Manufacturing methods and applications utilizing automation models, and research utilizing automation models in the field of composites. (A) Manufacturing methods and applications utilizing automation models; (B) Defect detection results using automation models in the automated fiber placement process.[141] Reprinted with permission from Tang *et al.*[141] Copyright © 2024 John Wiley and Sons; (C) Study on predicting mold filling patterns in the resin transfer molding process.[142]

Abbreviations: RNN: Recurrent neural network; LSTM: Long short-term memory.

deviations in the properties of composite materials. In particular, the performance of composite materials can be highly sensitive to external environments or specific conditions, making it crucial to analyze and manage these factors precisely. Therefore, the automation of composite material analysis using automation models for quality control is becoming increasingly important.[141-145]

In quality control applications, CNN-based DL models are extensively employed due to their optimized characteristics for processing image and spatial data through the convolution and pooling of nonlinear high-dimensional feature representations. Machado *et al.*[143] used CNNs to develop an automatic system for void content assessment in composite laminates. Voids were detected with high accuracy, and the approach delivered significant improvements over traditional optical microscopy methods by offering faster and more reliable results, even in challenging lighting conditions or with small void sizes. Furthermore, Tang *et al.*[141] applied a CNN-based DL model to the automated fiber placement (AFP) process, successfully detecting lay-up defects, such as bridging, wrinkles, and puckers, using 3D scanning data. The model demonstrated high accuracy, particularly for defects with significant height differences compared to the normal

region, as shown in Figure 11B. However, challenges remain in detecting more subtle defects, such as loose tows and twists, where boundary detection becomes more difficult due to minimal height variations or uneven distribution of defects. One of the reasons for this limitation is that CNNs focus on learning local regions, making it difficult to capture global relationships. To address this limitation, many studies have explored the use of other DL models.

For instance, Liu *et al.*[144] integrated a transformer-based neural network with a CNN for automatic delamination detection in composite curved structures. This transformer-based model can learn correlations among elements within the entire image through a self-attention mechanism, enabling the detection of defects with high accuracy by considering patterns and morphological information. Moreover, by utilizing enhanced terahertz time-domain spectroscopy signals for non-destructive testing and imaging of hidden delamination defects, the transformer-based approach demonstrated superior accuracy and generalization performance compared to traditional models, highlighting its potential for real-time defect detection in complex composite structures. This method could be particularly beneficial in industries such as aerospace, where structural integrity is critical. In addition, the potential for ML/DL-driven automation in the quality control of the RTM process was demonstrated by Wang *et al.*[142] The PixelRNN model, an image-based neural network architecture, was used to predict mold filling patterns with high accuracy given the resin injection location, as shown in Figure 11C. This model was particularly effective in handling nonlinear filling patterns and significantly reduced computational costs compared to traditional physics-based simulations. This highlights the increasing role of ML/DL in process monitoring and automatic detection of dry spots in resin impregnation processes.

In addition, as described in Sections 3.2 and 3.3, generative models, such as GANs,[126] VAEs,[118] and diffusion models,[131] were also used to detect and classify defects in composite materials. In contrast to the methods of defect detection, which require data from both normal and defective samples, Szarski and Chauhan[146] developed a model based on NFs to obtain the image likelihood of a new sample using the knowledge learned from input images of only normal samples. Considering the rarity and variety of defects, collecting training data is expensive and time-consuming, and supervised learning proves to be difficult. Instead of detecting the presence of defects, the model determines whether the sample is different from a set of normal samples, without requiring any data from defective samples. Furthermore, Zhang *et al.*[118] focused on the use of a VAE combined with Bayesian neural networks (BNN) to quantify damage in composite plates. This semi-supervised learning model helps with structural health monitoring by effectively handling the uncertainty and measurement errors prevalent in damage detection. The VAE-BNN model achieved high accuracy for several damage types, such as cracks and delamination, offering improved robustness against noise compared to traditional methods.

These studies exemplify the growing impact of automation models in improving quality control in composite material manufacturing. The presence of defects, such as voids or wrinkles, can significantly compromise the mechanical properties of composite parts. By automating defect detection and enhancing defect characterization, ML/DL technologies are transforming the production of composite materials, ensuring better quality, reducing production times, and achieving cost savings in the long run. Moreover, the integration of ML/DL allows for continuous monitoring and real-time adjustments to further enhance the precision and efficiency of the production process.

4.2. Machine learning/deep learning-driven process automation

The production of composite materials has traditionally relied on the expertise of skilled professionals. While the work of these skilled experts remains an effective method for producing composite materials, the manufacturing process is highly dependent on external environments and conditions and susceptible to human error, requiring advanced technical skills and labor-intensive efforts. In addition, some processes may generate harmful chemicals that might have negative impacts on the health of workers.

Due to these limitations, there has been an increasing interest in automation in composite material manufacturing. However, simple mechanical automation is insufficient considering the complex shapes and variable manufacturing conditions associated with composite materials. In other words, advanced AI-based automation technology with the flexibility to adapt to diverse shapes and complex conditions is essential for composite material manufacturing.

These innovations are particularly important in manufacturing processes, such as AFP, RTM, and composite curing, where high precision and efficiency are critical.[127-129] A hybrid framework combining spatial-temporal analysis, thermography, and ML algorithms was recently developed for process monitoring and defect detection in AFP.[147] In this framework, an extensive thermal image database was used to train the model, achieving an impressive accuracy

in defect detection. The approach demonstrates a good balance between real-time performance and accuracy, optimizing the AFP part quality and enhancing the overall process efficiency. In addition, the integration of decision support systems in AFP would be beneficial, as these systems assist in defect detection, segmentation, and precision assessment, further streamlining the process.

In terms of process optimization, a theory-guided probabilistic ML (TGML) approach has been proposed for minimizing process-induced deformations (PIDs) in composite materials.[148] This method provides a reliable prediction model for optimizing key process parameters, such as layup design and curing cycles, using minimal experimental data. By utilizing TGML, the study identified an optimal layup configuration and curing cycle, achieving significant reductions in PIDs and production costs. The study demonstrates how ML can be applied to optimize complex manufacturing processes without the need for extensive experimental trials.

In the domain of composite curing, deep reinforcement learning has been employed to optimize temperature profiles and tooling during the curing process.[76,127,130] Würth *et al.*[91] demonstrated the application of PINNs for cost optimization of the thermochemical curing process of a composite plate. The use of PINNs resulted in speed improvements by over 500 times compared with conventional finite element simulations, demonstrating their potential to significantly reduce simulation times and enhance process efficiency. Similarly, Humfeld *et al.*[149] optimized the air temperature profile for composite curing subject to process constraints, such as cure duration and maximum part and air temperatures, using a PINN framework. Their multiple neural network framework consisted of four neural networks, each representing a different process variable, and a series of transfer learning stages with increasing complexity to ensure training convergence. Through reinforcement learning-based process control, Szarski and Chauhan[146] improved the air temperature profile for CFRP curing, resulting in a 40% reduction in curing time compared to traditional methods. Furthermore, the study employed Bayesian optimization to adjust the mold thickness based on the geometry of the CFRP part, improving heat transfer and preventing local overheating. This approach demonstrates the potential of reinforcement learning as autonomous AI optimizes both process time and energy consumption, thereby significantly enhancing the efficiency of the composite curing process.

4.3. Summary of automation models for composite materials

These advancements highlight the growing role of AI in automating and optimizing the composite manufacturing process. To date, only a limited number of studies have applied autonomous AI in composite materials research. With continuous improvements in process monitoring, modeling, and optimization, ML/DL-driven approaches are paving the way for more efficient, reliable, and cost-effective production of composite materials. Table 3 provides a summary of the applications of automation models in the field of composite materials, with the advantages and limitations.

5. Conclusion and future perspectives

In this paper, the innovative potential of AI in the design, manufacturing, and analysis of composite materials is investigated through a systematic study of predictive, generative, and automation models.

Predictive models have shown exceptional performance in predicting the physical properties of composite materials, microstructure analysis, and design parameter estimation, utilizing techniques including DNNs, CNNs, transfer learning, and PINNs. Generative models play a crucial role in the design and optimization of new materials, microstructure design, and the discovery of novel materials, offering innovative solutions in the field of composite materials based on various techniques,

Table 3. Applications, advantages, and limitations of automation models for composite materials

Applications	Advantages	Limitations
Void detection in laminates using CNN,[143] defect detection in AFP using CNN,[141] delamination characterization using transformer, [144] RTM mold filling prediction using PixelRNN,[142] and defect detection using GAN/diffusion/NF[126,131,146]	-High defect detection accuracy -Automation of the detection process -Improved production quality and reduced time/cost	-Difficulty in detecting subtle defects -Challenges in data acquisition -Requirement for integration with manufacturing processes
AFP process monitoring using ML and thermal imaging, [147] curing process optimization with TGML,[148] curing profile optimization with reinforcement learning, [146] and composite curing optimization using multi-stage PINN[149]	-Optimization of manufacturing efficiency and precision -Reduction of human error -Lower production costs	-Complexity of system integration -Sensitivity to external environment variations

Abbreviations: AFP: Automated fiber placement; CNN: Convolutional neural network; GAN: Generative adversarial network; ML: Machine learning; NF: Normalizing flow; PINN: Physics-informed neural network; RNN: Recurrent neural network; RTM: Resin transfer modeling; TGML: Theory-guided probabilistic machine learning.

such as VAEs and GANs. Automation models, which make automated decisions during the manufacturing process through real-time data analysis, prediction, and optimization, play a significant role in improving efficiency and quality, and are expected to make key contributions to enable widespread adoption and popularization of composite materials. Through various research examples, the paper confirms that ML provides a new paradigm for research in composite materials.

Despite these advancements, several critical challenges remain. Data scarcity continues to limit ML performance, highlighting the need for data-efficient approaches, such as transfer learning, few-shot learning, and the development of large-scale open datasets. Enhancing data accessibility and promoting widespread data-sharing within the research community will be highly beneficial for accelerating ML-driven advancements in composite materials research. Moreover, to maximize the practical utilization of ML, combining and applying multiple ML methodologies appropriately becomes increasingly important. Generalization issues, particularly the difficulty of applying trained models to new materials or conditions, can be addressed by embedding physics-based knowledge into ML frameworks through hybrid modeling and domain adaptation techniques. In addition, rather than relying on blind data accumulation, more efficient learning through intentional human-driven data curation is expected to enhance ML performance. Challenges regarding training instability and lack of interpretability require further research on regularization and the adoption of XAI approaches. Furthermore, the real-world deployment of AI models faces significant challenges related to robustness, latency, and safety. These challenges can be mitigated through advances in edge computing, digital twin frameworks, real-time AI inference technologies, and specialized ML hardware, such as neural processing units. Finally, integrating emerging technologies, such as quantum computing, may further enhance the scalability, reliability, and industrial adoption of AI-driven solutions in the research and manufacturing of composite materials.

Acknowledgments

None.

Funding

This research was supported by the Nano & Material Technology Development Program through the National Research Foundation of Korea (NRF), funded by the Ministry of Science and ICT (No. RS-2024-00450477). This work was supported by the National R&D Program through the National Research Foundation of Korea (NRF), funded by the Ministry of Science and ICT (RS-2023-00260461).

Conflict of interest

Seong Su Kim is an Editorial Board Member of this journal but was not in any way involved in the editorial and peer-review process conducted for this paper, directly or indirectly. Separately, other authors declared that they have no known competing financial interests or personal relationships that could have influenced the work reported in this paper.

Author contributions

Conceptualization: Hyunsoo Hong, Samuel Kim
Visualization: Samuel Kim
Writing – original draft: Hyunsoo Hong
Writing – review & editing: All authors

Ethics approval and consent to participate

Not applicable.

Consent for publication

Not applicable.

Availability of data

No datasets were generated or analyzed during the current study.

References

1. Silver D, Schrittwieser J, Simonyan K, *et al*. Mastering the game of go without human knowledge. *Nature*. 2017;550(7676):354-359.

   doi: 10.1038/nature24270

2. Silver D, Huang A, Maddison CJ, *et al*. Mastering the game of Go with deep neural networks and tree search. *Nature*. 2016;529(7587):484-489.

   doi: 10.1038/nature16961

3. Brown T, Mann B, Ryder N, *et al*. Language models are few-shot learners. *Adv Neural Inf Process Syst*. 2020;33:1877-1901.

4. Bai Y, Kadavath S, Kundu S, *et al*. *Constitutional AI: Harmlessness From AI Feedback*. [arXiv Preprint]; 2022.

5. Grigorescu S, Trasnea B, Cocias T, Macesanu G. A survey of deep learning techniques for autonomous driving. *J Field Robot*. 2020;37(3):362-386.

   doi: 10.1002/rob.21918

6. Holzinger A, Keiblinger K, Holub P, Zatloukal K, Müller H. AI for life: Trends in artificial intelligence for biotechnology. *N Biotechnol*. 2023;74:16-24.

   doi: 10.1016/j.nbt.2023.02.001

7. Soori M, Arezoo B, Dastres R. Artificial intelligence, machine learning and deep learning in advanced robotics, a review. *Cogn Robot*. 2023;3:54-70.

doi: 10.1016/j.cogr.2023.04.001

8. Brunton SL, Nathan Kutz J, Manohar K, *et al*. Data-driven aerospace engineering: Reframing the industry with machine learning. *Aiaa J*. 2021;59(8):2820-2847.

doi: 10.2514/1.J060131

9. Lingitz L, Gallina V, Ansari F, *et al*. Lead time prediction using machine learning algorithms: A case study by a semiconductor manufacturer. *Procedia CIRP*. 2018;72:1051-1056.

doi: 10.1016/j.procir.2018.03.148

10. Hong H, Kim S, Kim W, Kim W, Jeong JM, Kim SS. Design optimization of 3D printed kirigami-inspired composite metamaterials for quasi-zero stiffness using deep reinforcement learning integrated with bayesian optimization. *Compos Struct*. 2025;359:119031.

doi: 10.1016/j.compstruct.2025.119031

11. Hong H, Kim W, Kim W, Jeong JM, Kim S, Kim SS. Machine learning-driven design optimization of buckling-induced quasi-zero stiffness metastructures for low-frequency vibration isolation. *ACS Appl Mater Interfaces*. 2024;16(14):17965-17972.

doi: 10.1021/acsami.3c18793

12. Hong H, Jeong KI, On SY, Kim W, Kim SS. Structural optimization of an arch-structured epoxy/rubber composite vibration isolator using deep Q-value neural network reinforcement learning. *Compos Struct*. 2023;323:117506.

doi: 10.1016/j.compstruct.2023.117506

13. Barile C, Casavola C, De Cillis F. Mechanical comparison of new composite materials for aerospace applications. *Compos Part B Eng*. 2019;162:122-128.

doi: 10.1016/j.compositesb.2018.10.101

14. Lee J, Lee D, Park J, Choi I, Lim JW, Kim S. Carbon/epoxy composite foot structure for biped robots. *Compos Struct*. 2016;140:344-350.

doi: 10.1016/j.compstruct.2016.01.022

15. Bank LC. *Composites for Construction: Structural Design with FRP Materials*. United States: John Wiley and Sons; 2006.

16. Sarfraz MS, Hong H, Kim SS. Recent developments in the manufacturing technologies of composite components and their cost-effectiveness in the automotive industry: A review study. *Compos Struct*. 2021;266:113864.

doi: 10.1016/j.compstruct.2021.113864

17. Mrazova M. Advanced composite materials of the future in aerospace industry. *Incas Bull*. 2013;5(3):139-50.

18. Galos J, Pattarakunnan K, Best AS, Kyratzis IL, Wang CH, Mouritz AP. Energy storage structural composites with integrated lithium-ion batteries: A review. *Adv Mater Technol*. 2021;6(8):2001059.

doi: 10.1002/admt.202001059

19. Resor BR. *Definition of a 5MW/61.5 m Wind Turbine Blade Reference Model*. California: Sandia National Laboratories; 2013.

20. Moein MM, Saradar A, Rahmati K, *et al*. Predictive models for concrete properties using machine learning and deep learning approaches: A review. *J Build Eng*. 2023;63:105444.

doi: 10.1016/j.jobe.2022.105444

21. Dijkstra M, Luijten E. From predictive modelling to machine learning and reverse engineering of colloidal self-assembly. *Nat Mater*. 2021;20(6):762-773.

doi: 10.1038/s41563-021-01014-2

22. Sengar SS, Hasan AB, Kumar S, Carroll F. Generative artificial intelligence: A systematic review and applications. *Multimed Tools Appl*. 2024;84:1-40.

doi: 10.1007/s11042-024-20016-1

23. Sarker IH. AI-based modeling: Techniques, applications and research issues towards automation, intelligent and smart systems. *SN Comput Sci*. 2022;3(2):158.

doi: 10.1007/s42979-022-01043-x

24. Agatonovic-Kustrin S, Beresford R. Basic concepts of artificial neural network (ANN) modeling and its application in pharmaceutical research. *J Pharm Biomed Anal*. 2000;22(5):717-727.

doi: 10.1016/S0731-7085(99)00272-1

25. Abiodun OI, Jantan A, Omolara AE, Dada KV, Mohamed NA, Arshad H. State-of-the-art in artificial neural network applications: A survey. *Heliyon*. 2018;4(11):e00938.

doi: 10.1016/j.heliyon.2018.e00938

26. Sze V, Chen YH, Yang TJ, Emer JS. Efficient processing of deep neural networks: A tutorial and survey. *Proceed IEEE*. 2017;105(12):2295-2329.

doi: 10.1109/JPROC.2017.2761740

27. Samek W, Montavon G, Lapuschkin S, Anders CJ, Müller KR. Explaining deep neural networks and beyond: A review of methods and applications. *Proceed IEEE*. 2021;109(3):247-278.

doi: 10.1109/JPROC.2021.3060483

28. Larochelle H, Bengio Y, Louradour J, Lamblin P. Exploring strategies for training deep neural networks. *J Mach Learn Res*. 2009;10(1):1-40.

29. Hong H, Sarfraz MS, Jeong M, *et al*. Prediction of ground reaction forces using the artificial neural network from capacitive self-sensing values of composite ankle springs for exo-robots. *Compos Struct*. 2022;301:116233.

doi: 10.1016/j.compstruct.2022.116233

30. Wang W, Wang H, Zhou J, Fan H, Liu X. Machine learning prediction of mechanical properties of braided-textile reinforced tubular structures. *Mater Design*. 2021;212:110181.

doi: 10.1016/j.matdes.2021.110181

31. Ding X, Gu Z, Hou X, Xia M, Ismail Y, Ye J. Effects of defects on the transverse mechanical response of unidirectional fibre-reinforced polymers: DEM simulation and deep learning prediction. *Compos Struct*. 2023;321:117301.

doi: 10.1016/j.compstruct.2023.117301

32. Hong H, Kim W, Kim S, Lee K, Kim SS. Deep transfer learning for efficient and accurate prediction of composite pressure vessel behaviors. *Compos Part A Appl Sci Manuf*. 2024;186:108413.

doi: 10.1016/j.compositesa.2024.108413

33. Zhang Z, Zhou H, Ma J, *et al*. Space deployable bistable composite structures with C-cross section based on machine learning and multi-objective optimization. *Compos Struct*. 2022;297:115983.

doi: 10.1016/j.compstruct.2022.115983

34. Tao F, Liu X, Du H, Yu W. Learning composite constitutive laws via coupling Abaqus and deep neural network. *Compos Struct*. 2021;272:114137.

doi: 10.1016/j.compstruct.2021.114137

35. Schmidt T, Natarajan DK, Duhovic M, Cassola S, Nuske M, May D. Numerical data generation for building machine learning models for permeability estimation of fibrous structures. *Polym Compos*. 2025:1-17.

doi: 10.1002/pc.29768

36. Tan C, Sun F, Kong T, Zhang W, Yang C, Liu C. *A Survey on Deep Transfer Learning*. Berlin: Springer; 2018. p. 270-279.

37. Long M, Zhu H, Wang J, Jordan MI. Deep Transfer Learning with Joint Adaptation Networks. In: *Proceedings of Machine Learning Research*; 2017. p. 2208-2217.

38. Zhuang F, Qi Z, Duan K, *et al*. A comprehensive survey on transfer learning. *Proceed IEEE*. 2020;109(1):43-76.

doi: 10.1109/JPROC.2019.2955636

39. O'shea K, Nash R. *An Introduction to Convolutional Neural Networks*. [arXiv Preprint]; 2015.

doi: 10.48550/arXiv.1511.08458

40. Yamashita R, Nishio M, Do RKG, Togashi K. Convolutional neural networks: An overview and application in radiology. *Insights Imaging*. 2018;9:611-629.

doi: 10.1007/s13244-018-0639-9

41. Gu J, Wang Z, Kuen J, *et al*. Recent advances in convolutional neural networks. *Pattern Recognit*. 2018;77:354-377.

doi: 10.1016/j.patcog.2017.10.013

42. Rawat W, Wang Z. Deep convolutional neural networks for image classification: A comprehensive review. *Neural Comput*. 2017;29(9):2352-2449.

doi: 10.1162/NECO_a_00990

43. Dhillon A, Verma GK. Convolutional neural network: A review of models, methodologies and applications to object detection. *Prog Artif Intell*. 2020;9(2):85-112.

doi: 10.1007/s13748-019-00190-9

44. Lawrence S, Giles CL, Tsoi AC, Back AD. Face recognition: A convolutional neural-network approach. *IEEE Trans Neural Netw*. 1997;8(1):98-113.

doi: 10.1109/72.554195

45. Hong H, Kim W, Lee K, Kim SS. Prediction of stacking angles of fiber-reinforced composite materials using deep learning based on convolutional neural networks. *Compos Res*. 2023;36(1):48-52.

46. Caglar B, Broggi G, Ali MA, Orgéas L, Michaud V. Deep learning accelerated prediction of the permeability of fibrous microstructures. *Compos Part A Appl Sci Manuf*. 2022;158:106973.

doi: 10.1016/j.compositesa.2022.106973

47. Kojima Y, Hirayama K, Endo K, Harada Y, Muramatsu M. Transfer-learning-aided defect prediction in simply shaped CFRP specimens based on stress distribution obtained from finite element analysis and infrared stress measurement. *Compos Part B Eng*. 2025;291:111958.

doi: 10.1016/j.compositesb.2024.111958

48. Guild F, Summerscales J. Microstructural image analysis applied to fibre composite materials: A review. *Composites*. 1993;24(5):383-393.

doi: 10.1016/0010-4361(93)90246-5

49. D'orazio T, Leo M, Distante A, Guaragnella C, Pianese V, Cavaccini G. Automatic ultrasonic inspection for internal defect detection in composite materials. *NDT E Int*. 2008;41(2):145-154.

doi: 10.1016/j.ndteint.2007.08.001

50. Bhaduri A, Gupta A, Graham-Brady L. Stress field prediction in fiber-reinforced composite materials using a deep learning approach. *Compos Part B Eng*. 2022;238:109879.

doi: 10.1016/j.compositesb.2022.109879

51. Kim DW, Lim JH, Lee S. Prediction and validation of the transverse mechanical behavior of unidirectional composites considering interfacial debonding through convolutional neural networks. *Compos Part B Eng*. 2021;225:109314.

doi: 10.1016/j.compstruct.2020.109314

52. Abueidda DW, Almasri M, Ammourah R, Ravaioli U, Jasiuk IM, Sobh NA. Prediction and optimization of mechanical properties of composites using convolutional

neural networks. *Compos Struct*. 2019;227:111264.

doi: 10.1016/j.compstruct.2019.111264

53. Shorten C, Khoshgoftaar TM. A survey on image data augmentation for deep learning. *J Big Data*. 2019;6(1):60.

doi: 10.1186/s40537-019-0197-0

54. Mikołajczyk A, Grochowski M. *Data Augmentation for Improving Deep Learning in Image Classification Problem*. New York: IEEE; 2018. p. 117-122.

55. Shim YB, Lee IY, Park YB. Predicting the material behavior of recycled composites: Experimental analysis and deep learning hybrid approach. *Compos Sci Technol*. 2024;249:110464.

doi: 10.1016/j.compscitech.2024.110464

56. Zhu X, Liu Y, Li J, Wan T, Qin Z. *Emotion Classification with Data Augmentation using Generative Adversarial Networks*. Berlin: Springer; 2018. p. 349-360.

57. Lata K, Dave M, Nishanth KN. Data Augmentation using Generative Adversarial Network. In: *Proceedings of 2nd International Conference on Advanced Computing and Software Engineering (ICACSE)*; 2019.

58. Shao S, Wang P, Yan R. Generative adversarial networks for data augmentation in machine fault diagnosis. *Comput Ind*. 2019;106:85-93.

doi: 10.1016/j.compind.2019.01.001

59. Liu C, Xu X, Wu J, Zhu H, Wang C. Deep transfer learning-based damage detection of composite structures by fusing monitoring data with physical mechanism. *Eng Appl Artif Intell*. 2023;123:106245.

doi: 10.1016/j.engappai.2023.106245

60. Xu Y, Weng H, Ju X, *et al*. A method for predicting mechanical properties of composite microstructure with reduced dataset based on transfer learning. *Compos Struct*. 2021;275:114444.

doi: 10.1016/j.compstruct.2021.114444

61. Yi J, Deng B, Peng F, *et al*. Study on the parameters optimization of 3D printing continuous carbon fiber-reinforced composites based on CNN and NSGA-II. *Compos Part A Appl Sci Manuf*. 2025;190:108657.

doi: 10.1016/j.compositesa.2024.108657

62. Yu C, Zheng S, Zhao X. A novel version of hierarchical genetic algorithm and its application for hyperparameters optimization in CNN models for structural delamination identification. *J Braz Soc Mech Sci Eng*. 2024;46(8):462.

doi: 10.21203/rs.3.rs-3620270/v1

63. DeMille KJ, Hall R, Leigh JR, Guven I, Spear AD. Materials design using genetic algorithms informed by convolutional neural networks: Application to carbon nanotube bundles. *Compos Part B Eng*. 2024;286:111751.

doi: 10.1016/j.compositesb.2024.111751

64. Liu C, Li X, Ge J, *et al*. A deep learning framework based on attention mechanism for predicting the mechanical properties and failure mode of embedded wrinkle fiber-reinforced composites. *Compos Part A Appl Sci Manuf*. 2024;186:108401.

doi: 10.1016/j.compositesa.2024.108401

65. Yousefi E, Shiri MB, Rezaei MA, Rezaei S, Band SS, Mosavi A. A novel long-term water absorption and thickness swelling deep learning forecast method for corn husk fiber-polypropylene composite. *Case Stud Construct Mater*. 2022;17:e01268.

doi: 10.1016/j.cscm.2022.e01268

66. Gao H, Zhai Y, Wang T. A deep LSTM-based constitutive model for describing the impact characteristics of concrete-granite composites with different roughness interfaces. *Sci Rep*. 2024;14(1):29129.

doi: 10.1038/s41598-024-80366-6

67. Cheung HL, Mirkhalaf M. A multi-fidelity data-driven model for highly accurate and computationally efficient modeling of short fiber composites. *Compos Sci Technol*. 2024;246:110359.

doi: 10.1016/j.compscitech.2023.110359

68. El Said B. Predicting the non-linear response of composite materials using deep recurrent convolutional neural networks. *Int J Solids Struct*. 2023;276:112334.

doi: 10.1016/j.ijsolstr.2023.112334

69. Maia M, Rocha IB, Kovačević D, Van der Meer F. Physically recurrent neural network for rate and path-dependent heterogeneous materials in a finite strain framework. *Mech Mater*. 2024;198:105145.

doi: 10.1016/j.mechmat.2024.105145

70. Chen Q, Jia R, Pang S. Deep long short-term memory neural network for accelerated elastoplastic analysis of heterogeneous materials: An integrated data-driven surrogate approach. *Compos Struct*. 2021;264:113688.

doi: 10.1016/j.compstruct.2021.113688

71. Borkowski L, Skinner T, Chattopadhyay A. Woven ceramic matrix composite surrogate model based on physics-informed recurrent neural network. *Compos Struct*. 2023;305:116455.

doi: 10.1016/j.compstruct.2022.116455

72. Arnold SM, Mital SK, Hearley BL. *Stiffness and Fatigue Life Estimator for Polymer Composite Laminates Using Machine Learning*. Ohio: Glenn Research Center; 2023.

73. Sun X, Yue L, Yu L, *et al*. Machine learning-evolutionary algorithm enabled design for 4D-printed active composite structures. *Adv Funct Mater*. 2022;32(10):2109805.

doi: 10.1002/adfm.202109805

74. Friemann J, Dashtbozorg B, Fagerström M, Mirkhalaf SM. A micromechanics-based recurrent neural networks model for path-dependent cyclic deformation of short fiber composites. *Int J Numer Methods Eng*. 2023;124(10):2292-2314.

doi: 10.1002/nme.7211

75. Qiu C, Gui Y, Ma J, Song H, Yang J. Machine learning-based determination of Mode II translaminar fracture toughness of composite laminates from simple V-notched shear tests. *Compos Part A Appl Sci Manuf*. 2024;184:108233.

doi: 10.1016/j.compositesa.2024.108233

76. Parida SP, Sahoo S, Jena PC. Prediction of multiple transverse cracks in a composite beam using hybrid RNN-mPSO technique. *Proc Inst Mech Engi Part C J Mech Eng Sci*. 2024;238(16):7977-7986.

doi: 10.1177/09544062241239415

77. Zhang F, Wang L, Ye W, Li Y, Yang F. Ultrasonic lamination defects detection of carbon fiber composite plates based on multilevel LSTM. *Compos Struct*. 2024;327:117714.

78. Kadri K, Kallel A, Guerard G, *et al*. Prediction of ductile damage in composite material used in type IV hydrogen tanks by artificial neural network and machine learning with finite element modeling approach. *Energy Technol*. 2025;13(1):2401045.

doi: 10.1002/ente.202401045

79. Ghane E, Fagerström M, Mirkhalaf M. *Recurrent Neural Networks and Transfer Learning for Elasto-Plasticity in Woven Composites*. [arXiv Preprint]; 2023.

80. Jian Y, Hu P, Zhou Q, *et al*. A novel bidirectional LSTM network model for very high cycle random fatigue performance of CFRP composite thin plates. *Int J Fatigue*. 2025;190:108627.

doi: 10.1016/j.ijfatigue.2024.108627

81. Ghane E, Fagerström M, Mirkhalaf M. Multi-fidelity data fusion for inelastic woven composites: Combining recurrent neural networks with transfer learning. *Compos Sci Technol*. 2025;267:111163.

doi: 10.1016/j.compscitech.2025.111163

82. Bahmanpour M, Kalhori H, Li B. A data-driven hybrid recurrent neural network and model-based framework for accurate impact force estimation. *Mech Syst Signal Process*. 2025;229:112503.

doi: 10.1016/j.ymssp.2025.112503

83. Shang T, Ge J, Yang J, Li M, Liang J. Spatiotemporal prediction of surface roughness evolution of C/C composites based on recurrent neural network. *Compos Part A Appl Sci Manuf*. 2024;186:108429.

doi: 10.1016/j.compositesa.2024.108429

84. Truong VH, Le QH, Lee J, Han JW, Tessler A, Nguyen SN. An efficient neural network approach for laminated composite plates using refined zigzag theory. *Compos Struct*. 2024;348:118476.

doi: 10.1016/j.compstruct.2024.118476

85. Du J, Zeng J, Wang H, Ding H, Wang H, Bi Y. Using acoustic emission technique for structural health monitoring of laminate composite: A novel CNN-LSTM framework. *Eng Fract Mech*. 2024;309:110447.

doi: 10.1016/j.engfracmech.2024.110447

86. Kovács N, Maia M, Rocha IB, Furtado C, Camanho PP, Van der Meer FP. Physically Recurrent Neural Networks for computational homogenization of composite materials with microscale debonding. *Eur J Mech A Solids*. 2025;112:105668.

doi: 10.48550/arXiv.2410.13774

87. Cuomo S, Di Cola VS, Giampaolo F, Rozza G, Raissi M, Piccialli F. Scientific machine learning through physics-informed neural networks: Where we are and what's next. *J Sci Comput*. 2022;92(3):88.

88. Raissi M, Perdikaris P, Karniadakis GE. Physics-informed neural networks: A deep learning framework for solving forward and inverse problems involving nonlinear partial differential equations. *J Comput Phys*. 2019;378:686-707.

doi: 10.1016/j.jcp.2018.10.045

89. Lee J, Duhovic M, May D, Allen T, Kelly P. Physics-informed neural networks for real-time simulation of transverse liquid composite moulding processes and permeability measurements. *Compos Part A Appl Sci Manuf*. 2025;193:108857.

doi: 10.1016/j.compositesa.2025.108857

90. Kalimullah NM, Shelke A, Habib A. A probabilistic framework for source localization in anisotropic composite using transfer learning based multi-fidelity physics informed neural network (mfPINN). *Mech Syst Signal Process*. 2023;197:110360.

doi: 10.1016/j.ymssp.2023.110360

91. Würth T, Krauß C, Zimmerling C, Kärger L. Physics-informed neural networks for data-free surrogate modelling and engineering optimization-an example from composite manufacturing. *Mater Design*. 2023;231:112034.

doi: 10.1016/j.matdes.2023.112034

92. Wang X, Kan Q, Petru M, Kang G. Study on the composition-property relationships of basalt fibers based on symbolic regression and physics-informed neural network. *Compos Part A Appl Sci Manuf*. 2024;185:108324.

doi: 10.1016/j.compositesa.2024.108324

93. Meng Q, Li Y, Liu X, Chen G, Hao X. A novel physics-informed neural operator for thermochemical curing analysis of carbon-fibre-reinforced thermosetting

composites. *Compos Struct*. 2023;321:117197.

doi: 10.1016/j.compstruct.2023.117197

94. Niaki SA, Haghighat E, Campbell T, Poursartip A, Vaziri R. Physics-informed neural network for modelling the thermochemical curing process of composite-tool systems during manufacture. *Comput Methods Appl Mech Eng*. 2021;384:113959.

95. Yuan L, Li J, Wang B, *et al*. Temperature dynamics and mechanical properties analysis of carbon fiber epoxy composites radiated by nuclear explosion simulated light source. *Sci Rep*. 2025;15(1):1799.

doi: 10.1038/s41598-025-85959-3

96. Wang S, Sankaran S, Wang H, Perdikaris P. *An Expert's Guide to Training Physics-Informed Neural Networks*. [arXiv Preprint]; 2023.

97. Fang Z. A high-efficient hybrid physics-informed neural networks based on convolutional neural network. *IEEE Trans Neural Netw Learn Syst*. 2021;33(10):5514-5526.

doi: 10.1109/TNNLS.2021.3070878

98. Nascimento RG, Corbetta M, Kulkarni CS, Viana FA. Hybrid physics-informed neural networks for lithium-ion battery modeling and prognosis. *J Power Sources*. 2021;513:230526.

99. Hanna JM, Aguado JV, Comas-Cardona S, Le Guennec Y, Borzacchiello D. *A Self-Supervised Learning Framework Based on Physics-Informed and Convolutional Neural Networks to Identify Local Anisotropic Permeability Tensor from Textiles 2D Images for Filling Pattern Prediction*. Amsterdam: Elsevier; 2024.

100. Korolev D, Schmidt T, Natarajan DK, *et al*. *Hybrid Machine Learning Based Scale Bridging Framework for Permeability Prediction of Fibrous Structures*. [arXiv Preprint]; 2025.

101. Gal Y, Islam R, Ghahramani Z. Deep Bayesian Active Learning with Image Data. In: *Proceedings of Machine Learning Research*; 2017. p. 1183-92.

102. Xu F, Uszkoreit H, Du Y, Fan W, Zhao D, Zhu J. *Explainable AI: A Brief Survey on History, Research Areas, Approaches and Challenges*. Berlin: Springer; 2019. p. 563-574.

103. Dwivedi R, Dave D, Naik H, *et al*. Explainable AI (XAI): Core ideas, techniques, and solutions. *ACM Comput Surv*. 2023;55(9):1-33.

doi: 10.1145/3561048

104. Yossef M, Noureldin M, Alqabbany A. Explainable artificial intelligence framework for FRP composites design. *Compos Struct*. 2024;341:118190.

doi: 10.1016/j.compstruct.2024.118190

105. Azad MM, Kim HS. An explainable artificial intelligence-based approach for reliable damage detection in polymer composite structures using deep learning. *Polym Compos*. 2025;46(2):1536-1551.

doi: 10.1002/pc.29055

106. Daghigh V, Ramezani SB, Daghigh H, Lacy TE Jr. Explainable artificial intelligence prediction of defect characterization in composite materials. *Compos Sci Technol*. 2024;256:110759.

doi: 10.3390/asi7060121

107. Song Y, Kim K, Park S, Park SK, Park J. Analysis of load-bearing capacity factors of textile-reinforced mortar using multilayer perceptron and explainable artificial intelligence. *Construct Build Mater*. 2023;363:129560.

doi: 10.1016/j.conbuildmat.2022.129560

108. Kulasooriya W, Ranasinghe R, Perera US, Thisovithan P, Ekanayake I, Meddage D. Modeling strength characteristics of basalt fiber reinforced concrete using multiple explainable machine learning with a graphical user interface. *Sci Rep*. 2023;13(1):13138.

doi: 10.1038/s41598-023-40513-x

109. Meister S, Wermes M, Stüve J, Groves RM. Investigations on explainable artificial intelligence methods for the deep learning classification of fibre layup defect in the automated composite manufacturing. *Compos Part B Eng*. 2021;224:109160.

doi: 10.1016/j.compositesb.2021.109160

110. Gupta S, Mukhopadhyay T, Kushvaha V. Microstructural image based convolutional neural networks for efficient prediction of full-field stress maps in short fiber polymer composites. *Defence Technol*. 2023;24:58-82.

doi: 10.1016/j.dt.2022.09.008

111. Baidoo-Anu D, Ansah LO. Education in the era of generative artificial intelligence (AI): Understanding the potential benefits of ChatGPT in promoting teaching and learning. *J AI*. 2023;7(1):52-62.

112. Fui-Hoon Nah F, Zheng R, Cai J, Siau K, Chen L. *Generative AI and ChatGPT: Applications, Challenges, and AI-Human Collaboration*. United Kingdom: Taylor and Francis; 2023. p. 277-304.

113. Mescheder L, Nowozin S, Geiger A. Adversarial Variational Bayes: Unifying Variational Autoencoders and Generative Adversarial Networks. In: *Proceedings of Machine Learning Research*; 2017. p. 2391-2400.

114. Mishra A, Krishna Reddy S, Mittal A, Murthy HA. A Generative Model for Zero Shot Learning using Conditional Variational Autoencoders. In: *Proceedings of the IEEE Conference on Computer Vision and Pattern Recognition (CVPR) Workshops*; 2018. p. 2188-2196.

115. Teimouri A, Li G. Machine Learning-driven discovery of thermoset shape memory polymers with high glass transition temperature using variational autoencoders. *J Polym Sci*. 2025;63:1095-1107.

doi: 10.1002/pol.20241095

.

116. Wang W, Cheney W, Amirkhizi AV. Generative design of graded metamaterial arrays for dynamic response modulation. *Mater Design*. 2024;237:112550.

doi: 10.1016/j.matdes.2023.112550

117. Sun H, Wang X, Li J, Li Z, Guan Z. Efficient property-oriented design of composite layups via controllable latent features using generative VAE. *Compos Sci Technol*. 2025;259:110936.

doi: 10.1016/j.compscitech.2024.110936

118. Zhang C, Liu X, Wei D, Bo L. Predicting damage and quantifying uncertainty in composite plates with semi-supervised VAE-BNN model. *Measurement*. 2024;236:115069.

doi: 10.1016/j.measurement.2024.115069

119. Wang G, Zhang L, Xuan S, *et al*. An efficient surrogate model for damage forecasting of composite laminates based on deep learning. *Compos Struct*. 2024;331:117863.

doi: 10.1016/j.compstruct.2023.117863

120. Jiang D, Qian H, Wang Y, Zheng J, Zhang D, Li Q. Data driven prediction of fatigue residual stiffness of braided ceramic matrix composites based on Latent-ODE. *Compos Struct*. 2023;323:117504.

doi: 10.1016/j.compstruct.2023.117504

121. Goodfellow IJ, Pouget-Abadie J, Mirza M, *et al*. Generative Adversarial Nets. In: *Advances in Neural Information Processing Systems*. Vol. 27; 2014 [arXiv Preprint].

122. Yang Z, Yu CH, Buehler MJ. Deep learning model to predict complex stress and strain fields in hierarchical composites. *Sci Adv*. 2021;7(15):eabd7416.

doi: 10.1126/sciadv.abd7416

123. Guo R, Alves M, Mehdikhani M, Breite C, Swolfs Y. Synthesising realistic 2D microstructures of unidirectional fibre-reinforced composites with a generative adversarial network. *Compos Sci Technol*. 2024;250:110539.

doi: 10.1016/j.compscitech.2024.110539

124. Wang Y, Sun J, Wang X, *et al*. Multi-objective optimization of engineered cementitious composite based on machine learning and generative adversarial network. *J Build Eng*. 2024;96:110471.

doi: 10.1016/j.jobe.2024.110471

125. Li M, Jia G, Cheng Z, Shi Z. Generative adversarial network guided topology optimization of periodic structures via Subset Simulation. *Compos Struct*. 2021;260:113254.

doi: 10.1016/j.compstruct.2020.113254

126. Cheng L, Tong Z, Xie S, Kersemans M. IRT-GAN: A generative adversarial network with a multi-headed fusion strategy for automated defect detection in composites using infrared thermography. *Compos Struct*. 2022;290:115543.

doi: 10.1016/j.compstruct.2022.115543

127. Yang L, Zhang Z, Song Y, *et al*. Diffusion models: A comprehensive survey of methods and applications. *ACM Comput Surv*. 2023;56(4):1-39.

doi: 10.1145/3626235

128. Lyu X, Ren X. Microstructure reconstruction of 2D/3D random materials via diffusion-based deep generative models. *Sci Rep*. 2024;14(1):5041.

doi: 10.1038/s41598-024-54861-9

129. Lee KH, Yun GJ. Microstructure reconstruction using diffusion-based generative models. *Mech Adv Mater Struct*. 2024;31(18):4443-4461.

doi: 10.1080/15376494.2023.2198528

130. Bastek JH, Kochmann DM. Inverse design of nonlinear mechanical metamaterials via video denoising diffusion models. *Nat Mach Intell*. 2023;5(12):1466-1475.

doi: 10.1038/s42256-023-00762-x

131. Huang T, Gao Y, Li Z, Hu Y, Xuan F. A hybrid deep learning framework based on diffusion model and deep residual neural network for defect detection in composite plates. *Appl Sci*. 2023;13(10):5843.

132. Kobyzev I, Prince SJ, Brubaker MA. Normalizing flows: An introduction and review of current methods. *IEEE Trans Pattern Anal Mach Intell*. 2020;43(11):3964-3979.

doi: 10.1109/TPAMI.2020.2992934

133. Mirzaee H, Kamrava S. Inverse design of microstructures using conditional continuous normalizing flows. *Acta Mater*. 2025;285:120704.

doi: 10.1016/j.actamat.2024.120704

134. Zhang C, Lu J, Zhao Y. Generative pre-trained transformers (GPT)-based automated data mining for building energy management: Advantages, limitations and the future. *Energy Built Environ*. 2024;5(1):143-169.

doi: 10.1016/j.enbenv.2023.06.005

135. Shah B, Sinha A, Saxena P. *Image GPT with Super Resolution*. Berlin: Springer; 2022. p. 99-107.

136. Hatamizadeh A, Song J, Liu G, Kautz J, Vahdat A. *Diffit: Diffusion Vision Transformers for Image Generation*. Berlin: Springer; 2024. p. 37-55.

137. Generale AP, Robertson AE, Kelly C, Kalidindi SR. Inverse stochastic microstructure design. *Acta Mater*. 2024;271:119877.

doi: 10.2139/ssrn.4590691

138. Murphy RR. *Introduction to AI Robotics*. Cambridge: MIT Press; 2019.

139. Yurtsever E, Lambert J, Carballo A, Takeda K. A survey

of autonomous driving: Common practices and emerging technologies. *IEEE Access*. 2020;8:58443-58469.

140. Arinez JF, Chang Q, Gao RX, Xu C, Zhang J. Artificial intelligence in advanced manufacturing: Current status and future outlook. *J Manuf Sci Eng*. 2020;142(11):110804.

doi: 10.1115/1.4047855

141. Tang C, Sun D, Zou J, Xiong Y, Fang G, Zhang W. Lay-up defects inspection for automated fiber placement with structural light scanning and deep learning. *Polym Compos*. 2025:1-11.

doi: 10.1002/pc.29672

142. Wang Y, Xu S, Bwar K, *et al*. Application of machine learning for composite moulding process modelling. *Compos Commun*. 2024;48:101960.

doi: 10.1016/j.coco.2024.101960

143. Machado JM, Tavares JMR, Camanho PP, Correia N. Automatic void content assessment of composite laminates using a machine-learning approach. *Compos Struct*. 2022;288:115383.

doi: 10.1016/j.compstruct.2022.115383

144. Liu Q, Wang Q, Guo J, *et al*. A Transformer-based neural network for automatic delamination characterization of quartz fiber-reinforced polymer curved structure using improved THz-TDS. *Compos Struct*. 2024;343:118272.

doi: 10.1016/j.compstruct.2024.118272

145. Fotouhi S, Pashmforoush F, Bodaghi M, Fotouhi M. Autonomous damage recognition in visual inspection of laminated composite structures using deep learning. *Compos Struct*. 2021;268:113960.

doi: 10.1016/j.compstruct.2021.113960

146. Szarski M, Chauhan S. Composite temperature profile and tooling optimization via Deep Reinforcement Learning. *Compos Part A Appl Sci Manuf*. 2021;142:106235.

147. Zemzemoglu M, Unel M, Tunc LT. Enhancing automated fiber placement process monitoring and quality inspection: A hybrid thermal vision based framework. *Compos Part B Eng*. 2024;285:111753.

doi: 10.1016/j.compositesa.2020.106235

148. Schoenholz C, Zobeiry N. An accelerated process optimization method to minimize deformations in composites using theory-guided probabilistic machine learning. *Compos Part A Appl Sci Manuf*. 2024;176:107842.

doi: 10.1016/j.compositesa.2023.107842

149. Humfeld KD, Kim GY, Jeon JH, *et al*. Co-training of multiple neural networks for simultaneous optimization and training of physics-informed neural networks for composite curing. *Compos Part A Appl Sci Manuf*. 2025;193:108820.

doi: 10.1016/j.compositesa.2025.108820

ACCSCIENCE PUBLISHING

International Journal of AI for Materials and Design

ORIGINAL RESEARCH ARTICLE

A biomimetic machine learning approach for predicting the mechanical properties of additive friction stir deposited aluminum alloy-based walled structures

Akshansh Mishra[1,2]*

[1]Department of Chemistry, Material and Chemical Engineering, School of Industrial and Information Engineering, Politecnico Di Milano, Milan, Italy

[2]Computational Materials Research Group, AI Fab Lab, Maharajganj, Uttar Pradesh, India

Abstract

Additive friction stir deposition (AFSD) is a solid-state manufacturing technique capable of producing high-strength, defect-free metal components. The complexity of its process parameters has driven growing interest in machine learning (ML) for improved predictive accuracy and process control. This study presents a novel biomimetic ML approach to predict the mechanical properties of AFSD-fabricated aluminum alloy-walled structures. The methodology integrates numerical modeling of the AFSD process with genetic algorithm (GA)-optimized ML models to predict von Mises stress and logarithmic strain. Finite element analysis was employed to simulate the AFSD process for five aluminum alloys: AA2024, AA5083, AA5086, AA7075, and AA6061, capturing the complex thermal and mechanical interactions involved. A dataset of 200 samples was generated from these simulations. Decision tree and random forest (RF) regression models, optimized using GAs, were developed to predict key mechanical properties. The RF model demonstrated superior performance, achieving R^2 values of 0.9676 for von Mises stress and 0.7201 for logarithmic strain. This innovative approach provides a robust tool for understanding and optimizing the AFSD process across a range of aluminum alloys, offering valuable insights into material behavior under various process parameters.

Keywords: Additive friction stir deposition; Additive manufacturing; Machine learning; Hybrid algorithms

***Corresponding author:**
Akshansh Mishra
(akshansh.mishra@mail.polimi.it)

Citation: Mishra A. A biomimetic machine learning approach for predicting the mechanical properties of additive friction stir deposited aluminum alloy-based walled structures. *Int J AI Mater Design*. 2025;2(3):31-44.
doi: 10.36922/ijamd.5014

Received: September 30, 2024

Revised: March 26, 2025

Accepted: March 28, 2025

Published online: July 9, 2025

1. Introduction

Additive friction stir deposition (AFSD) is a friction stir-based additive manufacturing process that enables the layer-by-layer deposition of materials using a combination of feedstock, substrate, and specialized tooling.[1-5] Derived from the principles of friction stir welding, AFSD relies on intense thermoplastic deformation rather than melting, resulting in a refined, equiaxed microstructure in the final product.

Friction stir-based additive manufacturing technologies include three primary variants: friction surface deposition additive manufacturing, friction extrusion additive manufacturing, and AFSD. In friction surface deposition additive manufacturing,

metal rods are employed as feedstock. These rods are fixed to a rotating spindle that exerts a downward force, generating frictional heat that plasticizes the material. The softened material is then layered onto the substrate to form the additive component. As the spindle moves along a predefined trajectory, the component takes shape. However, the material experiences unconstrained expansion in both radial and axial directions, often resulting in curled edges around the rod. Friction extrusion additive manufacturing also employs metal rods, which are transformed into a plastic state through friction with a rotating die driven by axial force. The plasticized metal is extruded from the die outlet and fills the gap between the substrate and the tool, forming the component as the spindle moves. However, this method tends to produce poorly bonded layers due to the frictional interaction between the feedstock and the rotating die.

AFSD, which involves a shoulder-assisted tool, typically employs rods, wires, or powders as raw materials.[6-10] These materials are introduced into a hollow, non-consumable tool and, under the combined effects of extrusion, friction, and stirring, become thermoplasticized and migrate downward to the substrate. Mechanical mixing between the softened substrate and the plasticized raw material creates a robust bond, after which the component is formed as the spindle traverses its predefined path. Compared to the other two techniques, AFSD offers more precise control over material flow and forming morphology. Several essential parameters influence the AFSD process, such as tool rotation speed, feed rate, and layer height. The rate of heat generation is primarily determined by the tool's spinning speed, while feed rate or axial force governs the rate of material deposition. Tool traverse velocity influences the spatial distribution of heat, and the layer height defines the vertical distance between the tool and the substrate. During the operation, material flow is driven by extrusion and shearing in the transition zone beneath the feedstock rod, with the tool's stirring action playing an important role.[11-14] Thermal evolution in AFSD is defined by heat generated from both friction and plastic deformation, with internal temperature distribution influencing material flow.

Garcia *et al.*[15] explored the thermal and material flow behavior in the AFSD process, enabling site-specific deposition of high-quality metals with refined microstructures. Their study addressed a critical gap in understanding the thermal fundamentals of AFSD by employing *in situ* monitoring techniques such as infrared imaging, thermocouple measurements, and optical imaging. Focusing on two materials – copper (Cu) and aluminum-magnesium-silicon (Al-Mg-Si) – they observed that while both materials exhibited similar thermal trends (e.g., peak temperature and cooling rate), key quantitative differences emerged. In Cu, heat generation was predominantly due to interfacial friction resulting from full slipping contact between the tool and the material. In contrast, for Al-Mg-Si, both interfacial friction and plastic energy dissipation contributed to heat generation under partial slipping and sticking conditions. The study highlights the significance of material-specific thermal behavior in AFSD and provides valuable insights for optimizing solid-state additive manufacturing processes. Stubblefield *et al.*[16] developed a fully coupled thermo-mechanical meshfree approach to simulate the AFSD process, marking a significant advancement in modeling this solid-state additive manufacturing technique. Their Lagrangian reference frame allowed for the tracking of material point history and accounted for both elastic and plastic strains. An explicit dynamics time-stepping scheme was implemented to handle the high non-linearity of the AFSD process. The study also introduced a novel thermo-mechanical joining contact algorithm and validated the simulation results by comparing them with experimental data from single-layer deposition tests. Patil *et al.*[17] estimated key parameters such as temperature and strain rate during multi-layer deposition based on existing thermo-pseudo-mechanical models of friction stir processes. Their findings revealed that variations in average deposition temperature and strain rate significantly influenced complex material deformation and flash formation. Microstructural analysis using electron backscatter diffraction showed the presence of fine equiaxed grains along the build direction and finer grain bands at layer interfaces, suggesting dynamic recrystallization as the dominant restoration mechanism. This grain refinement during AFSD significantly enhanced the yield strength of the deposited IN625 compared to both the feed material and as-cast IN625.

AFSD has great potential in industrial applications due to its ability to manufacture high-strength, defect-free components without melting.[18-24] In the aeronautic field, AFSD can be applied to both repair and manufacturing operations for low- and high-performance parts, such as turbine blades, fuselage panels, and structural components, using materials including titanium and high-strength aluminum alloys.[25-31] The repair phase, in particular, benefits most from AFSD through localized repairs, reduced material waste, and shortened lead times. In the automotive industry, AFSD is increasingly used to produce lightweight, high-strength components aimed at improving fuel efficiency and supporting sustainability. This is largely due to its capacity to fabricate complex geometries in critical parts. In the defense sector, AFSD offers the advantage of on-site manufacturing and repair of military equipment, especially in remote or resource-scarce locations.[32-37] Its capability to form gradient

structures enables the integration of multifunctional materials, further enhancing thermal, mechanical, and corrosion resistance properties. The versatility of AFSD also holds promise for the medical and energy sectors, where customized implants and components with tailored properties could noticeably improve performance and service life.

Machine learning (ML) integration into the AFSD process is driven by the need to improve efficiency, precision, and overall performance. This technology helps address key challenges in AFSD, such as managing numerous process parameters, anticipating material behavior, and ensuring product quality. AFSD involves a complex interplay of factors, including tool rotation speed, feed rate, and axial force, all of which influence material flow, temperature distribution, and the mechanical properties of the deposited layers. Traditional trial-and-error approaches to parameter optimization are both time-consuming and costly. ML algorithms offer a more efficient alternative by analyzing the vast datasets generated during AFSD to identify optimal parameter settings, thereby minimizing the need for extensive experimental runs. For example, Qiao *et al.*[38] investigated the use of ML approaches to optimize AFSD process parameters for improved component design flexibility and performance. They used support vector machine, random forest (RF), and artificial neural network models to predict the mechanical properties – specifically microhardness and ultimate tensile strength – of AFSD-based AA6061 depositions. Key parameters such as temperature, force, torque, rotation speed, traverse speed, feed rate, and layer thickness were monitored using a self-developed process-aware kit. Among the models tested, the artificial neural network model demonstrated the highest accuracy, with an R^2 of 0.9998, a mean absolute error (MAE) of 0.0050, and a root mean square error (RMSE) of 0.0063. The study also identified feed rate and layer thickness as the most influential factors on mechanical properties, contributing 24.8%/24.1% and 25.6%/26.6%, respectively. Zhu *et al.*[39] proposed a novel explainable artificial intelligence strategy that combines Bayesian learning with physics-based surrogate models. They developed a physics-informed, data-driven model capable of accurately forecasting temperature distribution during AFSD by calibrating and updating these models using ML on *in situ* monitoring data. The approach was validated through the AFSD of an Al-Mg-Si alloy, resulting in rapid and accurate temperature predictions with minimal reliance on physics-based simulations and *in situ* measurements. Similarly, Shi *et al.*[40] introduced a physics-informed ML approach known as AFSD-Nets, which integrates heat generation and heat transfer effects to predict temperature profiles. AFSD-Nets employs customized neural network approximators to model the coupled temperature evolution of the tool and the build during multilayer material deposition. The model's accuracy was validated through comparisons between predicted and actual temperature measurements.

Building on these advancements, the present study aims to develop a novel biomimetic ML approach for predicting the mechanical properties of AFSD-fabricated aluminum alloy-walled structures. Specifically, the study focuses on five aluminum alloys: AA2024, AA5083, AA5086, AA7075, and AA6061. The proposed method integrates genetic algorithm (GA)-optimized ML models with finite element analysis to predict von Mises stress and logarithmic strain.

AFSD holds significant promise as a manufacturing technique for aluminum alloy structures. However, due to the complicated interaction of thermal and mechanical processes inherent to AFSD, accurately predicting and controlling the mechanical properties of the final product remains a significant challenge. Traditional experimental approaches for optimizing process parameters and predicting material behavior are both time-intensive and costly. Furthermore, the variability in material properties among these different aluminum alloys, namely AA2024, AA5083, AA5086, AA7075, and AA6061, further complicates this task. Therefore, there is a pressing need for an effective and accurate method to predict critical mechanical parameters, such as von Mises stress and logarithmic strain, in AFSD-manufactured components across diverse aluminum alloys. This research seeks to address that need by introducing a novel biomimetic ML approach that integrates numerical modeling with GA-based optimization, offering a potentially revolutionary solution for process optimization and quality control in AFSD.

2. Materials and methods

The simulations were conducted using Abaqus finite element software to model the AFSD process for five aluminum alloys: AA2024, AA5083, AA5086, AA7075, and AA6061. The properties and typical applications of these alloys are summarized in Table 1.

Figure 1 illustrates the basic simulation setup. The modeling process begins with creating parts that represent both the substrate and the material to be deposited. Next, temperature-dependent material properties – including density, specific heat, thermal conductivity, and elastic/plastic properties – are defined and assigned to both the substrate and the deposited material.

A step in Abaqus represents a specific phase or period within the analysis during which specific loads, boundary conditions, and analysis procedures are applied. For the

Table 1. Material properties and typical applications of the alloys considered in the present work

Alloy	Temper	Tensile strength (MPa)	Yield strength (MPa)	Elongation (%)	Density (g/cm^3)	Typical applications
AA2024	T3	427 – 483	324 – 393	10 – 25	2.78	Aircraft structures, rivets, and truck wheels
AA5083	H116	283 – 303	193 – 214	16 – 22	2.66	Shipbuilding, pressure vessels, cryogenic tanks
AA5086	H116	290 – 324	172 – 193	18 – 25	2.66	Marine applications, automotive body panels
AA7075	T6	517 – 572	434 – 503	5 – 11	2.81	Aerospace components, bicycle frames, and rock climbing equipment
AA6061	T6	310	276	10 – 18	2.7	Architectural applications, bicycle frames, and automotive components

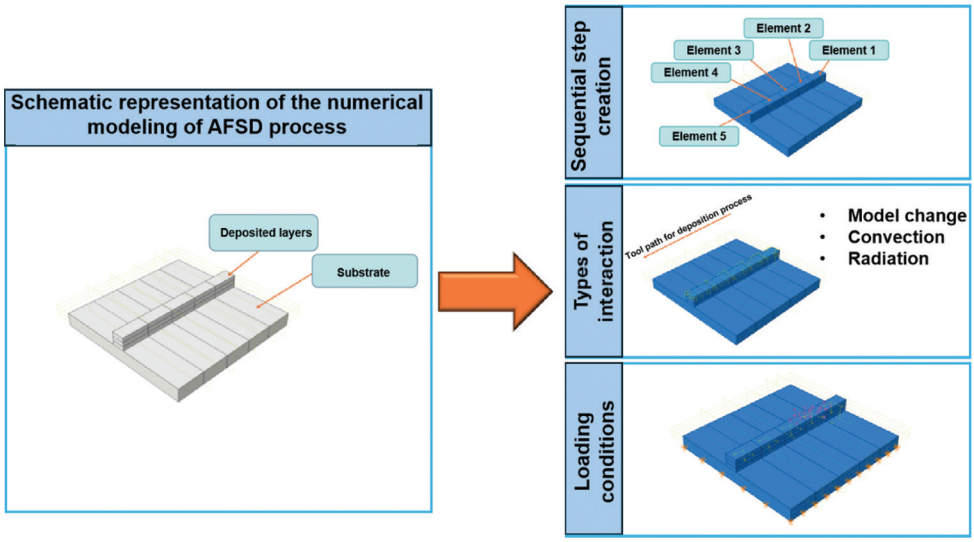

Figure 1. Schematic representation of the numerical modeling steps for the additive friction stir deposition process. The diagram consists of three main sections: sequential step creation, interaction types, and loading conditions. The simulation begins with the substrate and initially deactivated deposited layers. The model then incorporates element activation and various interaction types (mesh change, conversion, and radiation). Four distinct loading conditions are applied: heat source, pressure, and shear forces in both the longitudinal and rotational directions.

coupled temperature–displacement analysis in this study, a coupled temperature–displacement step is utilized. This type of step allows for the simultaneous analysis of both thermal and structural behavior, capturing the interaction between temperature changes and the resulting deformations or stresses. Figure 1 illustrates the top layer of the deposited material, where these steps are applied. Within each step, parameters such as step duration, loading conditions, boundary conditions, and the analysis procedure (e.g., static, dynamic, or explicit) can be specified according to simulation requirements.

To accurately simulate the complex physical processes involved in AFSD, three interaction types – model change, convection, and radiation – must be created, as shown in Figure 1. Model change interactions are essential for representing the additive nature of AFSD by simulating the sequential deposition of material layers. These interactions allow the model to depict the evolving geometry and thermal history of the build by activating different regions layer by layer. Convection interactions are required to model heat transfer between the deposited material, the tool, and the surrounding environment. This is essential for predicting cooling rates, temperature gradients, and possible defects such as distortions or residual stresses.

The loading parameters applied in Abaqus to simulate the AFSD process – namely, the heat source, pressure, shear longitude, and shear rotational – are all relevant and important for ensuring an accurate representation of the process, as depicted in Figure 1. The heat source plays a critical role by generating the necessary thermal energy through friction between the rotating tool and the substrate. The friction heat softens the material, enabling its deposition. The downward force exerted by the tool is essential for consolidating the deposited material and

ensuring a strong bond with the substrate. In addition, pressure influences both the material flow and the shape of the deposited bead. Shear longitude refers to the shear force acting in the direction of the tool's travel. This force plays an important role in material transport, mixing, and the formation of the characteristic AFSD microstructure. In contrast, shear rotational refers to the circumferential shear force generated around the tool. It contributes to material flow, stirring, and the development of the final part geometry.

Figure 2 displays the predicted outcomes of the AFSD simulations. One key parameter, AC YIELD, represents the accumulated equivalent plastic strain at the end of each increment. This parameter is crucial for understanding the extent of plastic deformation during the AFSD process and helps identify regions susceptible to material failure due to excessive strain. It also supports the optimization of process parameters to achieve desired material properties. Gradient of Temperature (GRADT), the spatial temperature gradient, reveals temperature distribution and heat flow within the material during AFSD. Sharp temperature gradients can induce thermal stresses and affect the microstructure and mechanical properties of the final part. NT11 represents the normal stress component in the 11-direction (typically aligned with the build direction in AFSD), allowing for the assessment of residual stresses caused by thermal and mechanical loads. Plastic strain (PEEQ) is a scalar measure of plastic deformation that complements AC YIELD in identifying regions where the material may fail or undergo significant changes in properties. LE, representing logarithmic strain, is used to analyze material behavior under large deformations, which are common in AFSD due to elevated temperatures and severe plastic deformation. HFL, the heat flux vector, indicates both the direction and magnitude of heat flow during AFSD, encompassing conduction, convection, and radiation. Understanding heat flux patterns is essential for optimizing process parameters and cooling strategies. The present work focused on the deposition of similar alloy layers onto a substrate of a similar alloy. The input parameters for these simulations included the elastic modulus of the alloys (GPa), specific heat (J/kg·K), shear translation (n), shear rotational (N·m), and heat source (W/m^3). These parameters were carefully selected to represent the key physical properties and process conditions influencing the AFSD process, as summarized in Table 2. The primary output parameters analyzed were the von Mises stress (MPa) and logarithmic strain

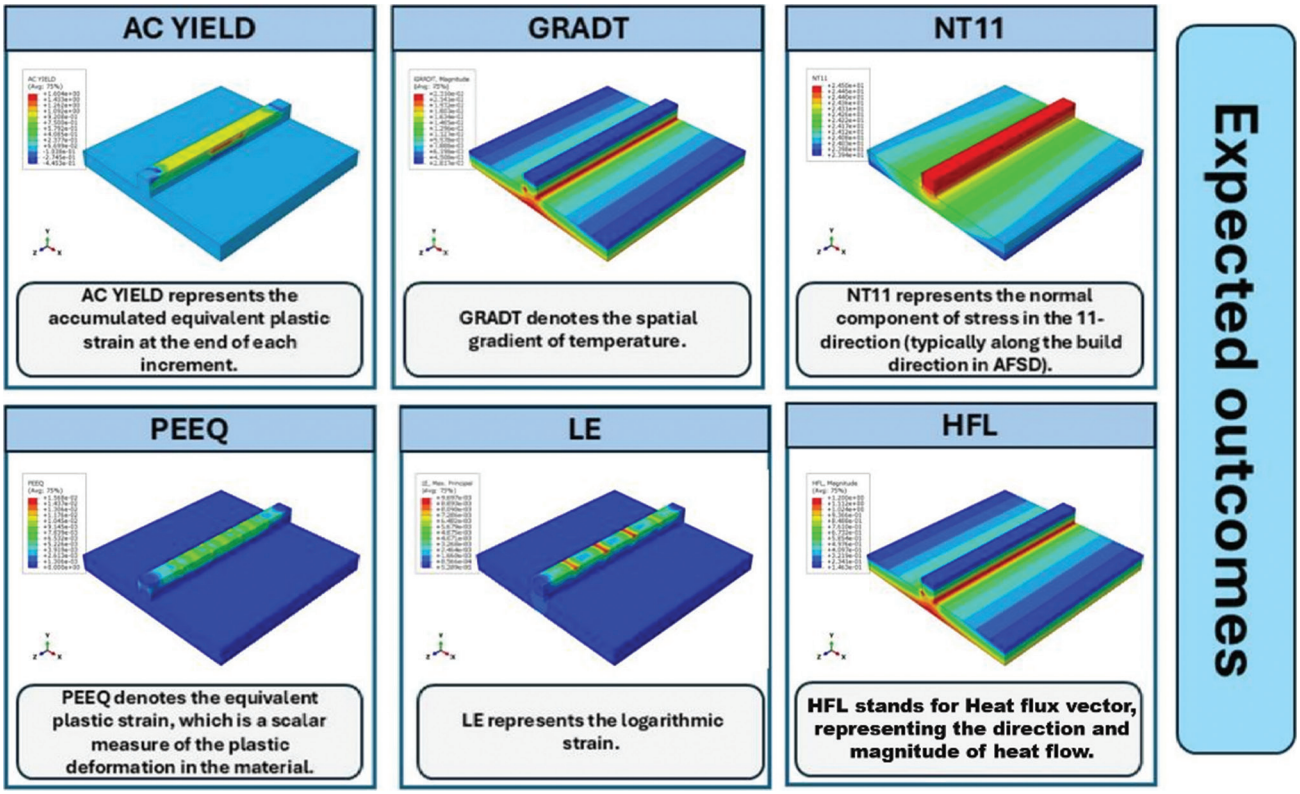

Figure 2. Visualization of predicted outcomes from the additive friction stir deposition numerical simulations, including accumulated equivalent plastic strain (AC YIELD), temperature gradient (GRADT), von Mises stress (NT11), and logarithmic strain (LE). These parameters are essential for assessing material properties and the overall performance of the deposited structures.

Table 2. Process parameters used in the present work

Elastic modulus (GPa)	Specific heat (J/kg·K)	Pressure (N)	Shear translation (N)	Shear rotation (N·m)	Heat source (W/m³)
73.1	0.875	50	10	10	500
73.1	0.875	75	20	20	700
73.1	0.875	100	30	30	800
73.1	0.875	125	40	40	900
73.1	0.875	150	50	50	1,000
73.1	0.875	175	60	60	1,100
68.9	0.896	50	10	10	500
68.9	0.896	75	20	20	700
68.9	0.896	100	30	30	800
68.9	0.896	125	40	40	900
68.9	0.896	150	50	50	1,000
71.7	0.96	50	10	10	500
71.7	0.96	75	20	20	700
71.7	0.96	100	30	30	800
71.7	0.96	125	40	40	900
71.7	0.96	150	50	50	1,000
71.7	0.96	175	60	60	1,100
71	0.9	50	10	10	500
71	0.9	75	20	20	700
71	0.9	100	30	30	800
71	0.9	125	40	40	900
71	0.9	50	10	10	500
71	0.9	75	20	20	700
71	0.9	100	30	30	800
71	0.9	125	40	40	900

(dimensionless), both of which are critical indicators of mechanical properties and performance of the deposited structures. From these simulations, a comprehensive dataset comprising 200 samples was generated, capturing a wide range of process conditions and material behaviors. This dataset was subsequently divided into training and testing subsets using an 80:20 split, with 160 samples allocated for training the ML models and 40 samples reserved for testing and validation. The coupled GA-ML models were evaluated using standard performance metrics, such as RMSE, MAE, and R^2 values.

3. Results and discussion

3.1. Numerical modeling of AFSD process

The element activation and deactivation technique is used in the numerical modeling of the AFSD process to simulate the sequential addition and removal of material. The method accurately captures the evolving geometry and thermal history of the deposited material. By activating specific regions in stages, the model closely simulates the real deposition process, guaranteeing that the growing structure and its thermal and mechanical properties are precisely represented. An essential component of this technique is the model change interaction, which enables the activation of new components corresponding to freshly deposited material and the deactivation of elements to represent removal or to disregard their influence at specified moments. This method is implemented within a coupled temperature–displacement analysis, allowing for the simultaneous assessment of thermal and structural behavior. The governing equations for this analysis include the heat transfer equation and the structural momentum balance, expressed in Equations 1 and 2, respectively:

$$\rho c_p . \frac{\partial T}{\partial t} = \nabla . \left(k \nabla T \right) + Q \quad \text{(I)}$$

$$\nabla . \sigma + f_b = \rho . \frac{\partial^2 u}{\partial t^2} \quad \text{(II)}$$

where ρ is density, c_p is the specific heat, T is the temperature, k is the thermal conductivity, Q is the internal heat generation per unit volume, σ is the stress tensor, f_b is the body force per unit volume, and is the displacement vector.

The simulation approach involves the incremental addition of material layers, controlled through element activation. Each simulation step corresponds to a distinct phase of the deposition process, during which specific components are activated. This sequential deposition enables the simulation to capture the thermal and mechanical changes, providing a realistic depiction of the AFSD process.

To account for thermal behavior, simulations of convection and radiation are incorporated to estimate heat transfer between the deposited material, the tool, and the surrounding environment. These heat transfer mechanisms influence cooling rates, temperature gradients, and potential distortions in the build. The applied loading conditions – including frictional heating, applied pressure, and both longitudinal and rotational shear forces – significantly impact material flow, interlayer bonding, and the final geometry of the deposited structure.

In the finite element formulation, the computational domain is discretized into smaller elements that can be selectively activated and deactivated to precisely model the material deposition process. The finite element equations are derived from the governing differential equations, and interpolation functions are used to estimate field

variables (e.g., temperature and displacement) within each element. An implicit temporal integration approach is widely employed to enhance numerical stability in coupled thermo-mechanical analyses. Accurate simulation also requires the application of adequate boundary and initial conditions.

The activation and deactivation of the elements are governed by the activation function A_c (t), which determines whether an element is active or inactive at a given time, as shown in Equation III:

$$A_c(t) = \begin{cases} 1 & \text{if element } e \text{ is active at time } t. \\ 0 & \text{if element } e \text{ is inactive at time } t. \end{cases} \quad \text{(III)}$$

The heat transfer equation for active elements is modified to incorporate the activation function and heat input from deposition, as given in Equation IV:

$$\rho c_p . \frac{\partial T}{\partial t} = \nabla . (k \nabla T) + Q + A_c(t) . H(t) \quad \text{(IV)}$$

where H (t) is the heat input modulated byA_c (t).

Similarly, the structural response for active elements is represented by Equation V:

$$\nabla . (\sigma . A_c(t)) + f_b = \rho . \frac{\partial^2 u}{\partial t^2} \quad \text{(V)}$$

The use of the element activation and deactivation technique in the numerical model enables accurate simulation of the dynamic nature of the AFSD process. This method provides valuable insights into the thermal and mechanical behavior of the deposited material, aiding in the prediction of material properties, the identification of possible flaws, and the assessment of overall structural performance (Figure 3). Additional simulation views and results for other alloy systems are provided in Supplementary File (Figure S1-S5 and Video S1).

3.2. Prediction of von Mises stress and logarithmic strain in additive friction stir deposited walled structures using GA-coupled ML algorithms

Von Mises stress and logarithmic strain are critical parameters in analyzing and optimizing the AFSD process. Von Mises stress is a widely used yield criterion that estimates the onset of yielding in materials under complex loading conditions. In AFSD, which involves severe plastic deformation, high strain rates, and elevated temperatures, evaluating von Mises stress is essential for determining whether the material will yield during deposition. This, in turn, is critical for maintaining strong interlayer bonding while avoiding material failure. In addition, von Mises stress offers information about material ductility and flow characteristics, which are key to achieving the

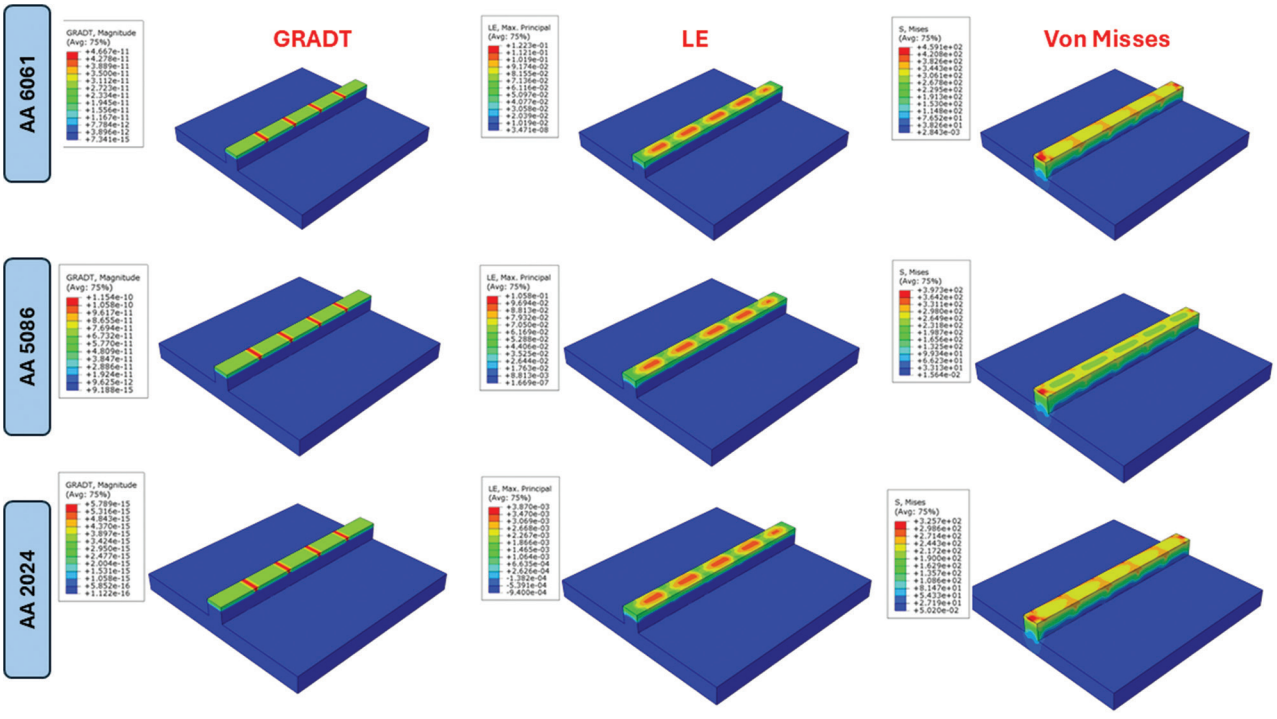

Figure 3. Thermal and mechanical responses of the alloys during the deposition process
Abbreviations: GRADT: Temperature gradient; LE: Logarithmic strain.

required bonding quality. By studying stress distributions, process parameters such as tool rotation speed, feed rate, and applied force can be optimized to ensure uniform deposition and minimize defects.

Logarithmic strain, also known as true strain, is equally important due to the large deformations involved in AFSD. Logarithmic strain offers a precise measure of material deformation, especially in scenarios involving extensive plastic deformation. Analyzing strain distribution helps identify regions experiencing high deformation, which is critical for ensuring the structural integrity of the deposited material. Understanding strain behavior also aids in characterizing the material response under high-strain and temperature conditions, which is essential for process optimization and achieving the desired material properties in the final structure.

Figure 4 presents contour plots illustrating the relationship between von Mises stress and the elastic modulus, in combination with other parameters such as specific heat, pressure, shear translation, shear rotation, and heat source. These plots demonstrate that higher elastic modulus values tend to result in higher stress levels, particularly when combined with elevated pressure and heat input. This implies that stiffer materials experience greater stresses under intense thermal and mechanical loading, highlighting the importance of balancing stiffness with other parameters to keep stresses within acceptable limits during deposition.

Figure 5 illustrates the influence of specific heat on the distribution of logarithmic strain, in combination with parameters such as pressure and heat source. The plots suggest that higher specific heat values tend to reduce stress accumulation. Materials with higher thermal capacity appear to distribute heat more uniformly, thereby resulting in lower peak stresses. This observation underscores the critical role of specific heat in thermal management during AFSD. Optimizing this parameter is essential for enhancing thermal stability and determining whether the material can withstand thermal stresses without failure.

In this study, reliable and efficient coupled algorithms were developed by combining decision tree (DT) regression and RF regression with GA optimization to predict von Mises stress and logarithmic strain in the AFSD process. The input parameters included elastic modulus, specific heat, shear translation, shear rotation, and heat source – all representing key physical and process characteristics of the alloys under consideration. By combining the predictive accuracy of DT and RF regressors with the optimization capabilities of GA, the proposed models demonstrated improved performance in predicting complex material behavior.

DT regression is a non-parametric, supervised learning technique used for regression tasks. It creates a tree where nodes represent input features (or attributes), branches define decision rules, and leaves represent the predicted outcomes. The goal is to develop a model that can predict the value of a target variable using a set of hierarchical, rule-based decisions derived from the input data. The key hyperparameters of a DT model include the maximum depth of the tree (d), the minimum number of samples required to split an internal node (s), and the minimum number of samples required to be at a leaf node (l).

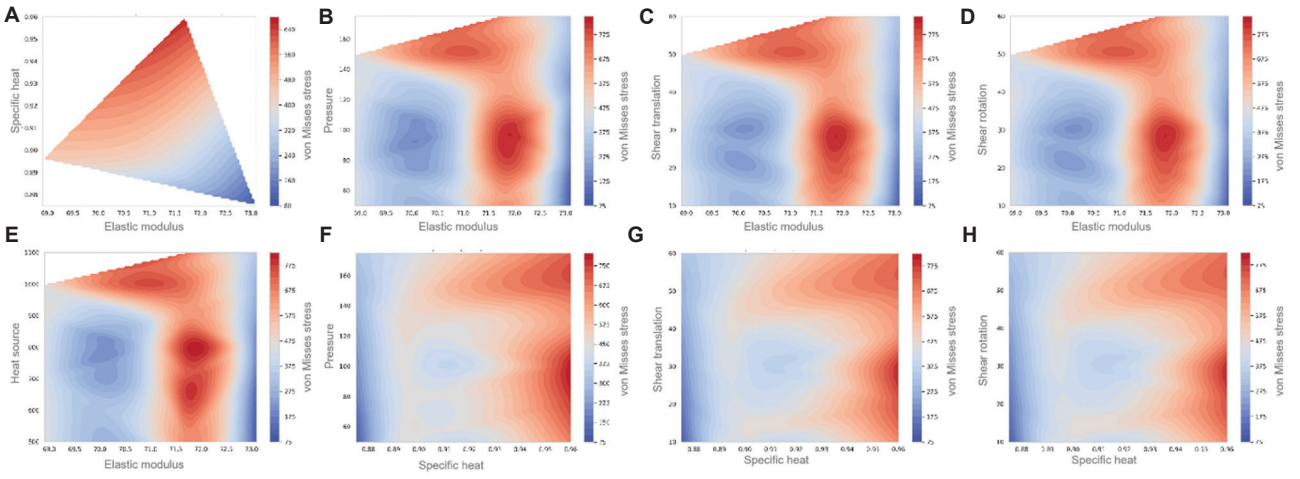

Figure 4. Contour plots of von Mises stress as a function of various parameter combinations: (A) elastic modulus and specific heat, (B) elastic modulus and pressure, (C) elastic modulus and shear translation, (D) elastic modulus and shear rotation, (E) elastic modulus and heat source, (F) pressure and specific heat, (G) shear translation and specific heat, and (H) shear rotation and specific heat. These plots illustrate how variations in elastic modulus, when paired with other parameters, influence von Mises stress and reveal sensitivity to specific combinations.

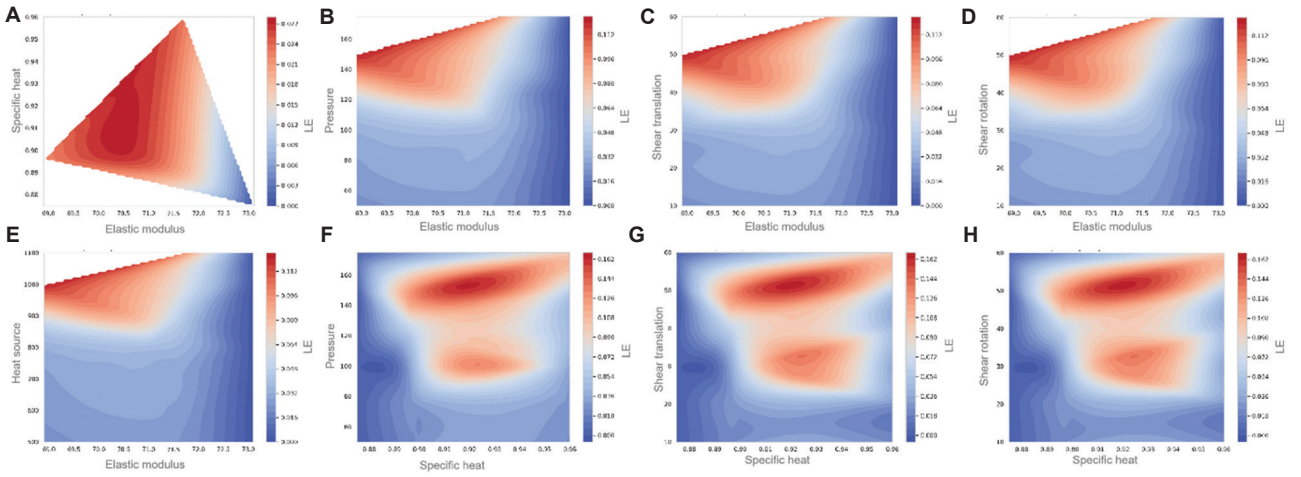

Figure 5. Contour plots of logarithmic strain (LE) as a function of various parameter combinations: (A) elastic modulus and specific heat, (B) elastic modulus and pressure, (C) elastic modulus and shear translation, (D) elastic modulus and shear rotation, and (E) elastic modulus and heat source (F) pressure and specific heat (G) shear translation and specific heat, and (H) shear rotation and specific heat. These visualizations emphasize how logarithmic strain depends on specific heat in conjunction with other process conditions, providing insights into thermal influences on material behavior during deposition.

RF regression extends the DT model by constructing an ensemble of DTs during training and calculating the average prediction of all trees. This method enhances predictive performance by reducing overfitting and improving generalization. Important hyperparameters for an RF model include the number of estimators (n), maximum depth (d), minimum sample split (s), and minimum sample leaf (l). The prediction of an RF model for an input is the average prediction from all the trees in the forest, as shown in Equation VI:

$$\hat{y} = \frac{1}{n}\sum_{i=1}^{n} h_i(X) \tag{VI}$$

where $h_i(X)$ is the prediction of the *i-th* tree.

In the GA, each individual in the population represents a set of model hyperparameters (Table 3). For a DT, an individual may be represented as (d,s,l), while for an RF, it may be (n,d,s,l). The fitness function evaluates the performance of the model with the given hyperparameters. The fitness functions for DT and RF models are defined in Equations VII and VIII, respectively:

$$Fitness(individual) = \frac{1}{MSE\left(y_{test}, h\left(X_{test}\right)\right)} \tag{VII}$$

$$Fitness\left(individual\right) = \frac{1}{MSE\left(y_{test}, \hat{y}\left(X_{test}\right)\right)} \tag{VIII}$$

In each generation, the GA selects individuals based on their fitness scores, performs crossover to generate offspring, and applies mutation to introduce variability. This iterative process continues for a predetermined number of generations or until convergence is achieved. The GA settings used in this study are summarized in Figures 6 and 7.

Table 3. Genetic algorithm parameters

Population size	Generations	Crossover probability	Mutation probability
50	200	0.8	0.1

Figure 6 shows the convergence curves of the GA-DT and GA-RF models for predicting von Mises stress. Both models demonstrate rapid improvement in the initial generations, with GA-RF achieving slightly better fitness in the later stages, suggesting superior predictive performance.

Figure 7 presents the convergence behavior for logarithmic strain prediction. Again, both GA-DT and GA-RF models demonstrate rapid initial improvement, but the convergence pattern is more erratic – particularly in the GA-RF model – indicating that predicting logarithmic strain is more challenging. This may be attributed to the greater sensitivity of strain to local variations in material properties and process parameters.

Tables 4 and 5 present the optimal hyperparameters obtained through GA optimization for the GA-DT and GA-RF models when predicting von Mises stress and logarithmic strain, respectively, in additive friction stir deposited aluminum-based walled structures. From

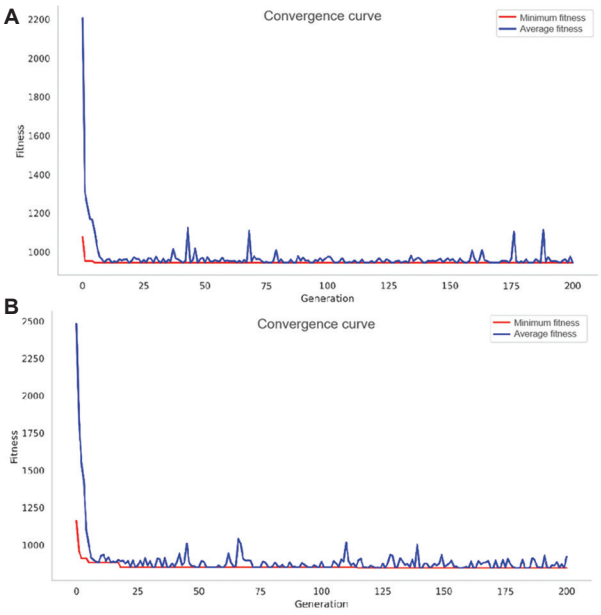

Figure 6. Convergence curves for GA-DT and GA-RF models in predicting von Mises stress in the additive friction stir deposition process. (A) GA-DT, (B) GA-RF. Both models show rapid improvement in initial generations, with GA-RF exhibiting slightly better convergence in later stages.
Abbreviations: GA-DT: Genetic algorithm-decision tree; GA-RF: Genetic algorithm-random forest.

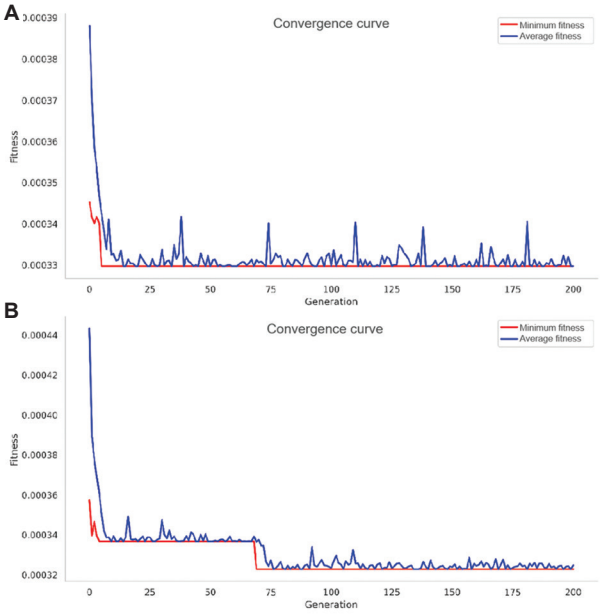

Figure 7. Convergence curves for GA-DT and GA-RF models in predicting logarithmic strain. (A) GA-DT, (B) GA-RF. The convergence process shows that predicting strain is more challenging, with erratic patterns in the GA-RF model compared to von Mises stress predictions.
Abbreviations: GA-DT: Genetic algorithm-decision tree; GA-RF: Genetic algorithm-random forest.

Table 4. Optimal hyperparameters for predicting von Mises stress in additive friction stir deposited aluminum-based walled structures

Algorithms	Best max depth	Best min samples split	Best min samples leaf	Best N estimators
GA-DT	10	2	1	-
GA-RF	5	3	1	93

Table 5. Optimal hyperparameters for predicting logarithmic strain in additive friction stir deposited aluminum-based walled structures

Algorithms	Best max depth	Best min samples split	Best min samples leaf	Best N estimators
GA-DT	5	2	1	-
GA-RF	11	2	1	23

Table 4, it is observed that the GA-DT model favors a deeper tree with a maximum depth of 10, while the GA-RF model uses shallower trees with a maximum depth of 5. This suggests that for von Mises stress, the DT benefits from more complex decision paths, while the RF achieves better results with simpler individual trees, leveraging the power of ensemble learning. Both models prefer a small minimum number of samples to split an internal node (2 for GA-DT, 3 for GA-RF) and the minimum possible number of samples at a leaf node (1 for both), indicating that fine-grained decision-making enhances model performance. The GA-RF model uses 93 estimators (trees), a relatively high number, implying that ensemble diversity significantly contributes to its predictive power for von Mises stress. Table 5 shows a reversed trend for tree depth in the context of logarithmic strain prediction: the GA-DT model uses shallower trees (depth of 5), while the GA-RF model uses deeper trees (depth of 11). This implies that logarithmic strain prediction benefits from different model architectures compared to von Mises stress prediction. Nevertheless, both models maintain a preference for a small minimum number of samples to split (2) and at leaf nodes (1), consistent with the von Mises stress prediction. Notably, the GA-RF model uses fewer estimators (23) for logarithmic strain prediction compared to von Mises stress, suggesting that fewer but more complex trees are more effective for this particular prediction task.

Tables 6 and 7, along with Figures 8 and 9, provide a comprehensive overview of the performance metrics for the GA-DT and GA-RF models in predicting von Mises stress and logarithmic strain, respectively, for AFSD aluminum-based walled structures.

For von Mises stress prediction, both models demonstrate excellent performance. The GA-RF model slightly outperforms GA-DT, achieving a lower RMSE (29.08 vs. 30.75), comparable MAE, and a higher R^2 value (0.9676 vs. 0.9638). This superior performance is visually confirmed in Figure 8, where both models exhibit a strong correlation between predicted and actual values. Notably, the GA-RF model (Figure 8B) displays slightly tighter clustering along the ideal prediction line compared to GA-DT (Figure 8A). In contrast, logarithmic strain prediction (Table 7 and Figure 9) shows lower overall performance for both models, although GA-RF again marginally outperforms GA-DT. Both models have identical RMSE values (0.017), with GA-DT showing a slightly lower MAE (0.010 vs. 0.011), while GA-RF achieves a marginally higher R^2 value (0.7201 vs. 0.7142). Figure 9 visually corroborates these results, showing more scattered predictions for both models compared to the von Mises stress, with GA-RF (Figure 9B) displaying a slightly better fit than GA-DT (Figure 9A).

The notable disparity in predictive performance between von Mises stress and logarithmic strain indicates that the latter is a more difficult quantity to forecast in the AFSD

Table 6. Performance metrics for predicting von Mises stress in additive friction stir deposited aluminum-based walled structures

Algorithms	RMSE	MAE	R^2 Value
GA-DT	30.75	22.75	0.9638
GA-RF	29.08	23.20	0.9676

Abbreviations: MAE: Mean absolute error; RMSE: Root mean square error.

Table 7. Performance metrics for predicting logarithmic strain in additive friction stir deposited aluminum-based walled structures

Algorithms	RMSE	MAE	R^2 Value
GA-DT	0.017	0.010	0.7142
GA-RF	0.017	0.011	0.7201

Abbreviations: MAE: Mean absolute error; RMSE: Root mean square error.

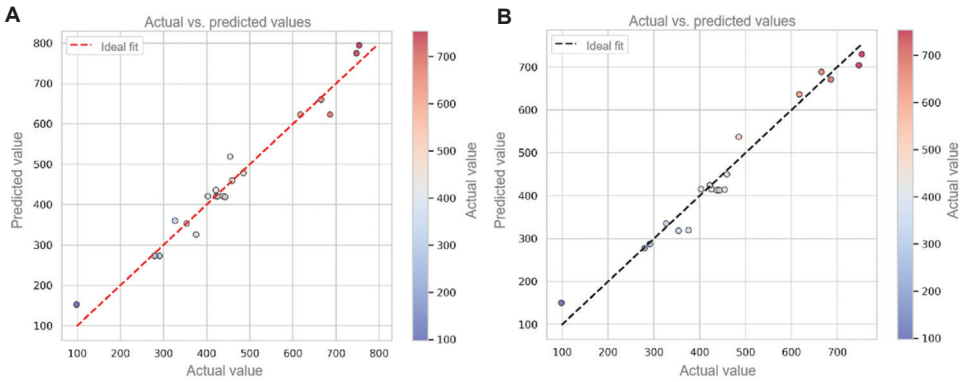

Figure 8. Actual versus predicted von Mises stress (MPa) for GA-DT and GA-RF models: (A) GA-DT and (B) GA-RF plots comparing actual versus predicted values. The GA-RF model demonstrates slightly higher accuracy, with predictions more closely clustered along the ideal prediction line.
Abbreviations: GA-DT: Genetic algorithm-decision tree; GA-RF: Genetic algorithm-random forest.

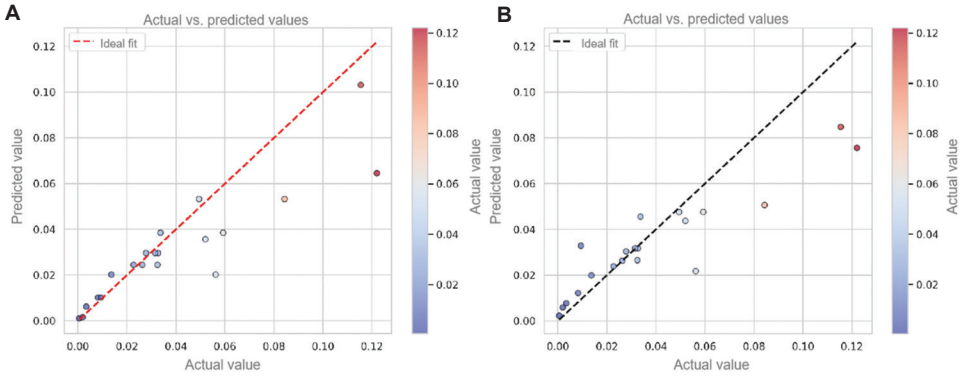

Figure 9. Actual versus predicted logarithmic strain for GA-DT and GA-RF models: (A) GA-DT and (B) GA-RF plots comparing actual versus predicted values. Both models show greater variability in prediction accuracy, with the GA-RF model achieving a marginally better fit.
Abbreviations: GA-DT: Genetic algorithm-decision tree; GA-RF: Genetic algorithm-random forest.

process. This may be due to logarithmic strain's heightened sensitivity to local fluctuations in material qualities or process parameters or to influences from factors not fully captured by the current set of input variables. Despite this, both GA-DT and GA-RF models demonstrate the ability to capture underlying patterns in the data, with GA-RF consistently outperforming GA-DT across both prediction tasks. These findings underscore the promise of ML techniques – particularly those optimized through GAs – for predicting complicated material behaviors in advanced manufacturing processes such as AFSD.

The proposed biomimetic ML approach effectively integrates finite element simulations with GA-optimized predictive models to estimate von Mises stress and logarithmic strain in AFSD aluminum alloy structures. This approach is consistent with previous studies, such as that conducted by Shi *et al.*[40], who developed AFSD-Nets to accurately predict temperature evolution during AFSD using physics-informed ML. Similarly, Qiao *et al.*[18] demonstrated the utility of ML techniques, such as RF models, in predicting the mechanical properties of AFSD-fabricated AA6061. Collectively, these findings support the viability of ML in enhancing process knowledge and optimization within solid-state additive manufacturing.

4. Conclusion

In this presented work, a biomimetic ML-based approach was developed for predicting two important mechanical properties – von Mises stress and logarithmic strain – in AFSD aluminum alloy-walled structures. The proposed method integrates finite element analysis with GA-optimized DT and RF models. This combined approach demonstrates strong predictive capability, with R^2 values of 0.9676 and 0.7201 for von Mises stress and logarithmic strain, respectively, utilizing the GA-RF model. These results indicate a high level of correlation within the simulated dataset; however, full experimental validation is needed to confirm the model's accuracy in real-world applications.

Future research will focus on validating the model against experimental data to strengthen confidence in its applicability. Expanding the model to encompass a broader range of alloy types and other relevant materials could further enhance its industrial utility. Incorporating real-time monitoring data during the AFSD process may improve predictive accuracy and facilitate adaptive control. In addition, the development of a user-friendly interface could accelerate adoption in industrial settings and contribute to transformative improvements in process optimization and quality control for the additive manufacturing of high-performance aluminum structures.

Acknowledgments

None.

Funding

None.

Conflict of interest

The author declares no competing interests.

Author contributions

This is a single-authored article.

Ethics approval and consent to participate

Not applicable.

Consent for publication

Not applicable.

Availability of data

The data will be provided to the readers upon reasonable request.

Further disclosure

The paper has been uploaded to or deposited in arXiv preprint server: https://arxiv.org/abs/2408.05237.

References

1. Yu HZ, Mishra RS. Additive friction stir deposition: A deformation processing route to metal additive manufacturing. *Mater Res Lett*. 2021;9(2):71-83.

   doi: 10.1080/21663831.2020.1847211

2. Patil SM, Sharma S, Joshi SS, Jin Y, Radhakrishnan M, Dahotre NB. Additive friction stir deposition of Al 6061-B4C composites: Process parameters, microstructure and property correlation. *Mater Sci Eng A*. 2024;910:146840.

   doi: 10.1016/j.msea.2024.146840

3. Korganci M, Bozkurt Y. Recent developments in additive friction stir deposition (AFSD). *J Mater Res Technol*. 2024;30:4572-4583.

   doi: 10.1016/j.jmrt.2024.04.179

4. Liu H, Xu M, Li X. Achievement of high-reliability and high-efficient deposit of PA66 by additive friction stir deposition. *Compos Part B Eng*. 2024;284:111682.

   doi: 10.1016/j.compositesb.2024.111682

5. Chen L, Lu L, Zhu L, *et al*. Microstructure evolution and mechanical properties of multilayer AA6061 alloy fabricated by additive friction stir deposition. *Metall Mater Trans A*. 2024;55(4):1049-1064.

doi: 10.1007/s11661-024-07303-0

6. Liu H, Liu Y, Liang T, *et al*. Effect of press depth on defect formation in friction-rolling additive manufacturing. *J Manuf Processes*. 2024;119:305-320.

   doi: 10.1016/j.jmapro.2024.03.097

7. Li X, Li X, Hu S, Liu Y, Ma D. Additive friction stir deposition: A review on processes, parameters, characteristics, and applications. *Int J Adv Manuf Technol*. 2024;133:1-18.

   doi: 10.1007/s00170-024-13890-4

8. Xu X, Qiu W, Wan D, Wu J, Zhao F, Xiong Y. Numerical modelling of the viscoelastic polymer melt flow in material extrusion additive manufacturing. *Virtual Phys Prototyp*. 2024;19(1):e2300666.

   doi: 10.1080/17452759.2023.2300666

9. Liu FC, Feng AH, Pei X, Hovanski Y, Mishra RS, Ma ZY. Friction stir based welding, processing, extrusion and additive manufacturing. *Prog Mater Sci*. 2024;146:101330.

   doi: 10.1016/j.pmatsci.2024.101330

10. Patel A, Taufik M. Extrusion-based technology in additive manufacturing: A comprehensive review. *Arab J Sci Eng*. 2024;49(2):1309-1342.

    doi: 10.1007/s13369-022-07539-1

11. Krishnanand, Singh V, Mittal V, Branwal AK, Sharma K, Taufik M. Extrusion strategies in fused deposition additive manufacturing: A review. *Proc Inst Mech Eng Part E J Process Mech Eng*. 2024;238(2):988-1012.

    doi: 10.1177/09544089221150709

12. Maurya M, Maurya A, Kumar S. Variants of friction stir based processes: Review on process fundamentals, material attributes and mechanical properties. *Mater Testing*. 2024;66(2):271-287.

    doi: 10.1515/mt-2023-0196

13. Gottwald RB, Gotawala N, Erb DJ, Hang ZY. An exploratory study on miniaturized additive friction stir deposition. *J Manuf Processes*. 2024;126:154-164.

    doi: 10.1016/j.jmapro.2024.07.076

14. Rao AG, Meena N. *Friction Stir Based Additive Manufacturing. Friction Stir Welding and Processing: Fundamentals to Advancements*. Hoboken: Wiley; 2024. p. 293-305.

15. Garcia D, Hartley WD, Rauch HA, *et al*. *In situ* investigation into temperature evolution and heat generation during additive friction stir deposition: A comparative study of Cu and Al-Mg-Si. *Addit Manuf*. 2020;34:101386.

    doi: 10.1016/j.addma.2020.101386

16. Stubblefield GG, Fraser K, Phillips BJ, Jordon JB, Allison PG. A meshfree computational framework for the numerical simulation of the solid-state additive manufacturing process, additive friction stir-deposition (AFS-D). *Mater Design*. 2021;202:109514.

    doi: 10.1016/j.matdes.2021.109514

17. Patil SM, Krishna KM, Sharma S, Joshi SS, Radhakrishnan M, Banerjee R, *et al*. Thermo-mechanical process variables driven microstructure evolution during additive friction stir deposition of IN625. *Addit Manuf*. 2024;80:103958.

    doi: 10.1016/j.addma.2024.103958

18. Sharifi A, Khodabakhshi F, Gerlich AP. Suppressing anisotropy in additive manufacturing by shear crystallographic texture development during multi-layer friction stir deposition. *Mater Sci Eng A*. 2024;903:146640.

    doi: 10.1016/j.msea.2024.146640

19. Agrawal P, Shiau CH, Sharma A, *et al*. Ion irradiation and examination of Additive friction stir deposited 316 stainless steel. *Mater Design*. 2024;238:112730.

    doi: 10.1016/j.matdes.2024.112730

20. Bagheri E, Zavari S, Adibi N, Ding H, Ghadimi H, Guo S. Additive friction stir deposition of al 7075 parts and the effect of heat treatment on microstructure, electroconductivity, and mechanical properties. *Int J Adv Manuf Technol*. 2024;135:763-774.

    doi: 10.1007/s00170-024-14582-9

21. Jin Y, Wang T, Liu T, *et al*. Gradient process parameter optimization in additive friction stir deposition of aluminum alloys. *Int J Mach Tools Manuf*. 2024;195:104113.

    doi: 10.1016/j.ijmachtools.2023.104113

22. Dong X, Zhou M, Geng Y, *et al*. Recent advances in additive friction stir deposition: A critical review. *Materials* (*Basel*). 2024;17(21):5205.

    doi: 10.3390/ma17215205

23. Zhang M, Jiang T, Feng X, *et al*. Investigation on *in-situ* tensile behaviors of 6061 aluminum alloy fabricated by wire additive friction stir deposition. *J Alloys Compds*. 2024;1008:176780.

    doi: 10.1016/j.jallcom.2024.176780

24. Sharma A, Jain R, Agrawal P, *et al*. Enhanced thermal stability in additive friction stir deposited ODS IN9052 Al alloy. *Acta Mater*. 2024;279:120284.

    doi: 10.1016/j.actamat.2024.120284

25. Pennington BK. *Frequency Response Modeling of Additive Friction Stir Deposition Parts with Print Defects* [Doctoral Dissertation, Virginia Tech]; 2024.

26. Merritt GR, Cousin CA, Yoon HS. Nonlinear temperature control of additive friction stir deposition evaluated on an echo state network. *J Dyn Syst Meas Control*. 2024;146(2):021004.

    doi: 10.1115/1.4064000

27. Wei J, He C, Dong R, Tian N, Qin G. Enhancing mechanical properties and defects elimination in 2024 aluminum alloy through interlayer friction stir processing in wire arc additive manufacturing. *Mater Sci Eng A*. 2024;901:146582.

doi: 10.1016/j.msea.2024.146582

28. Das A, Medhi T, Kapil S, Biswas P. Multi-track multi-layer friction stir additive manufacturing of AA6061-T6 alloy. *Prog Addit Manuf*. 2024;9(4):835-855.

doi: 10.1007/s40964-023-00485-w

29. Germano E, Walker J, Mills B, *et al*. Enhancing additive friction stir deposition through comprehensive ultrasonic defect detection and process optimisation. In: *UK and Ireland IEEE Ultrasonics, Ferroelectrics and Frequency Control Chapter*. Ireland: IEEE; 2024.

30. Wang H, Li Y, Zhang M, *et al*. Repairing the 7075 Al alloy plate by additive friction stir deposition with different feedstock rods. *Int J Adv Manuf Technol*. 2024;134(1):921-933.

doi: 10.1007/s00170-024-14186-3

31. Yakubov V, Ostergaard H, Bhagavath S, *et al*. Hardness Distribution and Defect Formation in Aluminium Alloys Fabricated Via Additive Friction Stir Deposition (AFSD). In 11th Australasian Congress on Applied Mechanics (ACAM2024). Brisbane: Engineers Australia; 2024. p. 244-251.

32. Kallien Z, Rath L, Roos A, Klusemann B. Application of friction surfacing for solid state additive manufacturing of cylindrical shell structures. *Addit Manuf Lett*. 2024;8:100184.

doi: 10.1016/j.addlet.2023.100184

33. Griffiths RJ, Garcia D, Hahn GD, Lua J, Phan N, Hang ZY. A non-melting additive approach to structural repair of aluminum aircraft fastener holes. *Addit Manuf Lett*. 2024;11:100249.

doi: 10.1016/j.addlet.2024.100249

34. Abbasi–Nahr M, Mirsalehi, SE. Additive friction stir deposition of AA5083/MoS2-diamond hybrid nanocomposites: Investigating their metallurgical, mechanical, tribological, and electrochemical characteristics, and process-structure-property relationships. *J Alloys Compd*. 2025;1013:178553.

doi: 10.1016/j.jallcom.2025.178553

35. Palya NI, Fraser K, Zhu N, *et al*. Microstructure prediction from smooth particle hydrodynamics process simulations of additive friction stir deposition. *Metall Mater Trans A*. 2024;55(9):3601-3616.

doi: 10.1007/s11661-024-07499-1

36. Modi U, Rai A, Ahmed S. Research prospects of friction stir additive manufacturing (FSAM). *AIP Conf Proc*. 2024;2960(1):030006.

doi: 10.1063/5.0183061

37. Rapaka R, Ladi H, Raja D, Muvvala G, Mukherjee T, Vicharapu B. Understanding in-process responses in multi-layer friction stir additive manufacturing: Temperature, viscosity, tool torque, and mechanical properties. *J Mater Process Technol*. 2024;330:118491.

doi: 10.1016/j.jmatprotec.2024.118491

38. Qiao Q, Liu Q, Pu J, *et al*. A comparative study of machine learning in predicting the mechanical properties of the deposited AA6061 alloys via additive friction stir deposition. *Mater Genome Eng Adv*. 2024;2(1):e31.

doi: 10.1002/mgea.31

39. Zhu Y, Wu X, Gotawala N, Higdon DM, Hang ZY. Thermal prediction of additive friction stir deposition through Bayesian learning-enabled explainable artificial intelligence. *J Manuf Syst*. 2024;72:1-15.

doi: 10.1016/j.jmsy.2023.10.015

40. Shi T, Wu J, Ma M, Charles E, Schmitz T. AFSD-Nets: A physics-informed machine learning model for predicting the temperature evolution during additive friction stir deposition. *J Manuf Sci Eng*. 2024;146(8):081003.

doi: 10.1115/1.4065178

ACCSCIENCE PUBLISHING

International Journal of AI for Materials and Design

ORIGINAL RESEARCH ARTICLE

Gesture recognition for engaging spatial experiences in healthcare: Co-design of intelligent interactive illuminative textiles

Ching Lee[1,2†], Jeanne Tan[1,2†*], Hiu Ting Tang[1,2†], Jun Jong Tan[2], Wing Ki Yip[1], and Ka Wing Tse[1,2]

[1]School of Fashion and Textiles, The Hong Kong Polytechnic University, Kowloon, Hong Kong Special Administrative Region, China

[2]Laboratory for Artificial Intelligence in Design, New Territories, Hong Kong Special Administrative Region, China

Abstract

The integration of artificial intelligence (AI) into textile design enhances functionality, automation, and user interaction. While gesture recognition has been explored in smart textiles, contactless interactive systems for healthcare remain underdeveloped. This study presents a human-centered co-design approach to the development of an AI-integrated gesture recognition system embedded in illuminative textile wall panels, aimed at enhancing spatial engagement in healthcare environments. The research was conducted in three key stages. First, a co-design workshop was conducted to explore user preferences in textile materials, graphic design, and gesture interaction. Second, intelligent illuminative textiles were developed by knitting polymeric optical fiber into base wool yarns to enable illumination. A camera was embedded and integrated with a computer vision-based deep learning model for detecting landmarks on the hands, shoulders, and head. The recognized gestures and body movements triggered specific pre-programmed color changes on the textile surface through edge-integrated light-emitting diodes. Finally, a prototype was fabricated and installed in a government-established District Health Centre in Hong Kong to support physical activity and rehabilitation for elderly users. Semi-structured interviews with stakeholders – including co-designers, users, and occupational therapists – were conducted to evaluate usability and inform design refinements. Stakeholders reported high levels of satisfaction, emphasizing the system's ability to enhance community connection, therapeutic engagement, intuitive usability, and compelling visual feedback. These findings suggest that AI-driven interactive textiles present promising opportunities for rehabilitation, therapeutic environments, and the promotion of elderly well-being.

Keywords: Interactive textiles; Illuminative textiles; Gesture recognition; Human-artificial intelligence interaction; Deep learning; Healthcare

[†]*These authors contributed equally to this work.*

***Corresponding author:**
Jeanne Tan
(jeanne.tan@polyu.edu.hk)

Citation: Lee C, Tan J, Tang HT, Tan JJ, Yip WK, Tse KW. Gesture recognition for engaging spatial experiences in healthcare: Co-design of intelligent interactive illuminative textiles. *Int J AI Mater Design*. 2025;2(3):45-63. doi: 10.36922/IJAMD025170013

Received: April 22, 2025

Revised: June 12, 2025

Accepted: June 24, 2025

Published online: July 10, 2025

1. Introduction

Artificial intelligence (AI) has significantly influenced modern textile design by promoting "smart fabrics" that adapt to external stimuli and enhance user experiences

across domains, such as fashion, sports, and healthcare.[1-4] These AI-driven textiles leverage innovations ranging from bio-signal monitoring and electronic components to contactless control, transforming conventional fabrics into dynamic, interactive platforms.[5] The growth of AI in textile applications is evident in examples, such as temperature-sensitive materials and motion-sensing garments, demonstrating real-time responsiveness in athletic training, safety gear, and medical diagnostics.[5-9] In the area of gesture recognition, most AI-powered textiles rely on wearable sensors (e.g., data gloves) to capture finger and hand movements for sign language translation or rehabilitation exercises.[5] However, limitations remain in fully contactless systems, as many solutions still depend on user touch or close-range sensing, underscoring a gap for more accessible, "touch-free" interfaces in healthcare.[5] As healthcare increasingly shifts toward unobtrusive tools for assisting seniors and individuals with mobility constraints, AI-integrated textiles can offer intuitive, hands-free interaction – an approach further explored in the next section on user-centered co-design. By seamlessly embedding computer vision and deep learning in interior textiles, researchers aim to expand usability from wearable contexts into rehabilitative, clinical, and everyday healthcare settings, thereby enhancing both patient engagement and therapeutic outcomes.[4,10] Proposing innovative healthcare solutions for the elderly is increasingly important, and the integration of AI offers significant potential to enhance well-being through personalized, responsive, and engaging interventions.

As global demographics shift toward an increasingly aging population, healthcare systems worldwide face unprecedented challenges in providing quality elderly care. The World Health Organization projects that by 2030, one in six individuals globally will be aged 60 or older, significantly straining healthcare infrastructure and resources.[11,12] This demographic shift demands transformative changes in elderly healthcare delivery, especially in densely populated urban areas where healthcare facilities already operate at capacity.[13] Older adults typically require up to 4 times more healthcare resources than younger adults due to the prevalence of chronic conditions, such as cardiovascular diseases, diabetes, and dementia, further amplifying pressures on healthcare systems.[13,14] In Asia, countries or regions such as Hong Kong, China, South Korea, and Japan are particularly impacted, with elderly populations projected to surpass 37% by 2050.[15] Specifically, Hong Kong is projected to have 40.6%, South Korea 39.4%, and Japan 37.5% of their populations aged 65 or older by 2050,[16,17] intensifying shortages of specialized healthcare professionals and highlighting the critical urgency for innovative healthcare solutions.[18] In Hong Kong specifically, the elderly population is expected to reach 26% by 2026, further exacerbating demands on local healthcare facilities.[19-21] Responding strategically, the Hong Kong government initiated the establishment of District Health Centres (DHCs) in 2019, aiming to enhance primary healthcare accessibility and effectiveness. By 2023, these centers expanded into comprehensive community-based networks, serving approximately 205,600 (provisional figures as of December 31, 2023) elderly residents.[22] The Wong Tai Sin DHC (WTSDHC), for example, exemplifies this approach by offering specialized services, such as health risk assessments, chronic disease management, and targeted rehabilitation programs delivered through multidisciplinary healthcare teams.[23]

Technological advancements globally illustrate how AI and digital innovations can significantly enhance healthcare efficiency and patient outcomes. International examples include Singapore's widespread adoption of AI initiatives, such as the SELENA+ system, AimSG, and ACE. Other examples include AI in community hospitals and Japan's Cancer Institute Hospital, where AI analyzes extensive clinical datasets annually.[24-27] In contrast, Hong Kong is still in its early stages of AI technology development. Hong Kong's DHCs currently utilize relatively basic technological tools, such as digital health records and standard health screening devices, reflecting limited AI integration.[28,29] Despite the evident potential and global trend toward AI-driven healthcare solutions, adoption remains limited among elderly populations in Hong Kong. Often attributed to technophobia or the grey digital divide, seniors' reluctance toward new technologies commonly stems from internalized ageism – self-imposed beliefs about their inability to learn or master digital tools. However, Köttl *et al.*[30] also highlight that many older adults genuinely desire to learn and can excel in technology use when provided with suitable support and accessible interfaces. Interactive textiles, as intuitive, tactile, and user-friendly platforms, present a valuable starting point for elderly individuals to engage with AI and other emerging technologies. By providing an accessible and reassuring interface, smart textiles offer older users an empowering opportunity to demonstrate their capacity to adopt, learn, and benefit from advanced technological solutions, ultimately bridging the existing digital divide and facilitating wider acceptance of AI-enhanced healthcare interventions.[31-33]

This study proposes an AI-driven gesture recognition textile-based system, developed through a co-design approach, to create interactive illuminative wall panels that integrate smart textiles and user-centered design principles for healthcare applications. As outlined in

Figure 1A, the research followed a structured process comprising three main stages: (i) a workshop (co-design session A) was conducted with the staff and elderly members in WTSDHC to explore preferences in soft textile materials, visually engaging and memorable imagery, and gesture-based interactions aimed at enhancing user engagement, (ii) development of intelligent textiles using knitted polymeric optical fiber (POF), integrated with a microcomputer running a deep learning-based model for real-time hand, shoulder, and head landmark detection, and (iii) prototype fabrication and installation at the WTSDHC, where semi-structured interviews (co-design session B and C) with stakeholders, including co-designers, users, and occupational therapists (OT), were conducted to assess overall satisfaction and gather feedback for system improvement. Figure 1B illustrates the workflow of the textile-based gesture and posture recognition system, from real-time gesture capture to visual output on the fabric's surface. The process begins with a user standing in front of the textile panel, where a

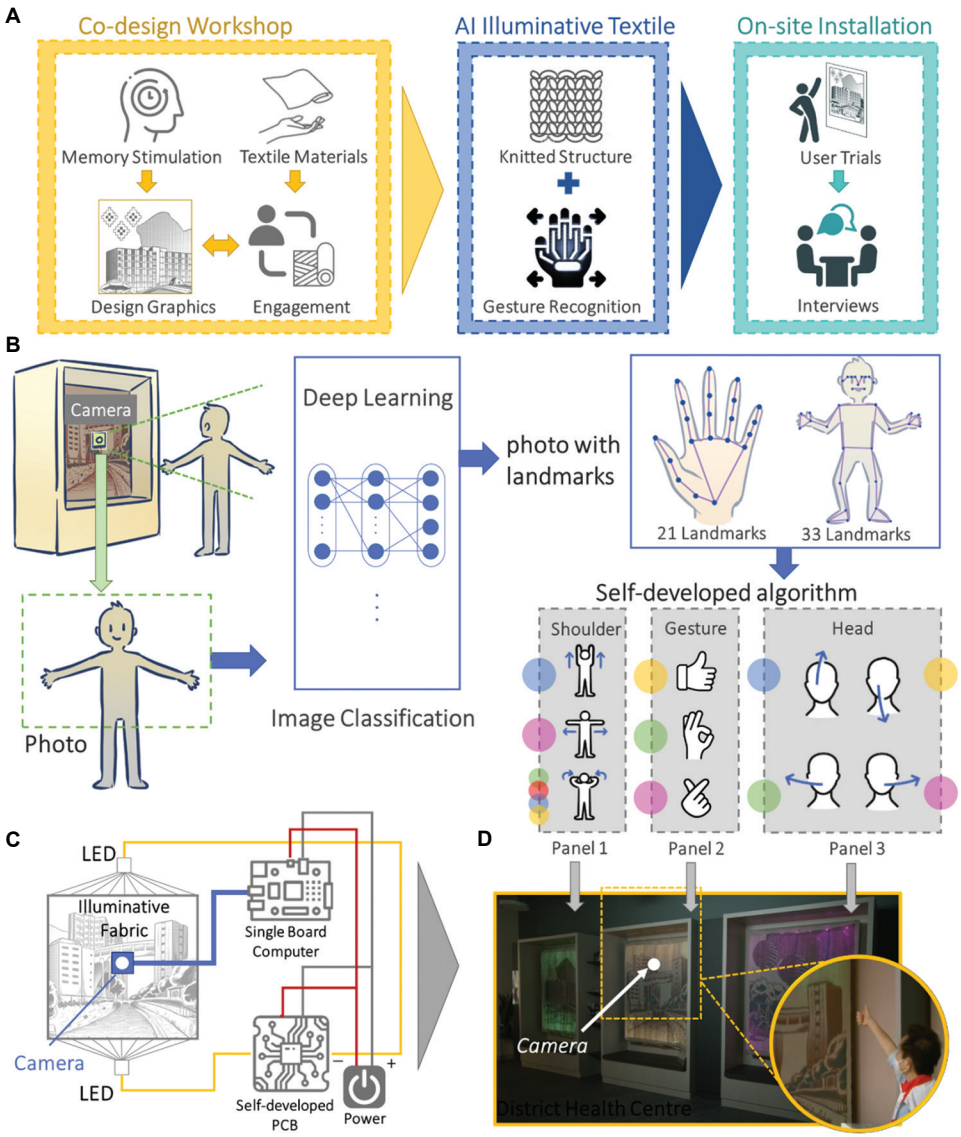

Figure 1. Overview of the co-design development process and artificial intelligence-based gesture recognition system for the interactive illuminative textile. (A) Structured research process, including a co-design workshop, intelligent textile development, and system deployment. (B) Computer vision-based deep learning model for gesture and posture recognition through landmark detection on hands, shoulders, and head. (C) Integration of polymeric optical fibers, edge-connected light-emitting diodes, camera, power supply, single-board computer, and custom printed circuit board to enable real-time color feedback on textile surfaces. (D) Installed prototype of three interactive textile wall panels at Wong Tai Sin District Health Centre, designed to enhance elderly engagement and spatial interaction.

camera captures a live image (photo) without storing it in memory. This image is passed to a deep learning model for image classification, which detects 21 hand landmarks or 33 body landmarks, depending on the type of input (e.g., hand gesture or full-body posture). The output of the deep learning model is a photo annotated with landmark points in (x, y) coordinate format. These landmarks are then processed by a self-developed algorithm, which interprets the spatial relationships between the landmarks to classify the user's physical position or gesture. Different gestures and body positions triggered distinct color responses on the surface of the illuminative fabric. These colors were activated through light-emitting diodes (LEDs) connected to the textile's edges, which were optically linked through the integrated POFs (Figure 1C). A camera was embedded within the textile system, and a single-board computer and a custom-designed printed circuit board (PCB) were connected to support real-time interaction. Figure 1D shows the installed prototype, consisting of three illuminative fabric wall panels in WTSDHC, designed to enhance engagement and promote well-being among elderly users.

2. Literature review

This research focused on achieving a user-centered design for intelligent interactive illuminative textiles to enhance spatial experiences through gesture recognition. The study was reviewed from three key aspects: (i) the co-design process, (ii) the design and development of interactive illuminative textiles, and (iii) the application of AI technology in gesture recognition. Finally, the research identified existing gaps in the literature.

2.1. Co-design

Design thinking is commonly applied within co-design processes, facilitating collaboration through structured, iterative methods. Popularized by IDEO and Stanford University's Hasso Plattner Institute of Design (also known as the Stanford d.school), design thinking integrates human needs, technological possibilities, and business viability through empathizing, defining, ideating, prototyping, and testing phases.[34] Specifically, when applied to designing solutions for older adults, design thinking bridges potential gaps between designers' assumptions and the actual needs and preferences of elderly users.[35] Co-design, representing the collective creativity of designers and non-designers collaborating in the development process, has become essential in creating user-centered solutions. This approach harnesses diverse expertise, benefiting from interdisciplinary contributions, which can lead to innovative and contextually appropriate designs.[36] For instance, Sanders and Stappers[35] highlight how co-design facilitates a richer understanding of user requirements and fosters a sense of ownership among end-users, ultimately leading to higher adoption rates and user satisfaction.[35] While co-design and design thinking often share overlapping tools and values – such as empathy, iteration, and participation – design thinking typically provides the structured methodology, whereas co-design emphasizes deeper user involvement as co-creators throughout the process. Distinguishing between them helps to clarify the specific roles of facilitated creativity and participatory engagement in the project context.

Experience-based co-design (EBCD) specifically applies co-design principles within healthcare service improvement contexts, systematically capturing and utilizing the lived experiences of service users and providers to enhance service quality.[37] For example, studies have shown EBCD's effectiveness in improving elderly care services by deeply engaging elderly individuals and caregivers in the design process, thereby ensuring solutions resonate with users' personal experiences and emotional needs.[38] Actively involving older adults through co-design processes, such as EBCD has demonstrated notable benefits, including improved service outcomes, increased user empowerment, and enhanced social connectedness.[39] Human-centered design further emphasizes placing human needs, capabilities, and behaviors at the forefront, making systems usable, accessible, and effective through ergonomic and usability principles.[40]

In designing for elderly users, methodologies, such as co-design, EBCD, and human-centered design are especially valuable, particularly when addressing cognitive or emotional connections to personal history and memory.[41] Research indicates that reminiscence therapy, commonly employed in dementia care and elderly mental health interventions, effectively utilizes personal memories and past experiences to improve psychological well-being and social engagement among elderly individuals.[42] Integrating reminiscence therapy principles within co-design methodologies has shown potential in creating solutions that significantly enhance elderly users' emotional health, autonomy, and dignity by actively involving them in crafting personalized and meaningful interventions.[43]

2.2. Interactive illuminative textiles

Interactive textiles, also known as e-textiles, are textiles designed to dynamically respond to external stimuli or user interactions through integrated electronic components and embedded technologies.[44-48] Illuminative interactive textiles specifically utilize lighting elements, such as POFs, to offer visual feedback and facilitate sensory stimulation.[49-52] POF textiles integrate flexible

polymer-based fibers, such as polymethyl methacrylate, into fabric structures to enable uniform side illumination. Light is transmitted through the fiber and emitted laterally through engineered surface modifications, allowing flexible, efficient, and interactive lighting within textiles.[53] Tan *et al.*[54] designed a gesture-controlled illuminated textile utilizing computer vision to recognize mid-air hand gestures, triggering corresponding color changes in the fabric. Prior research has primarily examined woven illuminative textiles designed for creating engaging sensory environments. However, recent innovations have begun exploring knitted textiles. Lam *et al.*,[55] investigated various knitted structures to optimize the illuminative effects of POFs, demonstrating the feasibility of integrating such technologies into wearable and interior applications, favored for their superior flexibility and user comfort, thereby enhancing interaction potential and application versatility, particularly in healthcare environments.[55,56] Data presented at the Hong Kong Geriatrics Society Annual Scientific Meeting showed that the use of knitted illuminative textiles, in the form of touch-and-proximity responsive cushions, substantially improved engagement in individuals with dementia.[57] Notably, 90% of participants with late-stage dementia demonstrated active participation during sensory interventions, and all participants (100%) reported positive experiences, providing strong empirical support for prior anecdotal observations. These findings affirm the potential effectiveness of interactive illuminative textiles in supporting elderly sensory therapies.

Nevertheless, a notable research gap persists regarding the comprehensive integration of advanced AI capabilities into knitted textile systems for wider healthcare applications. To address this gap, future research could emphasize AI integration to enhance user interactions and usability, especially among elderly populations who may experience reluctance due to perceptions of complexity or internalized ageism. Continued collaborative co-design efforts involving multidisciplinary teams and end-user participation are critical to developing solutions that closely align with user needs and enhance overall acceptance and effectiveness in healthcare applications.

2.3. Gesture recognition

Recent developments in smart textile research have opened new possibilities for gesture recognition interfaces within healthcare. By embedding sensor networks or computer-vision modules directly into fabrics, researchers aim to create seamless, intuitive systems that detect hand and finger movements with minimal user discomfort.[5] Early studies typically integrated wearable sensors – such as stretchable gloves or multiple inertial measurement units – for real-time motion capture[58,59]; however, the field still recognizes the potential of more ambient or contactless gesture solutions, particularly in clinical contexts.[10] A key impetus for pursuing AI-based gesture recognition in textiles is its potential application in rehabilitation and elderly care. With aging populations growing globally, there is an urgent need for unobtrusive monitoring technologies and interactive support for seniors.[60,61] Traditional camera-based systems may achieve high accuracy in controlled environments, but often face issues related to occlusion, lighting conditions, and perceived intrusiveness among older adults.[62] Consequently, intelligent textiles – integrated with conductive yarns, POFs, or advanced "smart glove" sensors – offer more user-friendly alternatives, minimizing external hardware and seamlessly blending into healthcare environments.[4]

2.3.1. Wearable and contactless frameworks

Early gesture-recognition textiles frequently relied on wearable forms, such as sensor-equipped gloves, to track finger angles or subtle hand movements.[10,61] These gloves typically embed pressure sensors or strain gauges in conductive yarns along finger segments, capturing real-time flexion–extension data. Complementary approaches integrate surface electromyography (sEMG) signals or multiple inertial measurement units to enhance motion capture accuracy, especially for dynamic tasks, such as stroke rehabilitation. Such gloves excel in precision and support personalized rehabilitation by offering biofeedback on gesture performance. However, some older patients or those with physical constraints may find gloves cumbersome or difficult to put on and remove daily, thus limiting practical adoption.

Recent studies acknowledge the potential of "contactless" gesture detection textiles, where embedded optical or capacitive sensors track mid-air hand movements. Tan *et al.*[54] propose an illuminative textile system using computer vision to detect mid-air number gestures without direct physical contact. This approach points toward fabric-based "wall panels" or "ambient curtains" capable of sensing gestures in healthcare environments where cleanliness and infection control are paramount. In addition, contactless designs can enhance accessibility for patients with limited dexterity or object-avoidance requirements.

2.3.2. AI and machine learning integration

Gesture recognition systems commonly integrate multiple stages: data collection from sensors or vision modules, preprocessing for noise reduction and feature extraction, classification using machine learning models, and real-time feedback or database storage. Databases containing gesture data – either from annotated video streams or sensor readings – are vital for training robust AI models.

Alternative gesture-tracking models comparable to popular hand landmark solutions include OpenPose, Leap Motion, and other proprietary landmark detection frameworks that similarly leverage neural networks for real-time gesture tracking.[63,64]

Raw data from e-textiles, such as pressure signals, optical signals, or electromyography, benefit from robust classification algorithms capable of interpreting complex spatiotemporal patterns.[5,59] Neural architectures, such as convolutional neural networks or attention-based transformers, interpret subtle gesture variations and adapt to user-specific differences. Guo *et al*.,[61] demonstrated that a one-dimensional convolutional neural network trained on sEMG signals could classify 10 distinct hand poses relevant to stroke therapy, achieving accuracy exceeding 90%. Such data-driven modeling is critical for real-time feedback, flagging suboptimal movements or guiding corrective steps during rehabilitation. Nevertheless, deep learning's power consumption and computational overhead pose challenges for embedded textile platforms with limited battery or hardware resources.[5] Researchers are thus exploring lightweight or optimized neural models deployable on microcontrollers. Edge computing can minimize reliance on cloud connectivity, which is advantageous for remote or resource-limited clinical environments.[60] Prototypes also employ data fusion techniques, combining optical gesture tracking with sEMG signals, refining gesture accuracy without significantly increasing hardware complexity.[61]

2.3.3. Healthcare applications and user acceptance

Gesture-driven textiles hold substantial promise in healthcare, including telemedicine, physical therapy, and elderly care.[54,62] A textile-based gesture interface could enable older adults to call for help using simple hand signs rather than navigating small buttons. In stroke recovery, interactive textiles or gloves could monitor progress during range-of-motion exercises, providing real-time feedback and gamified incentives. Practical deployment, however, demands attention to usability, washability, and robustness.[5,6] E-textiles integrated into hospital curtains or seat covers must withstand repeated cleaning cycles, and wearable gloves must maintain accurate sensor functions despite mechanical stresses.

User acceptance among older adults remains critical. Oudah *et al*.,[62] noted seniors' skepticism toward unfamiliar technologies as a potential barrier to adoption. Co-design strategies involving healthcare staff, caregivers, and older patients can yield intuitive gestures and esthetically pleasing fabrics. Studies like Tan *et al*.[54] emphasize visual feedback – illuminative textiles can confirm correct gesture detection by changing color or brightness, enhancing user confidence.[54] Future research could further explore these user-centered design approaches to ensure gesture recognition technologies feel neither intrusive nor burdensome.

3. Methodology

3.1. Interviews

This research adopted a multi-phase participatory design approach over a 37-month period. The study commenced with a workshop (co-design session A; December 22, 2021) at SKH Calvary Church in Wong Tin Sin, establishing the foundation for community-driven design principles. Subsequent semi-structured interviews (co-design session B) with the research lead and the OT lead (February 7, 2023) at the Core Centre at WTSDHC provided institutional perspectives on implementation requirements and healthcare objectives. User experience evaluation (co-design session C) was conducted through structured interviews with co-designers and end-users (March 25, 2024) at the same place. The study received ethical approval from the Institutional Review Board at the authors' affiliated university. All participants provided informed consent before the commencement of the interviews.

This methodological sequence allowed for iterative development while maintaining alignment with both community needs and healthcare requirements. The technical development phase implemented these insights through a gesture recognition illuminative knitted textile system, comprising three interactive interfaces. Each interface was developed using specific interaction modalities: hand gesture recognition, shoulder movement detection, and head movement recognition, with corresponding visual feedback mechanisms. The final evaluation phase employed qualitative user feedback, enabling systematic refinement of the system's technical parameters while maintaining therapeutic efficacy and user engagement objectives.

3.1.1. Co-design workshop

This study adopted a systematic participatory action research framework, comprising three distinct yet interconnected phases. The initial phase employed a participatory design methodology to engage members of the WTSDHC in a 3-h co-design workshop (co-design session A). A total of 11 participants, including five staff members and OTs and six center members, took part in the session. The workshop was divided into two parts. The first part consisted of a presentation introducing the concept and applications of intelligent illuminative textiles, aiming to provide participants with foundational

knowledge (Figure 2A). The second part focused on collecting participants' opinions regarding the design and development of an AI-enhanced, textile-based gesture recognition system tailored for use at WTSDHC. Structured activities and semi-structured discussions were utilized to elicit feedback on contextual needs, design esthetics, and relevant local cultural elements. This approach aimed to ensure that both user preferences and community values were reflected in the design process. A semi-structured interview guide was used during the co-design workshop

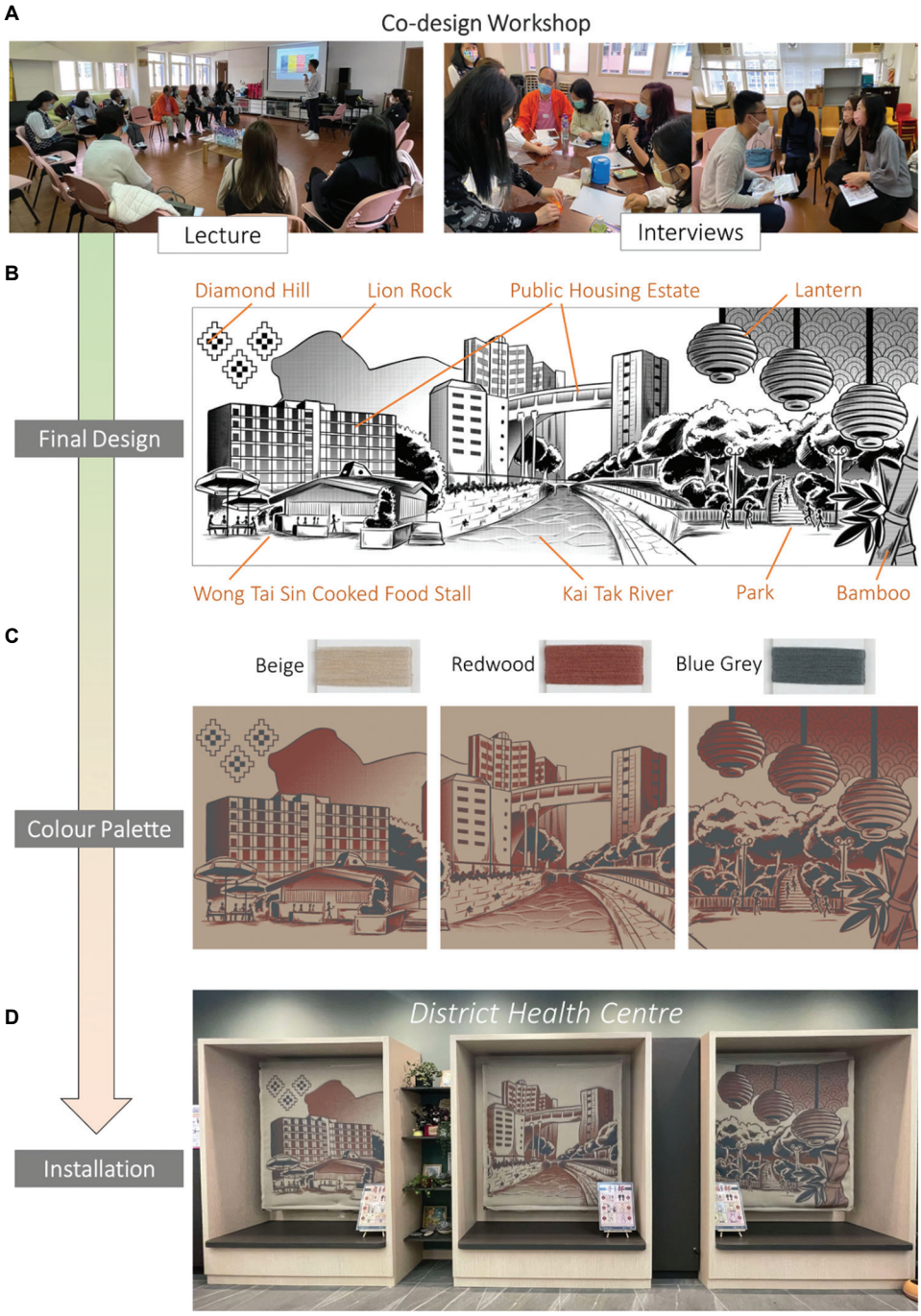

Figure 2. Co-design process. Photos from the co-design workshop showing (A) the lecture session and (B) interviews and group discussions. (C) Final illustration and design of the wall panels featuring several landmarks from the Wong Tai Sin district. (D) Color palette selected by co-designers for fabric development. (E) Installed wall panels in the Wong Tai Sin District Health Centre.

discussions, focusing on two main areas: (i) participants' background and experience with the social center, and (ii) their preferences regarding textile design. The first section explored general usage and engagement with the center through the following questions:

(i) Question 1: Have you visited a similar social center before?
(ii) Question 2: Approximately how long do you usually stay at the center during each visit?
(iii) Question 3: How frequently do you attend the center?
(iv) Question 4: Do you usually visit the center alone?
(v) Question 5: What activities are typically available to you?
(vi) Question 6: Which activities do you enjoy the most?
(vii) Question 7: Which activities do you think could be improved?
(viii) Question 8: What is your primary reason for visiting the center?
(ix) Question 9: Outside of the center, where do you usually spend your time, and what are your hobbies?

The second section addressed textile and design preferences:

(i) Question 1: What are your impressions of the sample illuminative textiles?
(ii) Question 2: Are you familiar with the concept of a sensory wall?
(iii) Question 3: Do you have suggestions for the design of the wall panels – for example, preferred themes, colors, or functional features?

3.1.2. Stakeholders' interviews after on-site installation

A systematic evaluation of the installation's efficacy was conducted through two methodologically distinct phases: expert interviews with the research lead and the OT lead (co-design session B) on February 7, 2023, followed by interviews with two co-designers and two end-user representatives (co-design session C) on March 25, 2024. This multi-phase assessment provided meaningful insights into the long-term impact of implementing co-designed, workshop-derived principles within a healthcare setting.

The expert interviews consisted of a series of structured questions aimed at understanding both conceptual foundations and practical applications of the intelligent textile system. Questions for the research lead included:

(i) Question 1: Could you share the background of this research study?
(ii) Question 2: Why do we need to use multisensory stimulation tools to treat or respond to this problem?
(iii) Question 3: What is the innovation or novelty of using intelligent textiles as a multisensory tool?
(iv) Question 4: Why is it important for the system to be contactless?
(v) Question 5: What is special about the fact that textile is soft or tactile, and how could that benefit this purpose?
(vi) Question 6: For this project with the WTSDHC, can you share the background – how did the collaboration come about?
(vii) Question 7: How much room is there for future improvement of this product or innovation?
(viii) Question 8: Can you describe the co-design process involved in developing these wall panels?

Questions for the OT lead focused on therapeutic impact, rehabilitation value, and real-world application. These included:

(i) Question 1: How have the intelligent textiles contributed to the multisensory experiences of users in your center?
(ii) Question 2: Is it important for visitors at your center to move around?
(iii) Question 3: Do you think the changing colors and AI-driven interactions on the wall provide an effective way to stimulate or engage users?
(iv) Question 4: What are the main benefits of using this new material in a rehabilitation context?
(v) Question 5: Why do you believe this AI textile system is unique?
(vi) Question 6: From your observation, how has this design engaged users?
(vii) Question 7: In your opinion, is there a need for intelligent materials in rehabilitation practices?
(viii) Question 8: Can you describe the effects of the AI wall and the benefits it has brought to your center?

Interviews with co-designers and end-users focused on their personal engagement in the co-design process and their perceptions of usability, esthetics, and experiential value after installation. Questions for the co-designers included:

(i) Question 1: How did participating in the co-design process make you feel?
(ii) Question 2: What are your thoughts on the final design, particularly considering it incorporates features inspired by the Wong Tai Sin District?
(iii) Question 3: How do you feel about seeing your ideas manifest in the design of the illuminative panels?
(iv) Question 4: What is your impression of the installed panels in the health center, particularly regarding texture and color change?
(v) Question 5: What do you think about the gestures selected for the gesture recognition technology integrated into the panels?

(vi) Question 6: How do you feel about the customized gesture design aligning with the center's slogan?
(vii) Question 7: In what ways did you feel engaged or connected to the community through the co-design process?
(viii) Question 8: Do you believe the panels will be adopted widely? Do you think elderly users will enjoy and regularly engage with them?
(ix) Question 9: Overall, how has participating in the co-design process influenced your sense of belonging to the center and the broader community?

Questions for the end-users focused on interaction experience, intuitiveness, comfort, and social aspects of engagement with the panels and included:

(i) Question 1: How was your overall experience interacting with the illuminative panels? Did you find the activity enjoyable and the instructions clear? Was the exercise easy or difficult to follow?
(ii) Question 2: Was interaction with the panels intuitive or challenging? How did your peers respond?
(iii) Question 3: Do you anticipate regularly using the panels and engaging with them socially alongside others?
(iv) Question 4: How do you feel about the color change feature that confirms your posture or gesture is correct?
(v) Question 5: What do you think of the visual esthetics of the panels, given that they were designed based on the features of the Wong Tai Sin District?
(vi) Question 6: Have you interacted with similar technologies or used AI-driven systems before?

3.2. Design and development of a textile-based gesture recognition system

3.2.1. Illuminative fabric development

Optical fiber made with polymethyl methacrylate, whose fiber diameter is 0.25 mm, was knitted with textile-based yarns to create the illuminative fabrics. Wool yarn was chosen to provide the users a soft and comfortable hand feel when touching the fabrics. A transparent yarn made with nylon and polyester was added in the second version to improve the illuminated effect. Table 1 shows the details of the POF and yarns used for the fabric development. The knitting process was conducted on a 14-gauge computerized v-bed knitting machine, which is an industrial machine and is able to realize scalable production. To knit out the design graphics, a knit structure of doubled jacquard in three colors was utilized. The design graphics were separated into three panels. Three fabric panels were knitted, each with a size of 123 cm in width and 139 cm in height. In the first version, the jacquard structure was only knitted with wool yarns. However, the illuminated area was not apparent, so the illuminative effect of the fabric panels was not satisfactory. Therefore, a transparent yarn was added when developing the second version to highlight the illuminated area.

3.2.2. Integration of illuminative fabrics and a gesture recognition system

The gesture recognition system consists of several key components working in an integrated pipeline. An embedded camera captured real-time images of the user's hand, arm, or head in front of the textile panel. The visual input was processed by a single-board computer, which runs a deep learning model to detect 21 landmarks on the hand, as well as 33 landmarks on the shoulder and head. A self-developed algorithm interpreted these landmark data coordinates to classify specific gestures. The recognized gestures were then converted into encoded serial data, which was transmitted to a self-developed PCB incorporating an ESP32 microcontroller (Espressif Systems, China). The PCB decoded the serial signal and transformed it into a pulse width modulation (PWM) signal that controls the illumination effect of RGB LEDs embedded in the illuminative textile panel. In addition, POFs were integrated into the fabric to emit the LED light, enabling gesture-driven color changes directly on the textile surface.

To clarify and expand upon the implementation of the gesture recognition system, the system leveraged Google's MediaPipe framework, specifically the MediaPipe Hand landmarks detection and Pose landmarks detection, which are pre-trained using over 30,000 real-world labeled images covering diverse hand and body postures.[65] These models enabled the detection of 21 hand landmarks and

Table 1. Polymeric optical fiber and yarn used for the illuminative fabric development

Materials	Details
Polymethyl methacrylate polymeric optical fiber	Fiber diameter: 0.25 mm, transmission loss: 350 dB/km, temperature range: −55°C to 70°C
Wool yarn	Count: Nm 2/48; composition: 100% extra fine merino wool; care label: machine wash cold or 40°C; do not bleach; dry flat; iron at low heat
Transparent yarn	Count: Nm 1/80; composition: 55% nylon, 45% polyester; care label: machine wash cold or 30°C; do not bleach; do not tumble dry; iron at low heat

33 pose landmarks (including head and shoulder) in real time without requiring additional custom training. The system operated on a Python-based software pipeline (version 3.12) deployed on a single-board computer (Raspberry Pi 4), achieving a processing rate of approximately 5 – 7 frames per second. This frame rate satisfied the application requirement.

Regarding algorithmic transparency, gesture classification was performed through a custom rule-based algorithm that interprets the relative x- and y-coordinates of the detected landmarks. Specific gestures were classified based on thresholds of angular relationships, spatial distances between relevant anatomical points (e.g., distance from index fingertip to thumb), and limb orientation. A finite state machine governed the gesture-to-command mapping, enhancing robustness by tolerating minor variations in gesture and posture.

Concerning AI model transparency and performance evaluation, the system utilized MediaPipe's pre-trained models without additional architectural modification or retraining. Detailed information regarding network architecture, training datasets, accuracy metrics, and optimization techniques is publicly available through official MediaPipe documentation.[65] Since the study focuses on real-time system integration and user interaction rather than novel model development, quantitative benchmarking (e.g., accuracy and latency) was not the primary evaluation method. Instead, performance was assessed qualitatively through stakeholder feedback collected during co-design workshops and prototype trials conducted in actual healthcare-related contexts. This approach facilitated iterative refinement of the system based on practical usability and user-centered design principles.

4. Results and discussion

4.1. User preferences in textile materials, design graphics, and gestures

Analysis of the co-design session A revealed critical insights into how interactive textile installations can effectively engage elderly users through visual, tactile, and interactive elements. The associated interview transcript is presented in Table S1. Through systematic examination of participant responses, four distinct themes emerged that significantly influenced the final design implementation:

(i) Incorporating local landmarks for memory stimulation and therapeutic engagement: The integration of local landmarks in graphic elements emerged as a powerful catalyst for memory stimulation and therapeutic engagement. Workshop participants emphasized that "remembering the past" was "helpful to the condition," specifically highlighting the significance of incorporating familiar elements like "Lion Rock plus Lion Pavilion. plus flowers and green grass." The strategic use of "eye-catching red, yellow, colorful" elements created visually comfortable environments that facilitated connections with past experiences and community identity.

(ii) Enhancing interaction through visual recognition: Visual recognition processes emerged as a crucial factor in ensuring effective user interaction with the installation. Participant feedback revealed that "simple things, let them associate them, and they can recognize them faster by looking at pictures than by reading words." This insight demonstrated the importance of developing intuitive visual elements that users could readily identify, emphasizing how graphic recognition served as a primary pathway for engagement.

(iii) The role of material tactility in user comfort and interaction: Material tactility emerged as a fundamental consideration that shaped the physical design and user comfort levels. Workshop participants explicitly articulated that "hard objects will make you nervous," while "touch and hearing, flow and sound" elicited "strong responses." Their emphasis on the need for "relaxing" elements and "soft music" underscored how material choices directly influenced user willingness to engage with the installation.

(iv) Gamification as a strategy for sustained engagement: Interactive engagement through gamification emerged as an essential strategy for sustained user participation. Participants observed that when users "press it, find it fun," indicating that "game elements attract the elderly" and should be "interesting, not preachy." This emphasis on playful interaction revealed how carefully designed interactive elements could overcome initial hesitation and encourage active participation among elderly users.

The graphic illustration was created using Clip Studio Paint EX (version 2.0) and Adobe Photoshop CS6 (version 13), with Drafts 1 and 2 presented in Figure S1. Both drafts featured signature landmarks from the Diamond Hill and Lion Rock areas, including the Wong Tai Sin Temple, a lantern representing Lok Fu Plaza, and bamboo symbolizing nature. Draft 1 included imagery of the Wong Tai Sin Temple and a dragon, symbolizing Kowloon. However, because SKH is a Christian organization, the depiction of the Wong Tai Sin Temple was replaced in Draft 2 with representations of public housing estates, sports elements, and parks. The final design, shown in Figure 2B, emphasizes local neighborhood landmarks, including the Wong Tai Sin Cooked Food Stall and Kai Tak River. In addition, four color palettes composed of three yarn colors each were proposed for the fabric knitting

process (Figure S2). The combination of beige, redwood, and blue-grey was selected by stakeholders and is shown in Figure 2C. Using this palette, three knitted fabric wall panels were fabricated and subsequently installed at the WTSDHC, as shown in Figure 2D.

4.2. Integration of illuminative fabrics into an AI-based system

Figure 3A presents a block diagram outlining the overall workflow of the gesture recognition pipeline used to drive the LED-based illumination of the textile surface. The process began with an integrated camera capturing real-time BGR images, which are sent directly to a deep learning model without being stored. The model included pre-trained hand-tracking and body pose detection networks capable of identifying 21 hand landmarks and 33 body landmarks (e.g., hands, shoulders, head) in each frame. The output is a set of landmark coordinates (x, y), which was processed by a self-developed algorithm to classify specific gestures and postures. The classified result was then converted into encoded serial data, later decoded by a custom-made PCB and transformed into PWM signals that controlled the RGB LED-based textile illumination. Figure 3B illustrates a specific example of this interaction workflow. When a user performs a "thumbs up" gesture, the camera captures the hand image, and the deep learning model identifies 21 corresponding landmark points. These landmarks – represented by their (x, y) coordinates – are analyzed by the self-developed algorithm, which identifies the gesture as "good" based on the relative positions and angles between landmark points. This classification is processed using simple state machine logic and converted into encoded serial data. The data are transmitted to the control unit, a self-developed PCB, where it is decoded and output as a PWM signal. This signal activates the appropriate LED channel, resulting in a yellow illumination on the textile surface, providing immediate visual feedback to the user. Figure 3C demonstrates the hand gesture, body, and head movement recognition.

4.3. Refinement in the textile-based gesture recognition system

The textile-based gesture recognition system was first installed at WTSDHC on June 29, 2021. After the initial installation, refinements were made to both the gesture recognition system and the three fabric wall panels to enhance the illuminative effect and expand the variation of color selection. The improved system and updated panels were reinstalled on January 22, 2025, as part of the system optimization and technical refinement phase. Transparent

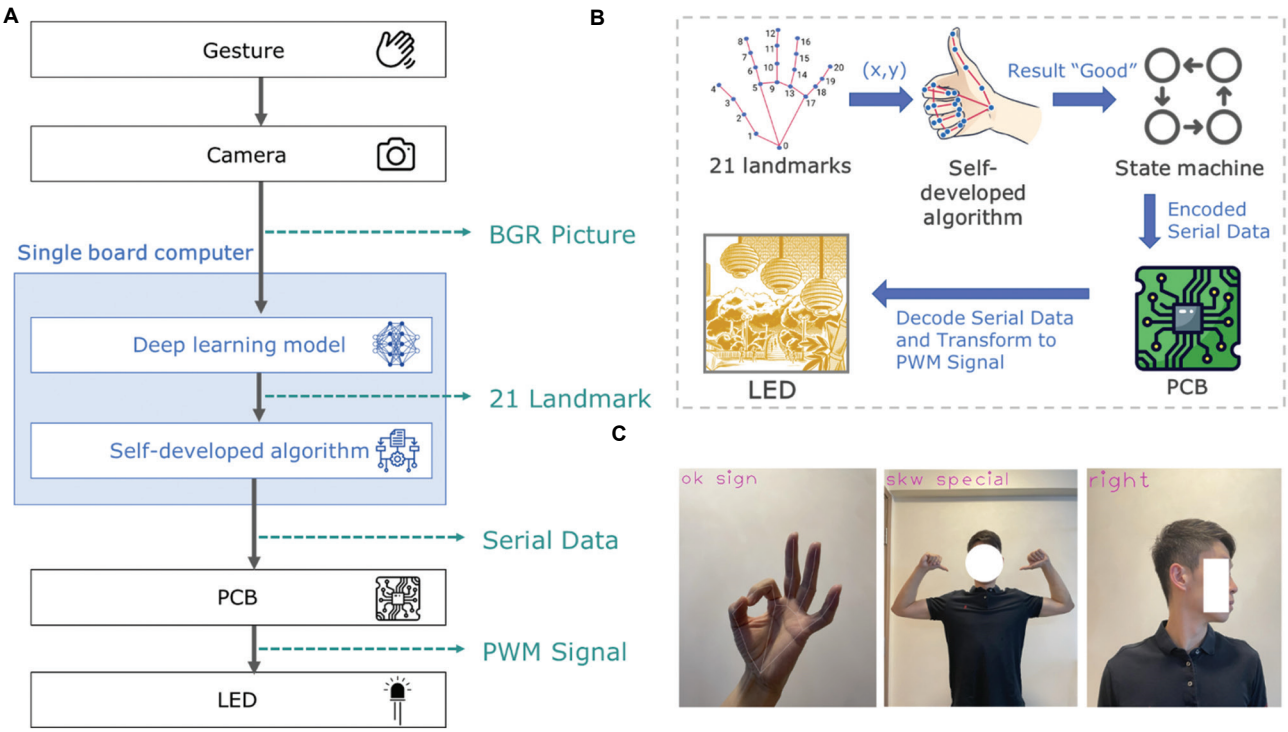

Figure 3. System architecture and workflow of the gesture recognition system. (A) Block diagram and (B) flowchart illustrating the process of the gesture recognition system. (C) Hand gesture, body, and head movement recognition.
Abbreviations: BGR: Blue, green, red; LED: Light-emitting diode; PCB: Printed circuit board; PWM: Pulse width modulation.

yarns were incorporated into the knitted structure to enhance the illuminative effect by better diffusing the emitted light across the textile surface (Figure 4A). Figure 4A shows the fabric in version A without transparent yarn, and the illuminative effect is not obvious, while the fabric in version B has transparent yarn, and the illuminative effect is apparent in the transparent parts. Furthermore, the upgraded configuration allows for a wider selection of color responses, enabling finer-tuned visual feedback in response to various gesture inputs. In Version 1, color output was restricted to basic RGB channels supporting only seven pre-defined colors (combinations of red, green, and blue at either 0 or 255 nm), as shown in Figure 4B. In contrast, Version 2 enables full-spectrum color control by allowing each RGB channel to range from 0 to 255 nm, resulting in up to 16,777,215 possible color combinations (Figure 4C).

In both the initial and advanced prototypes, the gesture recognition system was integrated into textile

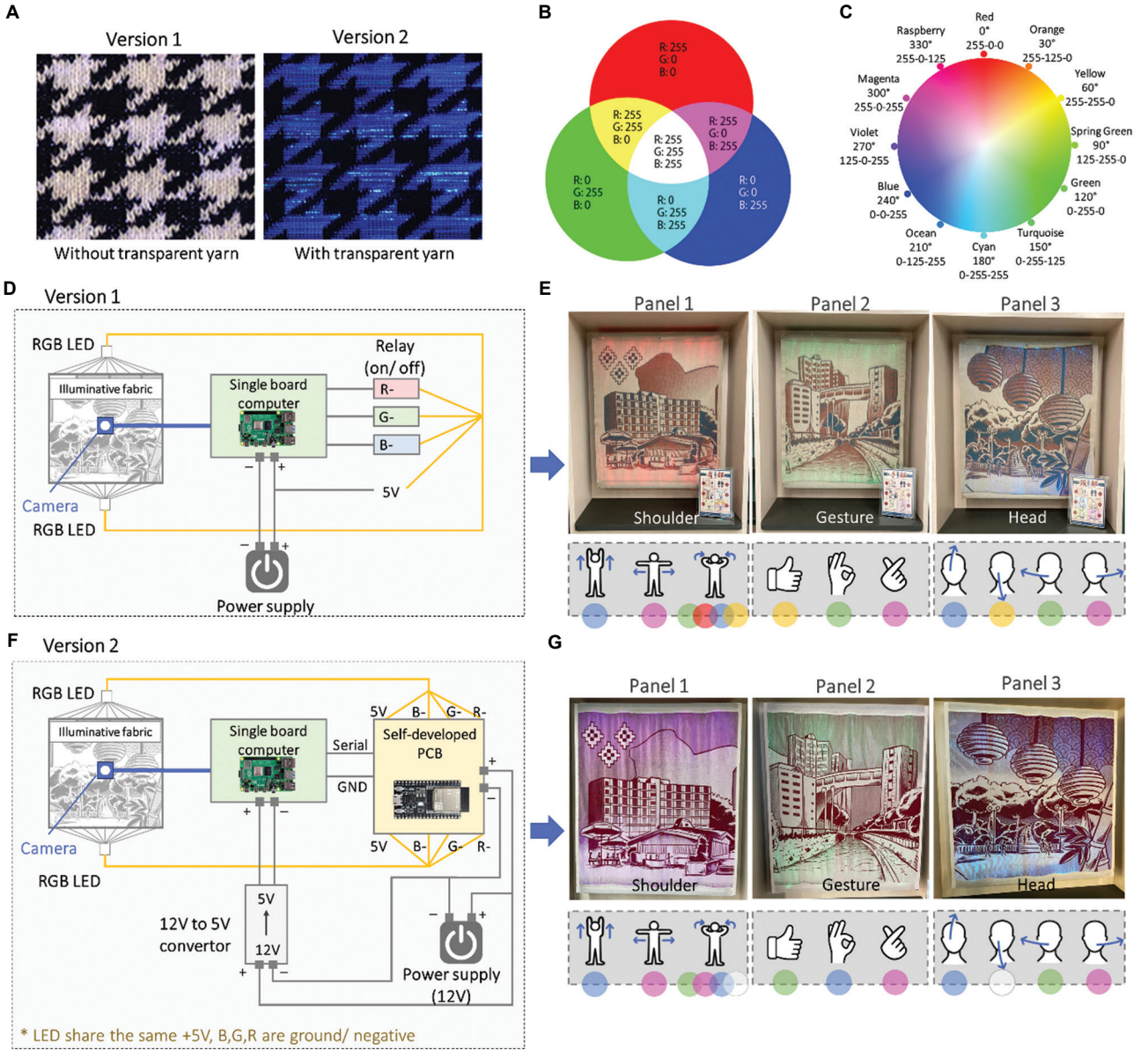

Figure 4. Light-emitting diode (LED) color configuration and system architecture of the textile-based gesture recognition panels. (A) Photos showing the illumination effects in wall panels for the first prototype (Version 1) and the advanced version (Version 2). LED color mapping in wall panels for (B) Version 1 and (C) Version 2. (D) Conceptual diagram illustrating the connection structure of the gesture recognition system in Version 1 and (E) Version 2. (F and G) Photos demonstrating different illumination colors in response to various gestures in Version 1 and Version 2, respectively.

wall panels that were knitted with POFs and embedded with RGB LEDs to enable illumination. These fibers guide emitted light across the textile surface, emitting the LED output and transforming it into soft, color-based visual feedback. In the first prototype (Version 1) shown in Figure 4D, the response system was relatively simple: Classified gesture data were sent from the Raspberry Pi to a basic relay switch connected to the RGB LEDs. This setup allowed the system to turn different colored light channels on or off based on the detected gesture or body posture, directly illuminating the textile surface in specific colors corresponding to each gesture and posture type. In the advanced version (Version 2) shown in Figure 4F, a more modular and intelligent infrastructure was implemented. The system included a self-developed PCB built around an ESP32 microcontroller, which decodes serial input from the single-board computer and distributes PWM signals to the RGB LEDs. The advanced system also supports potential Internet of Things applications, while simplifying hardware integration and improving system stability and responsiveness. The RGB LEDs, embedded along the edges of the textile panel and optically coupled through POFs, share a common +5V power source. Control signals (R, G, B) were adjusted through the PCB using serial data inputs processed by a state machine methodology, ensuring synchronized responses with gesture inputs. A unified 12V power supply supported all electronic components within the system, delivering power directly to the custom PCB and to a voltage converter that steps down the current to 5V for the single-board computer. This centralized power configuration ensures a compact, efficient, and easily maintainable setup, well-suited for integration in healthcare environments. Figure 4E and G show the color differences corresponding to various gestures and body movements in the fabric wall panels for Version 1 and Version 2, respectively. In Version 1, the left wall panel was designed to respond to shoulder movements. The illumination changed to blue, pink, and a dynamic "jumping" color effect when the system recognized the gestures "hands up," "open arms," and the WTSDHC slogan gesture "My Health, My Say!" performed by pointing to oneself, respectively. The middle panel was dedicated to hand gesture recognition, with color changes of yellow, blue, and pink corresponding to the gestures "good," "OK," and "love." The right panel was designed for head and neck movements; when the user turned their head "up," "down," "left," or "right," the textile illumination changed accordingly to blue, yellow, green, and pink. Figure S3 illustrates the infographic interaction with the illuminative fabric wall panels through (a) shoulder, (b) hand, and (c) head movements, respectively.

The integration of illuminative fabric into an AI-driven gesture recognition system creates a novel multi-sensory and contactless interaction platform, specifically aimed at promoting engagement, exercise, and therapy in healthcare settings. From a design and engineering perspective, the knitted POF fabric served both esthetic and functional goals by emitting programmable RGB light in response to validated gestures. This visual feedback mechanism – subtle, localized, and dynamic – provided a soft and non-intrusive way for users, particularly elderly individuals, to interact with therapy-driven content. The iterative transition from the first prototype, which relied on basic relay control, to an advanced custom-made PCB solution demonstrates the scalability of the design. The upgraded use of an ESP32 controller introduced advanced data handling, reduced latency, and allowed greater precision over RGB transitions, thereby enabling alignment with the AI model and optimizing the best color combinations across different panel designs and illumination patterns. This technical refinement enhanced the responsivity and fluidity of the textile interface, making the system feel more intuitive and responsive to natural body movement. Furthermore, the edge-mounted RGB LEDs, optically coupled to the textile through POFs, enabled a contactless yet emotionally resonant interaction method, particularly valuable in post-pandemic healthcare environments focused on hygiene and psychological comfort. The textile's ability to visually signify correct gestures with soft illuminations empowers elderly users through instant feedback, supporting self-guided physical and cognitive rehabilitation. Overall, this integration not only reinforces the practicality of smart textiles for ambient healthcare but also demonstrates how co-designed, AI-enhanced systems can drive inclusive and meaningful experiences in spatial interaction, particularly for vulnerable populations.

4.4. System validity and privacy considerations

To support real-world deployment in healthcare contexts, the design and implementation of the gesture recognition system deliberately accounted for environmental factors such as lighting conditions and gesture visibility. While no quantitative accuracy metrics were recorded at this stage, system latency was monitored through built-in software timers, which counted frame-processing loops based on timestamp differences. The average processing rate was approximately 5 – 7 times per second, confirming operational responsiveness suitable for real-time interaction. During participatory co-design workshops, the viewing angle and lighting conditions were thoroughly discussed with stakeholders. Based on this input, the optimal interaction distance was standardized at approximately 1 meter, with lighting conditions kept consistent to ensure

gesture reliability, thus reducing variation due to angle or environmental brightness. Although false positives were not formally measured, gesture set definitions were refined collaboratively with users to minimize misrecognition. Only movements that were clearly distinguishable in both posture and motion were selected as trigger gestures. This co-design-driven filtering process effectively reduced the risk of unintended activations.

Regarding privacy and ethical considerations, the image-capturing software does not include any recording or data storage functions. Images captured by the camera are processed in real time for landmark detection and are continuously overwritten with the next frame. No visual data are stored locally or remotely, and all content is deleted immediately upon device shutdown. As the textile panels are designed for use in public or semi-public spaces (such as DHC), where CCTV systems are already in operation, and the use of non-recording cameras falls within acceptable practices. Nonetheless, privacy concerns were considered during the design phase, and the current system meets ethical expectations for deployment in environments frequented by elderly users and vulnerable groups.

4.5. Stakeholders' feedback

Co-designers' feedback (co-design session C) highlighted multiple significant advantages of integrating textile wall panels with the gesture recognition system. Table 2 summarizes the stakeholders' feedback during the pre- and post-design stages of the co-design process. Co-designers A and B contributed essential community insights that directly informed the integration of familiar local landmarks into the design. This incorporation notably enhanced emotional engagement, strengthened community identity, and improved user connectivity. Their recommendations underscored the importance of visual familiarity, with participants expressing a strong emotional resonance rooted in their personal histories and lifelong proximity to landmarks, such as Lion Rock. Users A and B consistently reported high levels of comfort, positively evaluating the system's ease of access and intuitive interactions. They particularly praised the soft and approachable materials, noting their pleasant tactile qualities, which significantly contributed to overall user satisfaction and engagement. In addition, users emphasized the system's inclusive nature, highlighting how effectively the design accommodated diverse physical abilities and age groups. The OT lead (co-design session B) reported improvements in therapeutic outcomes, specifically noting the system's effectiveness in enhancing rehabilitation processes. They acknowledged that the integration of diverse technologies and intelligent solutions substantially increased rehabilitation efficiency and operational performance. Furthermore, OTs emphasized the system's high level of accessibility and intuitive usability across a broad demographic, supporting user within the age range of 6 to over 80 years old. A detailed summary of stakeholder feedback is presented in Table S2 for the research lead, Table S3 for the OT lead, Table S4 for co-designers, and Table S5 for the end-users. Complete transcripts of stakeholder interviews are included in the supplementary materials to ensure comprehensive documentation and research transparency.

The participatory design approach effectively engaged stakeholders through structured activities and semi-structured discussions, capturing precise community insights and user preferences that informed the systematic refinement of technical parameters. These structured interactions enabled stakeholders to articulate specific needs clearly, contributing significantly to the development process. Content analysis of interview data further identified clear, recurrent themes that were translated into actionable design criteria, emphasizing user-driven

Table 2. Stakeholders' feedback in pre- and post-stages of the co-design process

Design aspect	Co-design workshop input (2021)	Post-implementation feedback (2023 – 2024)
Community integration	• Emphasis on incorporating district landmarks and natural elements • Recognition of local cultural significance • Strong advocacy for familiar environmental elements	• Strong emotional connection to implemented landmarks • Enhanced sense of community identity • Effective integration of neighborhood characteristics
Material and interface	• Preference for soft, non-threatening materials • Emphasis on multi-sensory engagement • Identification of relaxation as a key design priority	• Positive user response to textile-based interfaces • Effective implementation of a gesture recognition system • Enhanced operational effectiveness in center activities
Visual design	• Prioritization of pictorial over textual elements • Recommendation for vibrant, age-appropriate color schemes • Focus on intuitive visual recognition	• High user comprehension rates • Effective visual communication strategy • Effective age-appropriate design implementation
User engagement	• Emphasis on gamification elements • Focus on enjoyment-driven interaction • Recommendation for a non-didactic approach	• High accessibility across age groups • Widespread user adoption • Effective integration into the center's daily operation

product development and iterative improvement. Stakeholders consistently expressed appreciation for the opportunity to contribute directly to the design process, reinforcing the perceived value of their participation.

The interactive textile wall panels significantly promoted physical engagement among elderly visitors by integrating intuitive, playful gesture recognition interactions rather than explicit instructional methods. By emphasizing an enjoyment-driven, non-didactic approach, the installation effectively facilitated greater acceptance and consistent use among elderly users, who frequently exhibit resistance to more traditional, overtly instructional exercise interventions. This approach effectively aligned with healthcare objectives by encouraging physical activity in a non-intrusive, enjoyable manner, thus fostering a more sustainable integration of exercise into daily routines.

Technologically, the system implemented a user-friendly gesture recognition interface allowing elderly users to interact effortlessly with illuminative knitted textiles, customizing colors and illumination without specialized technical knowledge. This ease of use substantially lowered barriers to technology adoption among elderly populations, who might otherwise find digital interactions challenging. A noteworthy technical enhancement included the development of a customized wooden frame specifically designed to optimize the illumination effectiveness of POF under regular lighting conditions. This improvement demonstrates an iterative and responsive problem-solving process, reflecting a robust commitment to addressing real-world operational challenges encountered during the development and deployment phases.

Expert participation provided academic insights and specialized technical expertise throughout the project, effectively combining established technological capabilities with stakeholder-driven esthetics and functional requirements. Experts' contributions ensured that the system was both scientifically robust and contextually appropriate, bridging theoretical knowledge and practical application seamlessly. The semi-structured virtual interviews conducted with stakeholders yielded rich, detailed qualitative insights, further ensuring that the final design effectively responded to user requirements and preferences. The systematic approach to collecting and analyzing qualitative data allowed for targeted refinements, ultimately achieving strong operational integration within the healthcare facility's daily practices and demonstrating improvements in user engagement and therapeutic outcomes.

5. Limitations and future work

The illumination effect of POF tends to weaken in well-lit environments, posing challenges for healthcare settings where bright lighting is essential. To compensate, a customized wooden frame was used to extend shadows and enhance visibility. This solution proved effective in improving the illuminative performance of the textile in this study; however, it may introduce venue restrictions and limit the flexibility of POF textile installations in certain scenarios. Therefore, future development should focus on miniaturizing panel sizes to support more diverse applications. Smaller POF textiles could enable the creation of portable therapeutic tools beyond fixed installations. Refining gesture recognition algorithms to improve responsiveness, particularly for users with limited mobility, is another priority. In addition, integrating the system with educational programs, digital applications, and interactive public spaces could further expand the technology's potential beyond healthcare environments.

Regarding the improvement in engagement and rehabilitation outcomes, findings at this early stage are based on qualitative user feedback collected during co-design workshops and preliminary trials. Due to time constraints and limited participant availability, no structured quantitative assessment of engagement levels or rehabilitation outcomes was conducted. The feedback gathered was used primarily to guide iterative design decisions and to evaluate initial system usability. Future work will incorporate standardized evaluation metrics and longitudinal studies to assess engagement and therapeutic impact more rigorously in real-world healthcare environments. While the initial user feedback during workshops and trials was largely positive, it is acknowledged that early-phase co-design processes inherently involve practical trade-offs. The limited duration and resources available for subject recruitment restricted the possibility of broader testing and capturing a more diverse range of inputs. Future iterations will aim to incorporate longer-term engagement and structured usability metrics that reflect both positive and critical experiences to achieve a more comprehensive understanding of the system's impact and adoption potential.

In addition, future work could explore the integration of new multimodal deep learning models, such as large language models and video language models, to capture complex human gestures through face and body pose analysis, as well as voice or sound recognition.[66] This would enhance the system's ability to interpret multi-sensory input, opening new possibilities for richer human-computer interaction. It would also be valuable to personalize textile responses by incorporating real-time emotional analysis through facial recognition and physiological signals. For example, systems such as Irida Health offer pathways for combining gesture evaluation with affective computing,

which may enrich the user experience and enable more human-centered therapeutic applications.[67,68]

6. Conclusion

This study presents a human-centered co-design approach to the design, development, and implementation of an AI-integrated gesture recognition system embedded in illuminative textile wall panels, aimed at enhancing spatial engagement in a healthcare setting. The findings demonstrate the effectiveness of the gesture-based illumination system, which provides immediate visual feedback through colored illuminations while accommodating ambidextrous gestures. Key contributions of the study include:

(i) Human-centered co-design and cultural integration: The study employed a co-design approach involving users, therapists, and stakeholders to develop an AI-integrated textile system. Workshops revealed preferences for soft materials, pictorial cues over text, and culturally significant graphic elements, aiming to create intuitive and emotionally resonant interactions, especially for elderly users.

(ii) AI and textile system development: Illuminative textile wall panels were fabricated using POF-knitted fabrics integrated with a computer vision-based deep learning model for gesture recognition. Two workflow configurations were proposed; enabling color-changing feedback based on hand movements. The system supports ambidextrous gestures and provides real-time, interactive visual feedback.

(iii) Real-world implementation and impact: The prototypes were installed in a DHC to promote elderly physical activity and engagement. Stakeholder feedback confirmed high usability, accessibility, and emotional connection to the design. The research demonstrates the potential of AI-driven textile interfaces in healthcare, offering a scalable model for creating responsive, human-centered environments.

In conclusion, this research offers insights into the fabrication of a textile-based gesture recognition system through a co-design framework. The design features demonstrated a seamless integration of AI tools into daily life and healthcare interventions, particularly benefiting elderly users. This study lays the groundwork for further exploration into textile-based AI systems in interactive environments and provides practical guidance for healthcare administrators planning similar installations. The integration of intelligent textiles into healthcare spaces represents a vital step toward creating responsive, engaging, and human-centered environments that align technological innovation with human needs.

Acknowledgments

We sincerely appreciate the valuable support and guidance provided by Dr. Elsa Lee and her team at the WTSDHC, whose assistance was instrumental in facilitating the placement of the textile wall panels within the center.

Funding

This research is funded by the Laboratory for AI in Design (Project Code: RP3-5) under the InnoHK Research Clusters, Hong Kong Special Administrative Region.

Conflict of interest

Jeanne Tan is an Editorial Board Member of this journal, but was not in any way involved in the editorial and peer-review process conducted for this paper, directly or indirectly. Separately, other authors declared that they have no known competing financial interests or personal relationships that could have influenced the work reported in this paper.

Author contributions

Conceptualization: Jeanne Tan, Hiu Ting Tang
Investigation: Ching Lee, Hiu Ting Tang, Jun Jong Tan
Methodology: Ching Lee, Hiu Ting Tang, Jun Jong Tan
Supervision: Jeanne Tan
Writing – original draft: Jeanne Tan, Ching Lee
Writing – review & editing: Jeanne Tan, Ching Lee, Hiu Ting Tang, Wing Ki Yip, Ka Wing Tse

Ethics approval and consent to participate

The study received ethical approval from the Hong Kong Polytechnic University's Institutional Review Board (Approval no.: HSEARS20200123003). All participants provided informed consent before the commencement of the interviews.

Consent for publication

Written informed consent for publication of the data was obtained from all participants involved in the study.

Availability of data

Data used in this work are available from the corresponding author upon reasonable request.

References

1. Islam S, Shekhar R. *Smart Textiles and Wearable Technology: Opportunities and Challenges in the Production and Distribution*. Singapore: Springer Nature; 2025. p. 267-303.

2. Scataglini S, Moorhead A, Feletti F. A systematic review of

smart clothing in sports: Possible applications to extreme sports. *Muscles Ligaments Tendons J*. 2020;10(2):333-342.

doi: 10.32098/MLTJ.02.2020.19

3. Wang C, Fu L, Ametefe DS, Wang S, John D. E-textiles in healthcare: A systematic literature review of wearable technologies for monitoring and enhancing human health. *Neural Comput Appl*. 2025;37(4):2089-2111.

doi: 10.1007/s00521-024-10947-z

4. Sajovic I, Kert M, Boh PB. Smart textiles: A review and bibliometric mapping. *Appl Sci.* 2023;13(18):10489.

doi: 10.3390/app131810489

5. Shajari S, Kuruvinashetti K, Komeili A, Sundararaj U. The emergence of ai-based wearable sensors for digital health technology: A review. *Sensors (Basel)*. 2023;23(23):9498.

doi: 10.3390/s23239498

6. Sarker MTH, Ahmed I, Rahaman MA. Ai-based smart textile wearables for remote health surveillance and critical emergency alerts: A systematic literature review. *Am J Scholarly Res Innov*. 2023;2(2):1-29.

doi: 10.63125/ceqapd08

7. Yadav A, Yadav K. Transforming healthcare and fitness with AI powered next-generation smart clothing. *Discov Electrochem*. 2025;2(1):2.

doi: 10.1007/s44373-025-00015-z

8. Avellar L, Stefano FC, Delgado G, Frizera A, Rocon E, Leal JA. AI-enabled photonic smart garment for movement analysis. *Sci Rep.* 2022;12(1):4067.

doi: 10.1038/s41598-022-08048-9

9. Akter A, Apu MMH, Veeranki YR, Baroud TN, Posada-Quintero HF. Recent studies on smart textile-based wearable sweat sensors for medical monitoring: A systematic review. *J Sens Actuator Netw*. 2024;13(4):40.

doi: 10.3390/jsan13040040

10. Tan J, Shao L, Lam NYK, Toomey A, Ge L. Intelligent textiles: Designing a gesture-controlled illuminated textile based on computer vision. *Text Res J*. 2022;92(17-18):3034-3048.

doi: 10.1177/00405175211034245

11. World Health Organization. *Decade of Healthy Ageing: Baseline Report*. Geneva, Switzerland: World Health Organization; 2021.

12. Department of Economic and Social Affairs, United Nations. *World Population Prospects*. New York, NY: United Nations; 2019.

13. Committee on the Future Health Care Workforce for Older Americans. *Retooling for an Aging America: Building the Health Care Workforce*. Washington, DC: National Academies Press; 2008.

14. Shah MN, Bazarian JJ, Lerner EB, *et al*. The epidemiology of emergency medical services use by older adults: An analysis of the national hospital ambulatory medical care survey. *Acad Emerg Med.* 2007;14(5):441-447.

doi: 10.1111/j.1553-2712.2007.tb01804.x

15. United Nations Economic and Social Commission for Asia and the Pacific (UN ESCAP). *Asia-Pacific Report on Population Ageing 2022: Trends, Policies and Good Practices Regarding Older Persons and Population Ageing*. Bangkok, Thailand: UN ESCAP; 2022.

16. United Nations Department of Economic and Social Affairs (UN DESA). *Countries Forecast to Have the Highest Share of 65-Year-Old People Worldwide in 2050*. New York, NY: UN DESA; 2023.

17. Wilmoth JR, Bas D, Mukherjee S, Hanif N. *World Social Report: Leaving no One Behind in an Ageing World*. New York, NY: United Nations; 2023.

18. McClellan CB. Health care utilization and expenditures in health professional shortage areas. *Med Care Res Rev*. 2024;81(4):335-345.

doi: 10.1177/10775587241235705

19. Research Office, Legislative Council Secretariat. *The 2025-2026 Budget.* Hong Kong: Legislative Council; 2025.

20. Wu X, Law CK, Yip PSF. A projection of future hospitalisation needs in a rapidly ageing society: A Hong Kong experience. *Int J Environ Res Public Health*. 2019;16(3):473.

doi: 10.3390/ijerph16030473

21. Choy R. Implementation of community care policy for older adults in Hong Kong. In: Law VTS, Fong BYF, editors. *Ageing with Dignity in Hong Kong and Asia: Holistic and Humanistic Care*. Ch. 3. Singapore: Springer Nature Singapore; 2022.

22. Government of the Hong Kong Special Administrative Region (HKSAR). LCQ11: District Health Centres and District Health Centre Expresses. Press Releases from the Government of the Hong Kong Special Administrative Region. Available from: https://www.info.gov.hk/gia/general/202403/27/P2024032700591.htm [Last accessed on 2024 Apr 25].

23. *Wong Tai Sin District Health Centre, Key functions and features of DHC*. Available from: https://www.dhc.gov.hk/en/healthcare-service-providers.html#key-functions-and-features-of-dhc [Last accessed on 2024 Apr 25].

24. Ta AWA, Goh HL, Ang C, Koh LY, Poon K, Miller SM. Two Singapore public healthcare AI applications for national screening programs and other examples. *Health Care Sci*. 2022;1(2):41-57.

doi: 10.1002/hcs2.10

25. Ang A. *Behind Singapore's Widespread AI Adoption in Public Health*. Healthc IT News. Available from: https://www.healthcareitnews.com/news/asia/behind-singapores-widespread-ai-adoption-public-health [Last accessed on

2024 Apr 25].

26. Raghavan A, Demircioglu MA, Taeihagh A. Public health innovation through cloud adoption: A comparative analysis of drivers and barriers in Japan, South Korea, and Singapore. *Int J Environ Res Public Health*. 2021;18(1):334.

    doi: 10.3390/ijerph18010334

27. Wright J. Inside Japan's long experiment in automating elder care. *MIT Technol Rev.* [Internet]. 2023. Available from: https://www.technologyreview.com/2023/01/09/1065135/japan-automating-eldercare-robots [Last accessed 2024 Apr 25].

28. Li LW, Ma CC. Application of AI in addressing challenges of primary healthcare in Hong Kong. In: *Ageing with Dignity in Hong Kong and Asia: Holistic and Humanistic Care*. Singapore: *Springer Nature Singapore*; 2025. p. 589-609.

29. Legislative Council. *Promotion of Smart Healthcare in Selected Places*. Hong Kong: Legislative Council; 2022.

30. Köttl H, Gallistl V, Rohner R, Ayalon L. But at the age of 85? Forget it!: Internalized ageism, a barrier to technology use. *J Aging Stud*. 2021;59:100971.

    doi: 10.1016/j.jaging.2021.100971

31. Zhang J, Wang H, Li Q, Luximon Y. What is the real-life experience of older adults on smart healthcare technologies? An exploratory interview study. *Gerontology*. 2024;70(9):978-990.

    doi: 10.1159/000539539

32. Millward P. The'grey digital divide': Perception, exclusion and barriers of access to the internet for older people. First Monday. Available from: https://firstmonday.org/ojs/index.php/fm/article/view/1066 [Last accessed on 2024 Apr 25].

33. Rice RE, Katz JE. Comparing internet and mobile phone usage: Digital divides of usage, adoption, and dropouts. *Telecomm Policy*. 2003;27(8-9): 597-623.

    doi: 10.1016/S0308-5961(03)00068-5

34. Brown T. Design thinking. *Harv Bus Rev.* 2008;86(6):84-92.

35. Sanders EBN, Stappers PJ. Co-creation and the new landscapes of design. *CoDesign*. 2008;4(1):5-18.

    doi: 10.1080/15710880701875068

36. Steen M, Manschot M, De KN. Benefits of co-design in service design projects. *Int J Des*. 2011;5(2):53-60.

37. Bate P, Robert G. Experience-based design: from redesigning the system around the patient to co-designing services with the patient. *Qual Saf Health Care*. 2006;15(5):307-310.

    doi: 10.1136/qshc.2005.016527

38. Robert G, Cornwell J, Locock L, Purushotham A, Sturmey G, Gager M. Patients and staff as codesigners of healthcare services. *BMJ*. 2015;350:g7741.

    doi: 10.1136/bmj.g7714

39. Locock L, Robert G, Boaz A, *et al*. Testing accelerated experience-based co-design: A qualitative study of using a national archive of patient experience narrative interviews to promote rapid patient-centred service improvement. *Health Serv Deliv Res*. 2014;2(4):1-122.

    doi: 10.3310/hsdr02040

40. Norman DA, Verganti R. Incremental and radical innovation: Design research vs. Technology and meaning change. *Des Issues*. 2014;30(1):78-96.

    doi: 10.1162/desi-a-00250

41. Rafael S, Santiago E, Rebelo F, Noriega P, Vilar E. Bio-centred interaction design: A new paradigm for human-system interaction. In: *International Conference on Human-Computer Interaction*. Cham: Springer International Publishing; 2022. p. 69-79.

42. Woods B, O'Philbin L, Farrell EM, Spector AE, Orrell M. Reminiscence therapy for dementia. *Cochrane Database Syst Rev.* 2018;2018(3):CD001120.

    doi: 10.1002/14651858.cd001120.pub3

43. Lazar A, Demiris G, Thompson HJ. Evaluation of a multifunctional technology system in a memory care unit: Opportunities for innovation in dementia care. *Inform Health Soc Care*. 2016;41(4):373-386.

    doi: 10.3109/17538157.2015.1064428

44. Poupyrev I, Gong NW, Fukuhara S, Karagozler ME, Schwesig C, Robinson KE. Project jacquard: Interactive digital textiles at scale. In: *Proceedings of the 2016 Chi Conference on Human Factors in Computing Systems*. New York: Association for Computing Machinery; 2016. p. 4216-4227

45. Gorka R, Subramaniyan AK, Velu R. Integrating advanced technologies in post-operative rehabilitation: 3D-knitting, 3D-printed electronics, and sensor-embedded textiles. In: Zheng Y, Chow H, editors. *Digital Health Innovation*. Ch. 10. Singapore: Springer Nature; 2023.

46. Caldani L, Pacelli M, Farina D, Paradiso R. E-Textile platforms for rehabilitation. In: *2010 Annual International Conference of the IEEE Engineering in Medicine and Biology Society*. Piscataway, NJ: IEEE; 2010. p. 5181-5184.

47. Meena JS, Choi SB, Jung SB, Kim JW. Electronic textiles: New age of wearable technology for healthcare and fitness solutions. *Mater Today Bio.* 2023;19:100565.

    doi: 10.1016/j.mtbio.2023.100565

48. Khatwani P, Desai K. Interactive smart textile fabrics. Interactive smart textile fabrics. In: *Functional and Technical Textiles.* United Kingdom: Woodhead Publishing; 2023. p. 293-311.

49. Bai ZQ, Tan J, Johnston CF, Tao XM. Connexion development of interactive soft furnishings with polymeric optical fibre (POF) textiles. *Int J Cloth Sci Technol.* 2015;27(6):870-894.

    doi: 10.1108/IJCST-05-2014-0058

50. Cochrane C, Mordon SR, Lesage JC, Koncar V. New design of textile light diffusers for photodynamic therapy. *Mater Sci Eng C Mater Biol Appl*. 2013;33(3):1170-1175.

doi: 10.1016/j.msec.2012.12.007

51. Schrank V, Beer M, Beckers M, Gries T. Polymer-optical fibre (POF) integration into textile fabric structures. In: *Polymer Optical Fibres*. United Kingdom: Woodhead Publishing; 2017. p. 337-348.

52. Avellar L, Frizera A, Leal JA. POF smart pants: A fully portable optical fiber-integrated smart textile for remote monitoring of lower limb biomechanics. *Biomed Opt Express*. 2023;14(7):3689-3704.

doi: 10.1364/BOE.492796

53. Gong Z, Xiang Z, OuYang X, *et al*. Wearable fiber optic technology based on smart textile: A review. *Materials*. 2019;12(20):3311.

doi: 10.3390/ma12203311

54. Tan J, Shao L, Lam NYK, *et al*. Evaluating the usability of a prototype gesture-controlled illuminative textile. *J Text Inst*. 2024;115(3):350-356.

doi: 10.1080/00405000.2023.2193790

55. Lam NYK, Tan J, Toomey A, Cheuk KCJ. Illuminative knitted textiles: Machine knitting with polymeric optical fibres (POFs). *Res J Text Appare*. 2024;28(2):317-335.

doi: 10.1108/RJTA-12-2021-0144

56. Chen A, Tan J, Henry P, Tao X. The design and development of an illuminated polymeric optical fibre (POF) knitted garment. *J Text Inst*. 2020;111(5):745-755.

doi: 10.1080/00405000.2019.1661937

57. Tam EY, Chi CM. The hong kong geriatrics society annual scientific meeting 2024. *Asian J Gerontol Geriatr*. 2024;19(2):50-51.

58. Park M, Park T, Park S, Yoon SJ, Koo SH, Park YL. Stretchable glove for accurate and robust hand pose reconstruction based on comprehensive motion data. *Nat Commun*. 2024;15(1):5821.

doi: 10.1038/s41467-024-50101-w

59. Glauser O, Wu S, Panozzo D, Hilliges O, Sorkine-Hornung O. Interactive hand pose estimation using a stretch-sensing soft glove. *ACM Trans Graph*. 2019;38(4):162.

doi: 10.1145/3306346.3322957

60. Panagiotou C, Faliagka E, Antonopoulos CP, Voros N. Multidisciplinary ML techniques on gesture recognition for people with disabilities in a smart home environment. *AI*. 2025;6(1):17.

doi: 10.3390/ai6010017

61. Guo K, Orban M, Lu J, Al-Quraishi MS, Yang H, Elsamanty M. Empowering hand rehabilitation with AI-powered gesture recognition: A study of an sEMG-based system. *Bioengineering (Basel)*. 2023;10(5):557.

doi: 10.3390/bioengineering10050557

62. Oudah M, Al-Naji A, Chahl J. Elderly care based on hand gestures using kinect sensor. *Computers*. 2020;10(1):5.

doi: 10.3390/computers10010005

63. Munoz NM, Kristoffersen MB, Sunnerhagen KS, Naber A, Alt MM, Ortiz CM. Upper limb stroke rehabilitation using surface electromyography: A systematic review and meta-analysis. *Front Hum Neurosci*. 2022;16:897870.

doi: 10.3389/fnhum.2022.897870

64. Jaramillo YA, Benalcázar ME, Mena ME. Real-time hand gesture recognition using surface electromyography and machine learning: A systematic literature review. *Sensors (Basel)*. 2020;20(9):2467.

doi: 10.3390/s20092467

65. MediaPipe. *MediaPipe - Hand Landmarker and Pose Landmarker*. Google AI; 2023. Available from https://ai.google.dev/edge/mediapipe/solutions/vision/hand-landmarker [Last accessed on 2024 Apr 28].

66. Anthropic. *Claude: Helpful, Honest, and Harmless AI Assistant*. Anthropic Website; 2023. Available from: https://www.anthropic.com [Last accessed on 2024 Apr 27].

67. IRIDA. *IRIDA Project - AI-Driven Mental Health Support Platform*. IRIDA Website; 2023. Available from: https://irida.health [last accessed on 2024 Apr 27].

68. Koulieris GA, Kannengiesser N, Noristani A. Affect recognition through multimodal fusion of face, body pose, and physiological data using deep learning. *Neurocomputing*. 2023;540:127171.

doi: 10.1016/j.neucom.2023.127171

ACCSCIENCE PUBLISHING

International Journal of AI for Materials and Design

ORIGINAL RESEARCH ARTICLE

Data-driven optimization of biaxial shrinkage and stability in electrospun membranes via machine learning and Monte Carlo simulation

Shiyu He[1,2], Chentong Gao[2,3], Runzhi Lu[2,4], Fei Xiao[1,5]*, Li Cong Huang[6], and Wei Min Huang[2]*

[1]State Key Laboratory of Metal Matrix Composites, School of Materials Science and Engineering, Shanghai Jiao Tong University, Shanghai, China

[2]School of Mechanical and Aerospace Engineering, Nanyang Technological University, Singapore

[3]College of Aerospace Engineering, Nanjing University of Aeronautics and Astronautics, Nanjing, Jiangsu, China

[4]School of Civil Engineering, Southeast University, Nanjing, Jiangsu, China

[5]Department of Computer Science, Institute of Medical Robotics, Shanghai Jiao Tong University, Shanghai, China

[6]School of Computing, National University of Singapore, Singapore

***Corresponding authors:**
Fei Xiao
(xfei@sjtu.edu.cn)
Wei Min Huang
(mwmhuang@ntu.edu.sg)

Citation: He S, Gao C, Lu R, Xiao F, Huang LC, Huang WM. Data-driven optimization of biaxial shrinkage and stability in electrospun membranes via machine learning and Monte Carlo simulation. *Int J AI Mater Design*. 2025;2(3):64-77.
doi: 10.36922/IJAMD025260022

Received: June 26, 2025

Revised: August 15, 2025

Accepted: August 21, 2025

Published online: September 9, 2025

Abstract

Controlling shrinkage behavior in electrospun membranes is critical for applications that require precise dimensional or mechanical performance. However, experimental variability and limited datasets often hinder the development of robust process models. This study introduces a data-driven framework that combines machine learning with Monte Carlo simulation to enable both accurate and stable shrinkage control in electrospinning using a small experimental dataset. Multiple regression models were trained to predict biaxial shrinkage ratios and their variability, with support vector regression and extreme gradient boosting showing the best performance for accuracy and stability prediction, respectively. Feature importance analysis revealed applied voltage and thermoplastic polyurethane concentration as the dominant parameters. A Monte Carlo-based optimization strategy was employed to identify process parameter sets that achieve target shrinkage ratios while minimizing output variability. The proposed approach enables multi-objective optimization in low-data, high-variability manufacturing environments, offering practical insights into precision fabrication of stimulus-responsive membranes.

Keywords: Electrospinning; Shrinkage stability; Machine learning; Monte Carlo simulation; Process parameter optimization

1. Introduction

Electrospinning has become a key nanofabrication technique in biomedical and engineering applications due to its simplicity, material adaptability, and ability to produce continuous fibers with diameters ranging from nanometers to micrometers.[1-3] Electrospun membranes, such as polyvinyl alcohol, poly(lactic acid), poly(lactide-co-glycolide), are widely employed in tissue engineering, drug delivery, smart materials, flexible electronics,

and filtration systems.[4-6] Notably, these membranes often undergo spontaneous and stimulus-responsive shrinkage when exposed to thermal, solvent, or moisture-based triggers.[7,8] Such shrinkage enables functional transformations, such as self-folding structures, yet its anisotropy and instability can cause severe deformation, critically limiting its reliability in applications such as tissue scaffolds.[9,10]

Recent studies suggest that the shrinkage of electrospun membranes originates from a gradient prestrain field within the cross-sectional area generated during fiber formation, driven by radial differences in solvent evaporation, prestraining from high-speed collectors, and the rapid fixation of polymer chain orientation.[11,12] Upon exposure to external stimuli, such as solvents, the shape memory effect[13,14] activates the prestrain, causing fiber buckling and resulting in macroscopic, anisotropic membrane contraction. Despite these insights, current models remain largely qualitative. Shrinkage control continues to rely on empirical parameter adjustments, lacking a predictive, quantitative framework capable of capturing the non-linear, multivariable nature of the process and its sensitivity to perturbations.[11]

Subtle variations in electrospinning parameters, such as applied voltage, rotation speed of the collator, distance between electrodes, and solvent concentration, can significantly affect jet dynamics, fiber solidification, and internal prestrain distribution, resulting in anisotropic and often unpredictable shrinkage behavior.[15] Due to the non-linear and multivariable nature of these effects, traditional modeling approaches often lack the accuracy and generalizability required for effective control.[16] Moreover, electrospinning experiments are typically labor-intensive and sensitive to environmental fluctuations, hindering the acquisition of high-throughput data.[17] As a result, available datasets are often limited in size and scope, further constraining the development of robust process control strategies.

Based on the experimental data reported in literature,[11] Figure 1 illustrates the distribution of system outputs along the rotational and transverse axes, with each data cluster (applied voltage [kV], rotation speed of collator [rpm], distance between electrodes [cm], and solvent concentration [%]) corresponding to a distinct combination of input parameters, denoted by unique "Combo" identifiers. To enable quantitative interpretation of cluster behavior, each group of data points is enclosed by a Gaussian confidence ellipse delineating the 68% probability region. These ellipses are computed based on the Mahalanobis distance, which incorporates the full covariance structure of each cluster to account for correlations and anisotropic variance. In contrast to Euclidean distance, the Mahalanobis metric provides scale-invariant and directionally sensitive distance measures, thereby yielding ellipses that more accurately reflect the underlying multivariate normal distribution of the data. The adoption of a 68% confidence level corresponds to one standard deviation from the mean in the bivariate normal case, thereby capturing the most statistically representative core of each distribution, while reducing sensitivity to outliers and extreme observations. This visualization framework supports inverse mapping, i.e., given a desired target output, its location on the plot can be used to identify the nearest confidence ellipse, and thus infer the most probable input parameter configuration that can produce the specified response. This approach enables principled, data-informed decision-making in predictive modeling and design selection.

According to Figure 1, the experimentally obtained biaxial shrinkage ratios only cover certain discrete regions. The same region can be covered by different combinations of processing parameters. Even when using identical parameters, the degree of result dispersion varies significantly depending on the parameter combination used. How can we optimally select a combination of processing parameters to achieve the desired biaxial shrinkage ratios of the electrospun membrane while minimizing variability?

More broadly, optimizing processing parameters in manufacturing is essential not only for achieving target performance but also for ensuring product stability and consistency across production. In processes such as electrospinning, small variations in parameters can lead to significant fluctuations in fiber morphology, internal stress distribution, and functional outcomes. With the recent emergence of machine learning in membrane science, there is increasing potential to address these challenges by enabling data-driven process optimization that simultaneously targets performance and stability, as demonstrated in recent studies on material discovery, process control, and performance prediction.[18-20] However, many artificial intelligence (AI)-based approaches focus primarily on predicting average performance, often overlooking process variability and robustness.[21] This limitation is particularly evident under small-sample conditions, where models may capture central trends but fail to reflect sensitivity to parameter fluctuations.[22] As a result, predictions may meet nominal targets while real-world performance remains unstable. Integrating both accuracy and stability into modeling frameworks is therefore vital for reliable, data-driven optimization in high-variability manufacturing scenarios.

More broadly, optimizing processing parameters in manufacturing is crucial not only to meet performance standards but also to ensure consistent product stability.

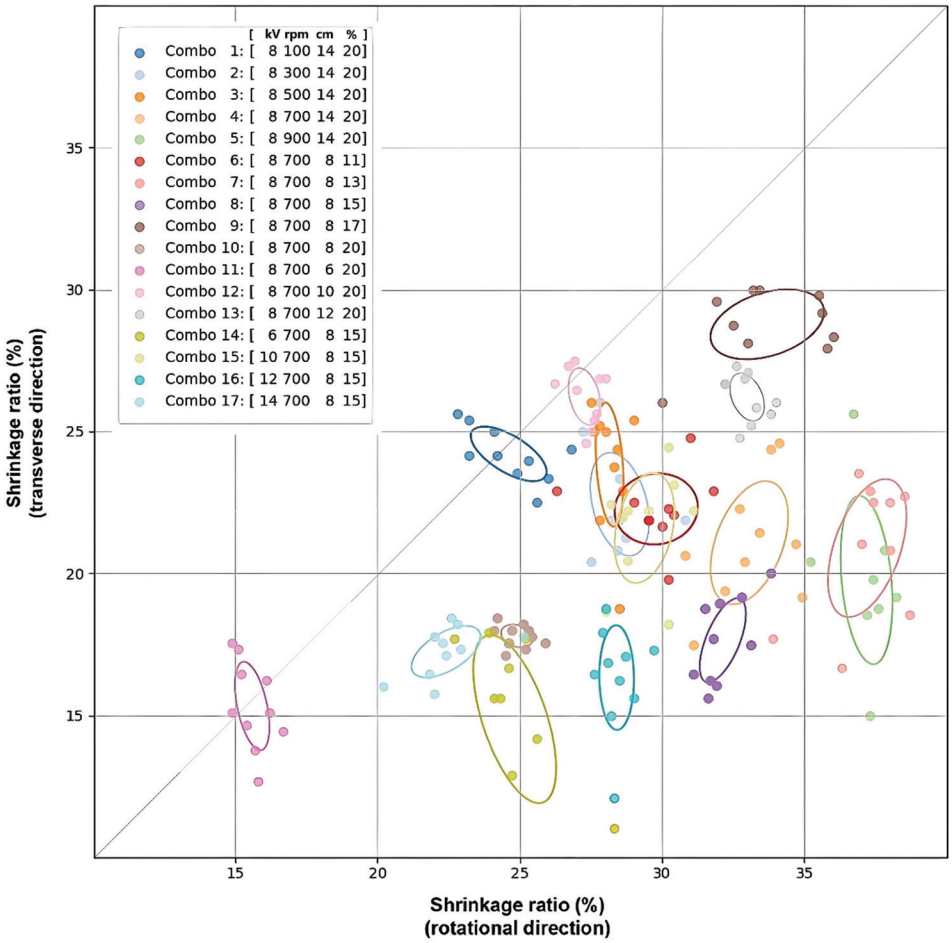

Figure 1. Scattered plot of measured shrinkage ratios in the transverse direction and rotational direction of each membrane in the literature,[11] with clusters highlighted and inner confidence contours

However, current AI applications largely focus on achieving performance targets, often neglecting stability, especially when data are limited.

To address these challenges, this study proposes a hybrid approach that integrates machine learning with Monte Carlo simulation to model and analyze the shrinkage behavior and stability of electrospun membranes based on a limited experimental dataset. A supervised learning model is first developed using experimental data (from literature;[11] Figure 1) to capture the non-linear relationships between processing parameters and shrinkage ratios under multifactorial conditions. On the other hand, a shrinkage stability coefficient is introduced to quantify the sensitivity of shrinkage to parameter perturbations, and the Monte Carlo simulation is employed to characterize its statistical distribution. This framework enables the identification of a controllable processing parameter space that ensures both target biaxial shrinkage performance and robustness in biaxial shrinkage. The proposed methodology establishes a data-driven and uncertainty-aware paradigm, offering both theoretical and practical guidance for designing tunable and stimulus-responsive electrospun membranes.

2. Methodology

This study presents a data-driven framework for optimizing electrospinning processes, which focuses on shrinkage behavior and stability. The proposed methodology consists of three main components: (i) dataset construction based on experimental measurements under controlled parameter variations; (ii) development and interpretation of machine learning models for predicting shrinkage ratios and their stability; and (iii) a Monte Carlo simulation-based strategy for identifying process conditions that satisfy target shrinkage values, while ensuring minimal variability.

2.1. Dataset construction

To develop a predictive and robust model for shrinkage behavior in electrospun membranes, we constructed an

experimental database from controlled electrospinning tests using thermoplastic polyurethane (TPU) solutions. Shrinkage ratios in the rotational direction (RD) and transverse direction (TD) were obtained by measuring the linear dimensions of the membrane before and after ethanol activation, where RD is parallel to the axis of rotation of the roller collector and TD is perpendicular to it. The shrinkage ratio in each direction was calculated as the percentage reduction in length relative to the initial length, that is, the difference between the initial and final lengths divided by the initial length. The four input features (solvent concentration, distance between electrodes, collector speed, and applied voltage) were selected for their direct influence on jet formation, fiber deposition, and solvent evaporation, which together determine the internal prestrain distribution. The solution flow rate was maintained at a fixed constant value throughout all experiments to avoid introducing additional variability from unstable jet formation. Each parameter combination was tested at least five times under controlled conditions, revealing up to 10% variation in shrinkage ratios under identical settings. This variability was expressed as the confidence interval width (CIW), the range between the upper and lower bounds of the 95% confidence interval, with a smaller CIW indicating higher stability. CIW was used as the stability metric alongside mean shrinkage values. The dataset spans practical parameter ranges, ensuring representativeness and reliability for model training. The details of the materials and experimental procedures are described in.[11] The measured shrinkage ratios (%RD and %TD) of each tested membrane are presented in Figure 1.

2.2. Model development and interpretation

In this study, predictive models were developed for both the shrinkage ratio and shrinkage stability. The shrinkage stability metric was defined based on the CIW of repeated measurements under identical processing conditions, with lower values indicating higher process robustness and consistency. To identify the most effective predictive model for shrinkage behavior, several machine learning algorithms were assessed, including support vector regression (SVR),[23] random forest (RF),[24] extreme gradient boosting (XGBT),[25] artificial neural networks (ANN),[26] and linear regression (LR).[27] These models were selected to cover kernel-based, ensemble, neural network, and linear paradigms, offering complementary strengths for small-sample, non-linear, and high-variability systems, and providing a balanced basis for robust model selection.

The dataset was randomly partitioned into a training set (80%) and a testing set (20%) to ensure robust model validation. Each model was trained to establish the non-linear mapping from processing parameters (applied voltage, TPU concentration, collector speed, electrode distance) to shrinkage ratios (%RD and %TD). Model performance was evaluated on the testing set using a set of complementary metrics, including mean squared error (MSE), root mean square error (RMSE), mean absolute error (MAE), mean absolute percentage error (MAPE), coefficient of determination (R^2), and Pearson correlation coefficient (R). These metrics capture different aspects of predictive accuracy: MSE and RMSE emphasize penalization of large errors, MAE reflects the average magnitude of deviation, MAPE provides a relative error assessment normalized to the scale of measurement, and R^2, along with R, quantify the proportion of variance explained and the degree of linear correlation between predicted and observed values. The optimal model was selected based on a composite assessment of these metrics. Priority was given to models achieving low error values (MSE, RMSE, and MAE) and high consistency indicators (R^2, R). The selected model was then integrated into the stability evaluation framework, providing a reliable predictive core for Monte Carlo-based optimization.

Subsequently, the Shapley Additive Explanations (SHAP) method[18,28-33] was applied to interpret the trained model and reveal the relationship between electrospinning parameters and shrinkage behavior. This analysis enabled the identification of key process features that most strongly influence shrinkage, providing a clear basis for understanding and optimizing critical factors in membrane fabrication. Mathematically, SHAP values are derived from the cooperative game theory framework, where each feature is considered a "player" contributing to the model prediction. For a model prediction $f(x)$, the SHAP value for the i^{th} feature is computed with Equation I,

$$\phi_i = \sum_{S \subseteq N \setminus \{i\}} \frac{|S|!\left(M-|S|-1\right)!}{M!}\left[f_{S\cup\{i\}}\left(x_{S\cup\{i\}}\right) - f_S\left(x_S\right)\right] \quad \text{(I)}$$

where M is the total number of features, S represents a subset of features excluding i; $f_S(x_S)$ is the model output when only features in S are included; ϕ_i quantifies the average marginal contribution of feature i over all possible feature combinations.

In the context of this study, the trained regression model $f(x)$ maps the four process parameters (voltage, TPU concentration, collector speed, and electrode distance) to the predicted shrinkage ratios and stability. The SHAP value ϕ_i for each parameter represents its average contribution to increasing or decreasing the predicted shrinkage outcome, aggregated over all permutations of feature inclusion. By summing all contributions and the

base value f_0 (mean model output), the prediction can be decomposed as Equation II.

$$f(x) = f_0 + \sum_{i=1}^{M} \phi_i \quad \text{(II)}$$

This additive decomposition provides a transparent interpretation of how each electrospinning parameter affects the model output, enabling a parameter-sensitive optimization strategy.

2.3. Optimization of shrinkage stability

To identify optimal processing parameters that achieve target shrinkage ratios with maximal stability, a Monte Carlo simulation[34-38] framework was established by integrating shrinkage prediction and shrinkage stability models. The Monte Carlo method is a stochastic simulation technique that estimates numerical results by performing repeated random sampling over the parameter space. In this study, each process parameter, including applied voltage, TPU concentration, collector speed, and electrode distance, is treated as a random variable within experimentally feasible bounds. A large number N of parameter sets is generated from the joint distribution of process parameters to explore the multidimensional process space in an unbiased and comprehensive manner. Compared with Bayesian optimization or other sequential search algorithms, this one-step large-scale sampling can simultaneously evaluate shrinkage accuracy and stability without iterative model updates, making it particularly suitable for our non-linear, high-variability system with a pre-trained predictive model.

Mathematically, for a target shrinkage function $f(x)$ and stability metric $g(x)$, the expected values are approximated as Equation III,

$$E[f(x)] \approx \frac{1}{N}\sum_{k=1}^{N} f(x_k), E[g(x)] \approx \frac{1}{N}\sum_{k=1}^{N} g(x_k) \quad \text{(III)}$$

where x_k is the kth random sample of process parameters. Through sufficient sampling, the distribution of predicted shrinkage ratios (%RD, %TD) and stability coefficient (CIW) can be estimated.

By filtering all samples that meet the target shrinkage tolerance, the Monte Carlo method provides a numerical approximation to the feasible design domain. The subsequent ranking by predicted CIW corresponds to an optimization over the estimated probability distribution of outcomes. This enables the selection of parameter combinations that maximize process robustness while satisfying the desired biaxial shrinkage performance. The method proceeds as follows:

(i) Step 1: Initialization
The optimization process begins by specifying the target shrinkage ratios in the radial direction (RD) and TD, denoted as R_{RD}^{target} and R_{TD}^{target}. In addition, tolerance limits Δ_{RD} and Δ_{TD} are defined to account for permissible deviations from the target values. These targets are determined based on the desired dimensional accuracy of the electrospun mat after post-processing, ensuring the end product meets application-specific requirements (e.g., biomedical scaffolds or filtration membranes). This initialization step provides clear quantitative objectives for subsequent parameter screening.

(ii) Step 2: Monte Carlo sampling
A large set of candidate processing parameter combinations is generated via Monte Carlo sampling within predefined practical ranges. The considered parameters include applied voltage (kV), solution concentration (wt%), collector distance (cm), and rotation speed (rpm). Random sampling ensures comprehensive coverage of the parameter space, enabling the identification of non-intuitive optimal combinations that conventional trial-and-error methods may miss.

(iii) Step 3: Shrinkage prediction
Each sampled parameter set is evaluated using a previously trained shrinkage prediction model, which was constructed based on experimental data and machine learning algorithms. The model outputs predicted shrinkage ratios in $RD\left(\hat{R}_{RD}\right)$ and $TD\left(\hat{R}_{TD}\right)$, capturing the non-linear dependencies between processing parameters and shrinkage behavior. This predictive approach greatly reduces the number of costly experimental trials.

(iv) Step 4: Feasibility filtering
Only those parameter sets whose predicted shrinkage ratios satisfy Equation IV,

$$|\hat{R}_{RD} - R_{RD}^{target}| \leq \Delta_{RD}, |\hat{R}_{TD} - R_{TD}^{target}| \leq \Delta_{TD} \quad \text{(IV)}$$

are retained for further analysis. This filtering step eliminates parameter combinations that would produce excessive dimensional deviation, thus narrowing the candidate pool to only potentially viable solutions.

(v) Step 5: Stability assessment
For each feasible parameter set, shrinkage stability is evaluated using a trained stability prediction model. The stability metric is expressed as the predicted CIW, which reflects the sensitivity of shrinkage behavior to process fluctuations. A smaller CIW corresponds to a more robust process configuration, less prone to variation due to environmental changes or equipment drift. This step ensures that the selected parameters are not only accurate but also reproducible in real production.

(vi) Step 6: Pareto front construction
The feasible samples are mapped onto a Pareto front by jointly considering two competing objectives: Shrinkage deviation from the target values and the predicted CIW (robustness). This multi-objective optimization framework enables the identification of trade-offs between dimensional accuracy and process stability, guiding informed decision-making rather than relying on a single metric.

(vii) Step 7: Optimal parameter selection.
Based on the Pareto front constructed in Step 6, the optimal processing configuration is selected by prioritizing the lowest CIW to maximize stability while maintaining an acceptable deviation from the target shrinkage ratios, ensuring dimensional precision. This integrated approach effectively balances product quality with manufacturing consistency, providing a practical and reliable processing window for electrospinning applications.

3. Results and discussion

3.1. Shrinkage ratio prediction model

Figure 2 illustrates the predictive performance of six machine learning models in estimating the shrinkage ratio in the %RD, namely RF, SVR, XGBT, ANN, decision tree regressor (DTR), and LR. Among them, RF, SVR, and XGBT exhibit high prediction accuracy, as evidenced by the close alignment of predicted values with the ideal diagonal line on both training and test sets, indicating strong generalization capability across varying input conditions. The ANN, DTR, and LR models display noticeably larger deviations from the ground truth, suggesting the presence of underfitting, model bias, or limited capacity to capture the complex, non-linear relationships inherent in the dataset. Notably, certain predicted %RD values correspond to multiple experimentally observed outcomes. This phenomenon does not originate from predictive ambiguity in the models but rather reflects the intrinsic instability of the electrospinning process itself. The shrinkage ratios are susceptible to fluctuations arising from subtle variations in ambient environment, equipment status, and material heterogeneity, all of which can introduce non-negligible noise into the output. Such variability highlights the necessity of incorporating both accuracy and stability into the modeling framework to ensure reliable shrinkage control.

Figure 3 presents the performance of six machine learning models in predicting %TD, including RF, SVR, XGBT, ANN, DTR, and LR. Among them, RF, SVR, and XGBT achieve relatively accurate predictions on both training and test sets, with predicted values closely matching observed values, and the points clustering tightly around

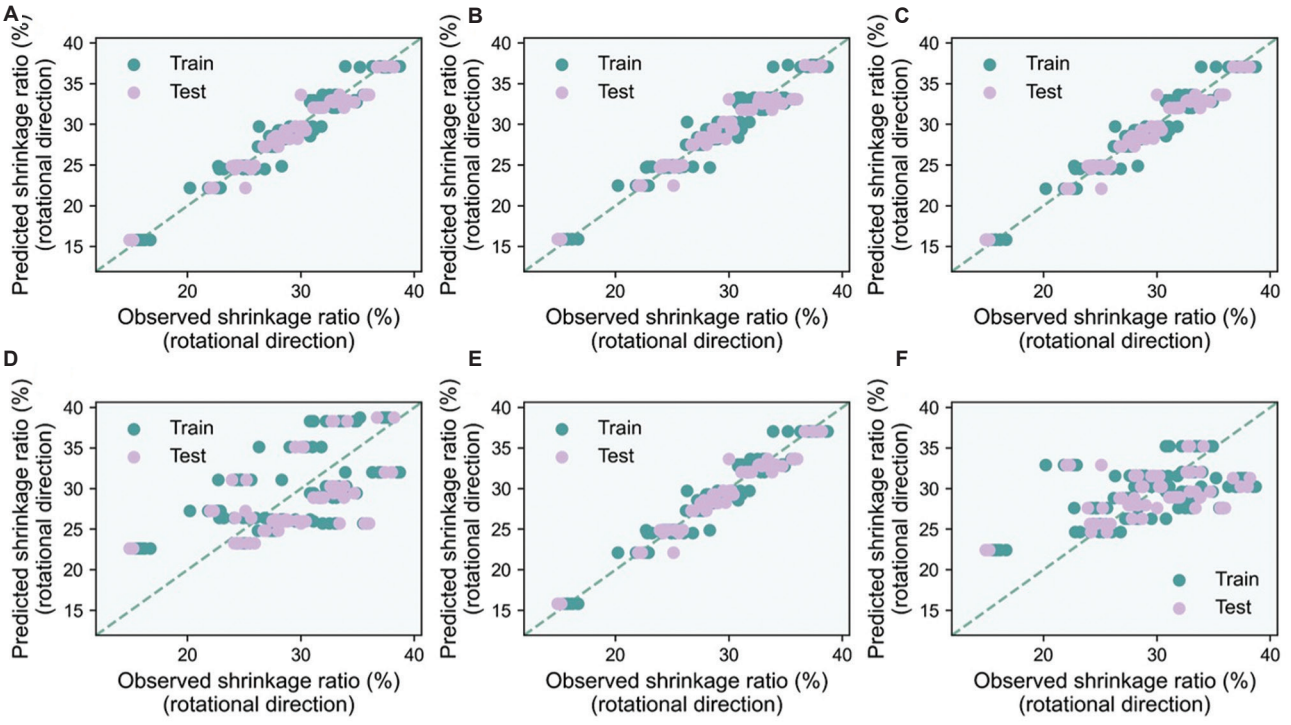

Figure 2. Performance of different machine learning models in predicting the percentage of rotational direction on the test set. (A) Random forest. (B) Support vector regression. (C) Extreme gradient boosting trees. (D) Artificial neural networks. (E) Decision tree regressor; (F) Linear regression.

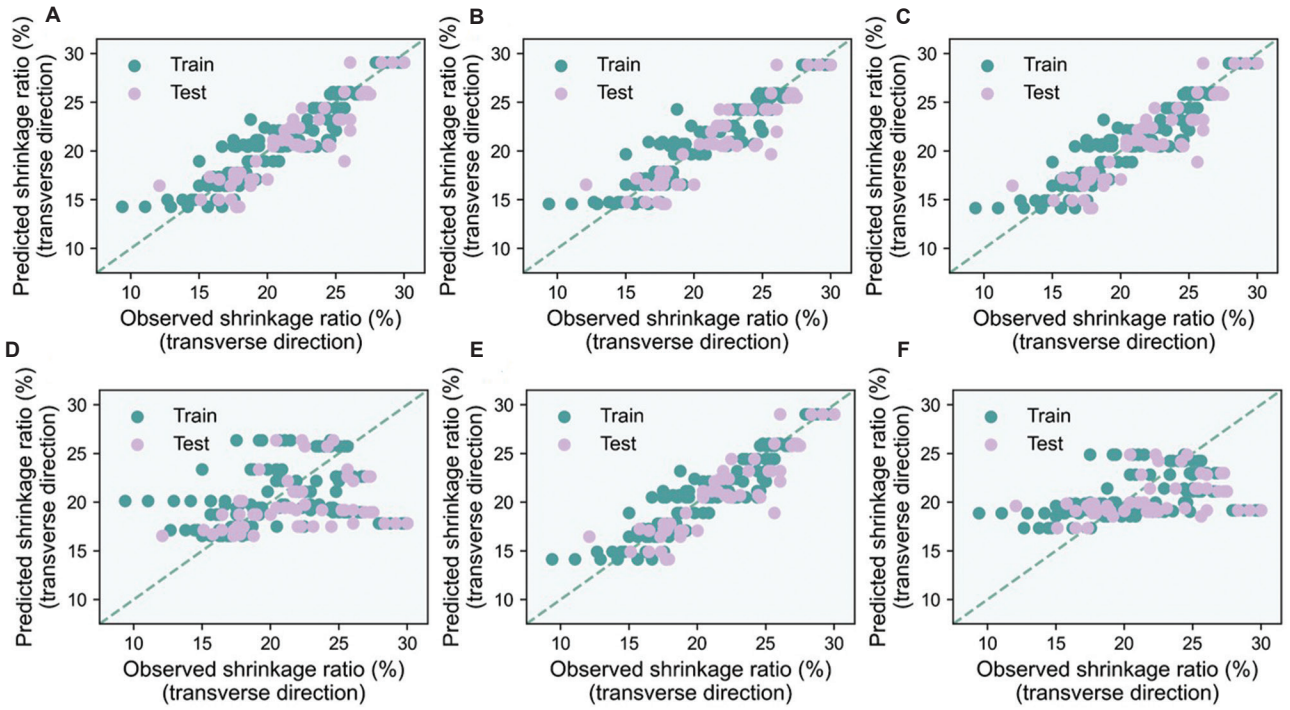

Figure 3. Performance of different machine learning models in predicting the percentage of transverse direction on the test set. (A) Random forest. (B) Support vector regression. (C) Extreme gradient boosting trees. (D) Artificial neural networks. (E) Decision tree regressor; (F) Linear regression.

the diagonal line. The SVR and XGBT models demonstrate slightly better consistency and convergence, particularly on the test set, which suggests that they are more robust in handling high-dimensional interactions under small-sample conditions. However, the ANN and LR models exhibit considerably lower predictive accuracy, particularly on the test set. The ANN model, while theoretically capable of modeling non-linearities, shows significant scatter in the prediction results, indicating that it may have overfit the training data or failed to generalize due to limited data and suboptimal hyperparameter tuning. The LR model, which relies on a strictly linear approximation of the feature space, consistently underperforms across the entire prediction range, suggesting that it is fundamentally inadequate for capturing the multivariate non-linear dependencies inherent in the electrospinning process.

Table 1 presents the performance comparison of different machine learning models in predicting %RD and %TD. The RF, SVR, XGBT, and DTR models exhibit relatively low prediction errors (MSE = 1.04–1.10, MAE = 0.74–0.79, MAPE = 2.6–2.8) and high goodness-of-fit metrics (R^2 = 0.96, R = 0.98). Notably, the SVR, XGBT, and DTR models achieve the highest R^2 (0.96), indicating excellent predictive performance for %RD. In the case of %TD prediction, the SVR model demonstrates superior performance, achieving the lowest MSE (4.00),

Table 1. Performance comparison of different machine learning models in predicting %RD and %TD evaluated by MSE, RMSE, MAE, MAPE, R^2, and R

Properties	Model	MSE	RMSE	MAE	MAPE	R^2	R
%RD	RF	1.1	1.05	0.79	2.78	0.96	0.98
	SVR	1.04	1.02	0.74	2.59	0.96	0.98
	XGBT	1.04	1.02	0.74	2.59	0.96	0.98
	ANN	19.38	4.4	3.82	14.03	0.27	0.59
	DTR	1.04	1.02	0.74	2.59	0.96	0.98
	LR	19.62	4.43	3.32	12.55	0.26	0.52
%TD	RF	4.08	2.02	1.51	7.2	0.74	0.9
	SVR	4	2	1.53	7.35	0.75	0.9
	XGBT	4.13	2.03	1.53	7.27	0.74	0.9
	ANN	19.45	4.41	3.24	13.89	-0.23	0.35
	DTR	4.13	2.03	1.53	7.27	0.74	0.9
	LR	14.74	3.84	2.94	13.16	0.07	0.42

Abbreviations: %RD: Shrinkage ratio (%) in rotational direction; %TD: Shrinkage ratio (%) in transverse direction; ANN: Artificial neural networks; DTR: Decision tree regressor; LR: Linear regression; MAE: Mean absolute error; MAPE: Mean absolute percentage error; MSE: Mean squared error; R: Pearson correlation coefficient; R^2: Coefficient of determination; RF: Random forest; RMSE: Root mean square error; SVR: Support vector regression; XGBT: Extreme gradient boosting trees.

the smallest RMSE (2.00), the highest R^2 (0.75), and a relatively low MAPE (7.35). In contrast, the RF, XGBT, and DTR models exhibit higher prediction errors in %TD forecasting. The ANN and LR models perform poorly across both tasks, with particularly unsatisfactory results from the ANN model in %TD prediction, where it yields a negative R^2 (−0.23), likely due to the limited dataset size and suboptimal model parameterization. The relatively lower accuracy for %TD compared with %RD can be attributed to its higher experimental variability and sensitivity to uncontrolled factors, such as ambient humidity and fiber deposition heterogeneity, which were not included in the model inputs.

3.2. Shrinkage stability prediction model

Figure 4 illustrates the performance of six machine learning models in predicting the stability of %RD, including RF, SVR, XGBT, ANN, DTR, and LR. Figure 4A-F presents the comparison between the predicted and actual observed values on both the training and testing sets for each model, while Figure 4G-I depicts the evaluation metrics MSE, RMSE, and MAE on the testing set. From the scatter plots

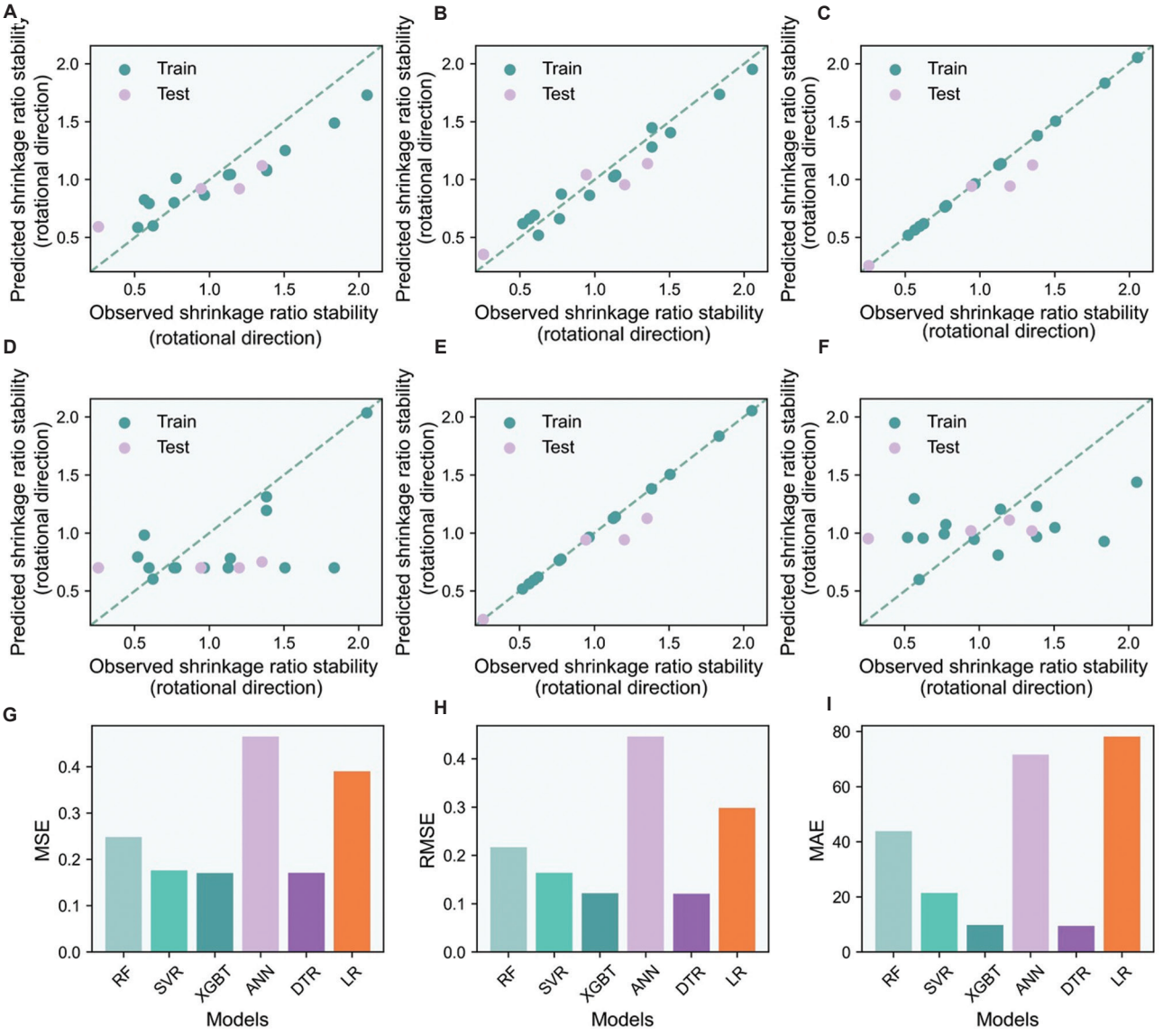

Figure 4. Performance of different machine learning models in predicting the stability of %RD on the test set. (A) RF. (B) SVR. (C) XGBT. (D) ANN. (E) DTR. (F) LR. (G) MSE of the models. (H) RMSE of the models. (I) MAE of the models.

Abbreviations: %RD: Shrinkage ratio (%) in rotational direction; ANN: Artificial neural networks; DTR: Decision tree regressor; LR: Linear regression; MAE: Mean absolute error; MSE: Mean squared error; RF: Random forest; RMSE: Root mean square error; SVR: Support vector regression; XGBT: Extreme gradient boosting trees.

(Figure 4A-F), it is evident that the XGBT and DTR models produce predictions that are more closely aligned with the ideal diagonal line on the test set, indicating superior fitting accuracy and generalization performance. In contrast, the LR, ANN, and SVR models exhibit larger deviations in their predictions. In terms of error metrics, the XGBT and DTR models achieve the lowest values across all three indicators (MSE, RMSE, and MAE), demonstrating the highest accuracy in capturing variations in %RD stability.

Figure 5 presents the performance of six machine learning models in predicting %TD stability, including RF, SVR, XGBT, ANN, DTR, and LR. The fitting plots reveal that the XGBT model exhibits outstanding predictive capability on both the training and testing sets, with nearly all predicted values closely aligned with the ideal diagonal line. RF and SVR also demonstrate strong performance, whereas the ANN and LR models show significant prediction deviations. In particular, LR substantially overestimates or underestimates the stability of several samples, making it the least effective model. This observation is further supported by the bar charts of error metrics, where the XGBT model consistently achieves the

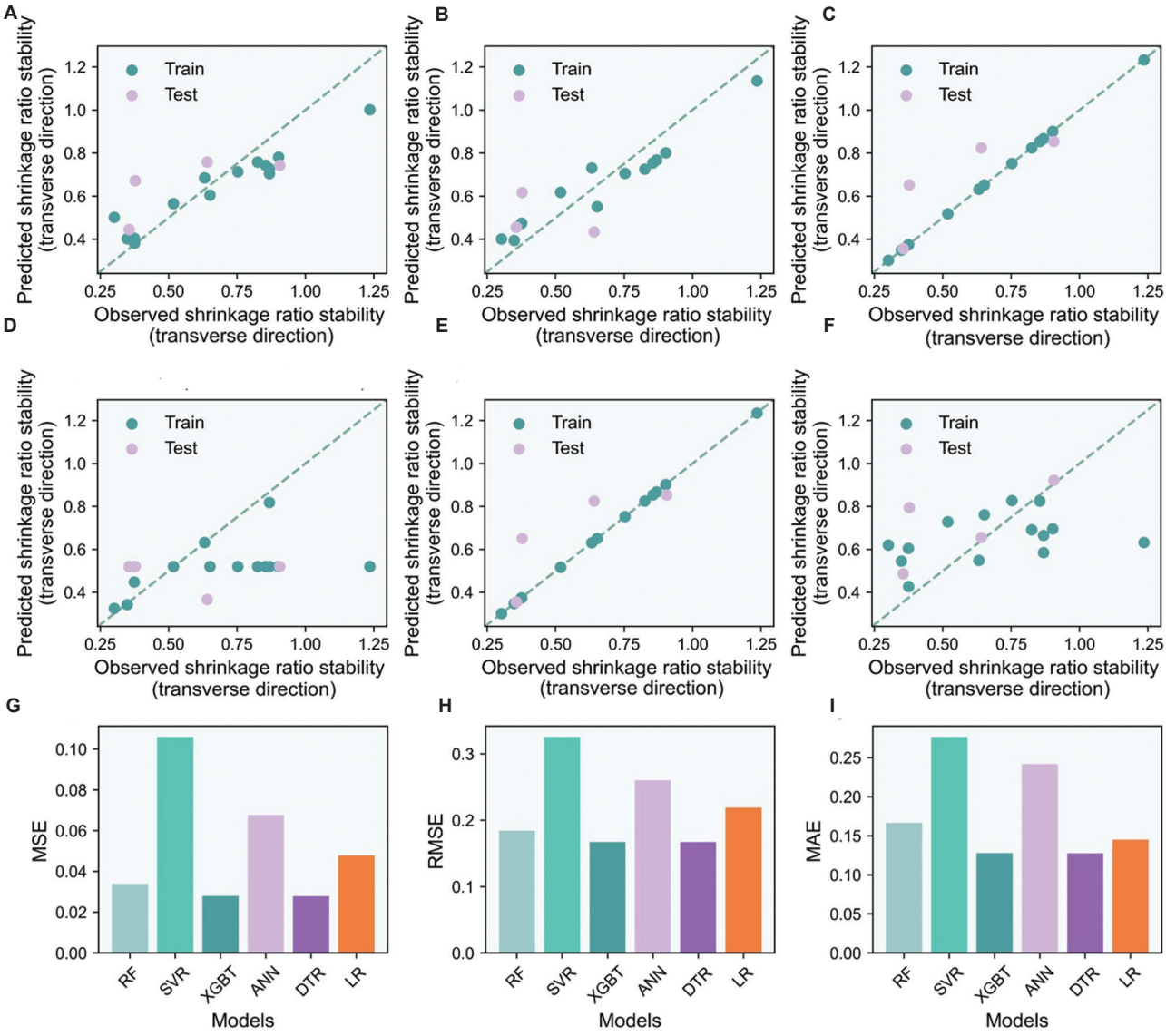

Figure 5. Performance of different machine learning models in predicting the stability of %TD on the test set. (A) RF. (B) SVR. (C) XGBT. (D) ANN. (E) DTR. (F) LR. (G) MSE of the models. (H) RMSE of the models. (I) MAE of the models.

Abbreviations: %TD: Shrinkage ratio (%) in transverse direction; ANN: Artificial neural networks; DTR: Decision tree regressor; LR: Linear regression; MAE: Mean absolute error; MSE: Mean squared error; RF: Random forest; RMSE: Root mean square error; SVR: Support vector regression; XGBT: Extreme gradient boosting trees.

lowest values in MSE and RMSE, confirming its superior accuracy and robustness in modeling TD stability. In contrast, the ANN and LR models yield significantly higher errors, indicating poor predictive reliability. Overall, the results indicate that XGBT is the most effective model for predicting %RD stability and %TD stability, outperforming other approaches in both accuracy and robustness.

3.3. Model interpretation by SHAPs

Figures 6 and 7 present the mean absolute SHAP values for the stability predictions of %RD and %TD, respectively, which quantify the relative importance of the four input features: Applied voltage, TPU concentration, collector speed, and distance between electrodes. These SHAP values represent the average magnitude of each feature's contribution to the model's output across all samples, thereby enabling a global interpretation of feature relevance. However, it is important to note that while SHAP values effectively capture feature importance, they do not indicate the directionality of influence; in other words, they do not reveal whether an increase in a given parameter enhances or diminishes stability. Applied voltage and TPU concentration consistently rank as the most influential factors in both RD and TD stability models, underscoring their critical role in governing shrinkage stability during electrospinning. Voltage controls the electrostatic field strength, directly influencing jet acceleration, elongation, and fiber morphology.[6,11,39-41] Even slight variations can induce significant changes in jet dynamics and deposition patterns, thereby altering internal stress distributions and post-activation stability. TPU concentration affects the solution's viscosity and molecular entanglement,[42,43] helping to stabilize jet morphology and reduce deformation. Speed and distance contribute less, suggesting a more indirect impact. Collector speed can affect fiber alignment,

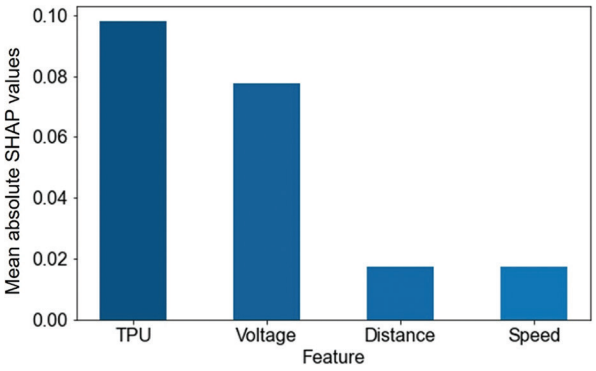

Figure 6. The mean absolute SHAP values of features for the percentage of rotational direction
Abbreviations: SHAP: Shapley additive explanations; TPU: Thermoplastic polyurethane.

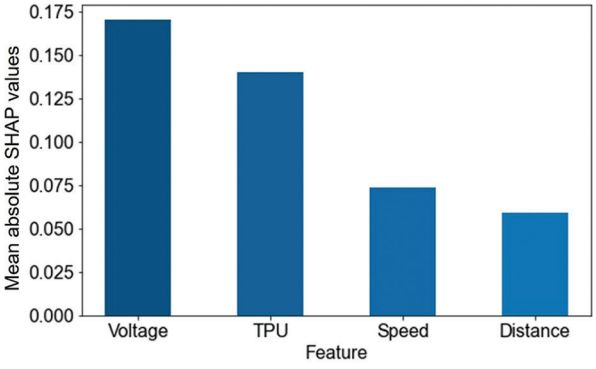

Figure 7. The mean absolute SHAP values of features for the percentage of the transverse direction
Abbreviations: SHAP: Shapley additive explanations; TPU: Thermoplastic polyurethane.

Table 2. Partial results of Pareto front screening obtained by the Monte Carlo method

TPU (%)	Distance (cm)	Speed (rpm)	Voltage (kV)	%RD	%TD	CIW
15	8	701	13	26.36	15.43	0.36
15	9	700	13	25.69	16.48	0.37
15	9	705	13	25.76	16.44	0.37
15	9	707	13	25.78	16.43	0.38
15	9	709	13	25.81	16.41	0.38
15	8	715	13	26.57	15.31	0.38
15	8	716	13	26.58	15.31	0.38
15	9	711	13	25.83	16.40	0.38
15	8	718	13	26.61	15.29	0.38
15	8	723	13	26.68	15.26	0.39
15	8	724	13	26.69	15.25	0.39
15	8	726	13	26.72	15.24	0.39
15	9	727	13	26.03	16.29	0.40
15	9	732	13	26.08	16.27	0.40
15	8	769	14	23.48	17.00	0.41
15	8	770	14	23.49	16.99	0.41
15	8	772	14	23.52	16.99	0.41
15	9	740	13	26.17	16.23	0.41
15	8	773	14	23.53	16.99	0.41
15	8	745	13	26.94	15.15	0.41
15	8	776	14	23.58	16.98	0.42
15	9	745	13	26.22	16.21	0.42
15	9	745	13	26.22	16.21	0.42
15	8	778	14	23.60	16.98	0.42
15	8	780	14	23.63	16.98	0.42

Abbreviations: %RD: Shrinkage ratio (%) in rotational direction; %TD: Shrinkage ratio (%) in transverse direction; CIW: Confidence interval width; TPU: Thermoplastic polyurethane.

potentially influencing %RD more than %TD. Distance influences jet flight time and solvent evaporation, but its effect appears less consistent. Although SHAP values cannot reveal directional effects, the results highlight voltage and polymer concentration as key parameters for controlling shape stability.

3.4. Monte Carlo simulation-based optimization

In electrospinning, required shrinkage ratios (%RD and %TD) vary across applications. To enable customized control of target shrinkage while maximizing process stability, we developed a process optimization framework that combines shrinkage prediction and stability prediction models. Using %RD = 25% and %TD = 15% with a ± 2% tolerance as a representative case to demonstrate the optimization process, 10,000 sets of process parameters were randomly generated via Monte Carlo sampling. These parameter sets were first evaluated by the shrinkage prediction model to identify those that met the target range. The qualified candidates were then assessed using the stability prediction model, which outputs the predicted CIW for both %RD and %TD. Since a smaller CIW indicates higher process stability, the parameter set with the minimum combined CIW was selected as the optimal condition. This approach enables simultaneous optimization of shrinkage accuracy and process robustness in electrospinning.

Table 2 presents a subset of process conditions generated via Monte Carlo simulation and screened using the shrinkage prediction model to meet the target values of %RD = 25% ± 2% and %TD = 15% ± 2%. Although all candidates fall within the target range, their predicted CIW vary from 0.36 to 0.42. The combination with the lowest CIW (TPU = 15%, distance = 8 cm, speed = 701 rpm, voltage = 13 kV) shows the highest predicted stability, indicating reduced sensitivity to process variability while maintaining the desired shrinkage levels.

Figure 8 shows the scatter plots of %RD and %TD for the Pareto-optimal sets across four key process variables, including TPU concentration (%), distance (cm), speed (rpm), and voltage (kV). As the TPU concentration was fixed at 15%, no variation is observed in Figure 8A. Figure 8B shows minor fluctuations in %RD and %TD at collector distances of 8 cm and 9 cm. In Figure 8C, %RD decreased notably at speeds above 800 rpm, whereas %TD

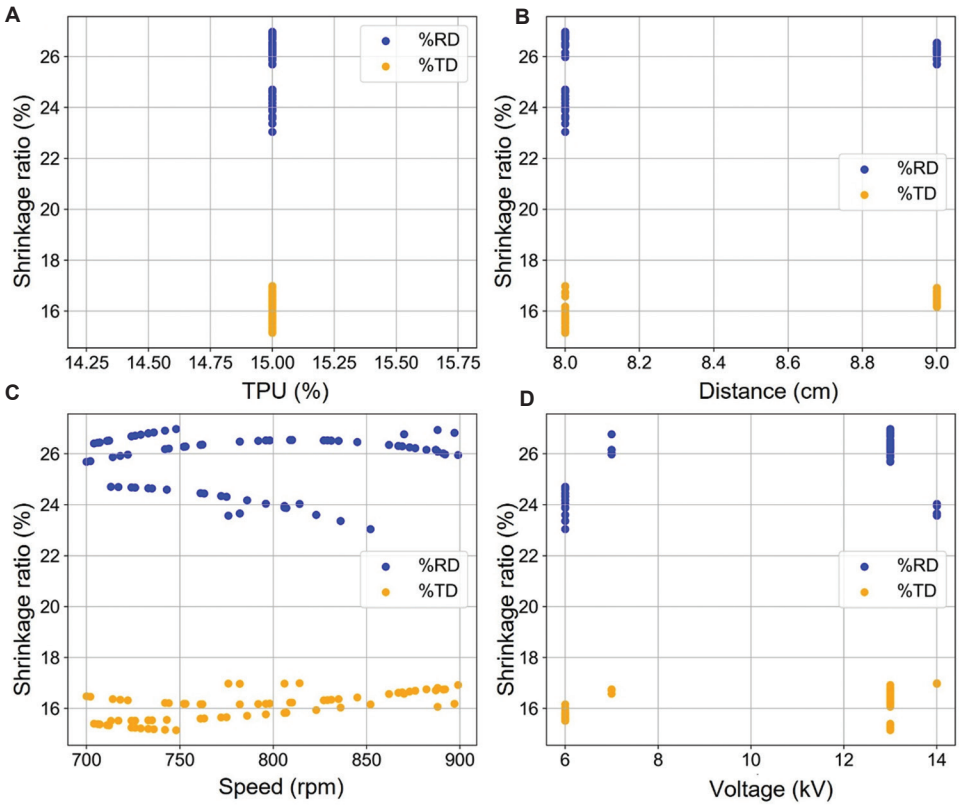

Figure 8. Scatter plots of each feature versus %RD and %TD in the results of the Pareto front. (A) TPU concentration (%). (B) Distance (cm). (C) Speed (rpm). (D) Voltage (kV).
Abbreviations: %RD: Shrinkage ratio (%) in rotational direction; %TD: Shrinkage ratio (%) in transverse direction; TPU: Thermoplastic polyurethane.

exhibited a slight increase. In Figure 8D, both %RD and %TD elevated with increasing voltage, indicating voltage as a key parameter in shrinkage control. These results demonstrate that meeting shrinkage targets alone is insufficient for ensuring process reliability. Incorporating CIW as a stability metric allows selection of process conditions that are both accurate and robust, providing a practical basis for optimizing electrospinning parameters in scalable production.

The machine learning models in this study were developed and validated using experimental data from controlled electrospinning trials of TPU membranes, with repeated measurements used to capture both mean shrinkage and variability via the CIW metric. Monte Carlo optimization was conducted on these validated models within practical parameter ranges, ensuring physically relevant predictions. The modeling framework is material-agnostic and, in principle, applicable to other polymers; extending it requires retraining with high-quality data specific to the target material to capture its unique processing-structure-property relationships. Direct experimental validation of our multi-objective optimization framework was not performed due to the high cost and time required. Future work will address this to further enhance the model's robustness and generalizability.

4. Conclusion

This paper presents a data-driven framework that combines machine learning with Monte Carlo simulation to achieve accurate and stable control of biaxial shrinkage in electrospun membranes, even under limited data conditions.

By modeling shrinkage ratios in both RD and TD along with their stability, the framework enables multi-objective optimization of process parameters. Among the evaluated models, SVR demonstrated the highest accuracy in predicting shrinkage behavior, achieving an RMSE of 1.04% for RD and 2.00% for TD. XGBT was most effective in forecasting shrinkage stability, with RMSE of 0.16 for RD and 0.17 for TD. SHAP analysis identified applied voltage and TPU concentration as the most influential factors governing shrinkage stability, whereas collector speed and distance between electrodes had relatively minor effects.

Using the Monte Carlo-based parameter screening, the framework successfully identified sets of process parameters that met predefined shrinkage targets while minimizing variability.

In conclusion, this methodology offers a robust and generalizable strategy for high-variability, small-sample manufacturing scenarios, with significant potential for broader applications in smart material design and precision fabrication.

Acknowledgments

None.

Funding

This work was funded by the National Natural Science Foundation of China (grant no.: 52031005, 52571227), Natural Science Foundation of Shanghai (grant no.: 24ZR1438200), Shanghai Academy of Spaceflight Technology Joint Research Fund (grant no.: USCAST2023-19), Equipment Development Department Huiyan Action (grant no.: 5D3D1365), and China Scholarship Council (grant no.:202406230025).

Conflict of interest

The authors declare they have no competing interests.

Author contributions

Conceptualization: Wei Min Huang, Shiyu He
Formal analysis: Shiyu He, Li Cong Huang
Investigation: Shiyu He, Wei Min Huang, Fei Xiao
Methodology: Shiyu He, Chentong Gao, Runzhi Lu
Writing–original draft: Shiyu He, Wei Min Huang
Writing–review & editing: Shiyu He, Wei Min Huang, Fei Xiao

Ethics approval and consent to participate

Not applicable.

Consent for publication

Not applicable.

Availability of data

Data are available from the corresponding author upon reasonable request.

References

1. Cheng F, Song D, Li H, Ravi SK, Tan SC. Recent progress in biomedical scaffold fabricated via electrospinning: Design, fabrication and tissue engineering application. *Adv Funct Mater*. 2025;35(1):2406950.

   doi: 10.1002/adfm.202406950

2. Cho Y, Beak JW, Sagong M, Ahn S, Nam JS, Kim ID. Electrospinning and nanofiber technology: Fundamentals, innovations, and applications. *Adv Mater*. 2025;37:2500162.

   doi: 10.1002/adma.202570190

3. Wang C, Su Y, Xie J. Advances in electrospun nanofibers: Versatile materials and diverse biomedical applications. *Acc*

Mater Res. 2024;5(8):987-999.

doi: 10.1021/accountsmr.4c00145

4. Yadav S, Sharma A, Kurmi BD, *et al*. Nanofiber drug delivery systems: Recent advances in nanofabrication and their role in targeted therapy in cancer, neurodegenerative, and cardiovascular diseases. *Polym Adv Technol*. 2025;36(5):e70198.

   doi: 10.1002/pat.70198

5. Wang Z, Gao C, Yang R, Xiong F. The interface effect of electrospun fiber promotes wound healing. *Macromol Rapid Commun*. 2025:2500038.

   doi: 10.1002/marc.202500038

6. Wang J, You C, Xu Y, Xie T, Wang Y. Research advances in electrospun nanofiber membranes for non-invasive medical applications. *Micromachines*. 2024;15(10):1226.

   doi: 10.3390/mi15101226

7. Wu H, Zheng Y, Zeng Y. Fabrication of helical nanofibers via co-electrospinning. *Ind Eng Chem Res*. 2015;54(3):987-993.

   doi: 10.1021/ie504305s

8. Zhao Y, Miao X, Lin J, *et al*. Coiled plant tendril bioinspired fabrication of helical porous microfibers for crude oil cleanup. *Glob Challenges*. 2017;1(3):1600021.

   doi: 10.1002/gch2.201600021

9. Wang M, Li W, Tang G, Garciamendez Mijares CE, Zhang YS. Engineering (bio) materials through shrinkage and expansion. *Adv Healthc Mater*. 2021;10(14):2100380.

   doi: 10.1002/adhm.202100380

10. Mandal A, Chatterjee K. 4D printing for biomedical applications. *J Mater Chem B*. 2024;12(12):2985-3005.

    doi: 10.1039/D4TB00006D

11. Fang F, Wang H, Wang H, *et al*. Stimulus-responsive shrinkage in electrospun membranes: Fundamentals and control. *Micromachines*. 2021;12(8):920.

    doi: 10.3390/mi12080920

12. Zaarour B, Liu W, Omran W, *et al*. A mini-review on wrinkled nanofibers: Preparation principles via electrospinning and potential applications. *J Ind Text*. 2024;54:15280837241255396.

    doi: 10.1177/15280837241255396

13. Wang CC, Zhao Y, Purnawali H, Huang WM, Sun L. Chemically induced morphing in polyurethane shape memory polymer micro fibers/springs. *React Funct Polym*. 2012;72:757-764.

    doi: 10.1016/j.reactfunctpolym.2012.07.013

14. Aadithiya D, Fang FY, Wang H, Huang WM. Stimulus-induced shrinkage in electrospun polymeric fibres: An investigation on thickness of prestretched shell and prestrain via finite element analysis. *Fibers Polym*. 2023;24(2):525-536.

    doi: 10.1007/s12221-023-00133-8

15. Ahmadi Bonakdar M, Rodrigue D. Electrospinning: Processes, structures, and materials. *Macromol*. 2024;4(1):58-103.

    doi: 10.3390/macromol4010004

16. El Ferik S, Adeniran AA. Modeling and identification of nonlinear systems: A review of the multimodel approach-Part 2. *IEEE Trans Syst Man Cybern Syst*. 2016;47(7):1160-1168.

    doi: 10.1109/TSMC.2016.2560129

17. Subeshan B, Atayo A, Asmatulu E. Machine learning applications for electrospun nanofibers: A review. *J Mater Sci*. 2024;59(31):14095-14140.

    doi: 10.1007/s10853-024-09994-7

18. Shastry T, Basdogan Y, Wang ZG, Kunmar SK, Carbone MR. Machine learning-based discovery of molecular descriptors that control polymer gas permeation. *J Membr Sci*. 2024;697:122563.

    doi: 10.1016/j.memsci.2024.122563

19. Ignacz G, Beke AK, Toth V, Szekely G. A hybrid modelling approach to compare chemical separation technologies in terms of energy consumption and carbon dioxide emissions. *Nat Energy*. 2025;10(3):308-317.

    doi: 10.1038/s41560-024-01668-7

20. Lee S, Shirts MR, Straub AP. Molecular fingerprint-aided prediction of organic solute rejection in reverse osmosis and nanofiltration. *J Membr Sci*. 2024;705:122927.

    doi: 10.1016/j.memsci.2024.122927

21. He S, Wang Y, Zhang Z, *et al*. Interpretable machine learning workflow for evaluation of the transformation temperatures of TiZrHfNiCoCu high entropy shape memory alloys. *Mater Des*. 2023;225:111513.

    doi: 10.1016/j.matdes.2022.111513

22. He SY, Xiao F, Hou RH, *et al*. Accelerated learning and co-optimization of elastocaloric effect and stress hysteresis of elastocaloric alloys. *Rare Met*. 2024;43(12):6606-6624.

    doi: 10.1007/s12598-024-02827-1

23. Rigatti SJ. Random forest. *J Insur Med*. 2017;47(1):31-39.

    doi: 10.17849/insm-47-01-31-39.1

24. Osman AIA, Ahmed AN, Chow MF, Huang YF, EI-Shafle A. Extreme gradient boosting (Xgboost) model to predict the groundwater levels in Selangor Malaysia. *Ain Shams Eng J*. 2021;12(2):1545-1556.

    doi: 10.1016/j.asej.2020.11.011

25. Zou J, Han Y, So SS. Overview of artificial neural networks. In: *Artificial Neural Networks: Methods and Applications*.

Springer; 2009.

doi: 10.1007/978-1-60327-101-1_2

26. Su X, Yan X, Tsai CL. Linear regression. *Wiley Interdiscip Rev Comput Stat*. 2012;4(3):275-294.

doi: 10.1002/wics.1198

27. Mosca E, Szigeti F, Tragianni S, Gallagher D, Groh G. SHAP-based explanation methods: A review for NLP interpretability. In: *Proceedings of the 29th International Conference on Computational Linguistics*; 2022.

doi: 2022.coling-1.406

28. Antwarg L, Miller R M, Shapira B, Rokach L. Explaining anomalies detected by autoencoders using Shapley Additive Explanations. *Expert Syst Appl*. 2021;186:115736.

doi: 10.1016/j.eswa.2021.115736

29. Van den Broeck G, Lykov A, Schleich M, Suciu D. On the tractability of SHAP explanations. *J Artif Intell Res*. 2022;74:851-886.

doi: 10.1613/jair.1.13283

30. Li Z. Extracting spatial effects from machine learning model using local interpretation method: An example of SHAP and XGBoost. *Comput Environ Urban Syst*. 2022;96:101845.

doi: 10.1016/j.compenvurbsys.2022.101845

31. Zhang J, Ma X, Zhang J, *et al*. Insights into geospatial heterogeneity of landslide susceptibility based on the SHAP XGBoost model. *J Environ Manag*. 2023;332:117357.

doi: 10.1016/j.jenvman.2023.117357

32. Wang H, Liang Q, Hancock JT, Khoshgoftaar TM. Feature selection strategies: A comparative analysis of SHAP value and importance based methods. *J Big Data*. 2024;11(1):44.

doi: 10.1186/s40537-024-00905-w

33. Harrison RL. Introduction to monte carlo simulation. *AIP Conf Proc*. 2010;1204:17.

doi: 10.1063/1.3295638

34. Metropolis N, Ulam S. The monte carlo method. *J Am Stat Assoc*. 1949;44(247):335-341.

doi: 10.2307/2280232

35. Raychaudhuri S. Introduction to monte carlo simulation. In: *Proceedings of the 2008 Winter Simulation Conference*; 2008.

doi: 10.1109/WSC.2008.4736059

36. Kroese DP, Rubinstein RY. Monte carlo methods. *Wiley Interdiscip Rev Comput Stat*. 2012;4(1):48-58.

doi: 10.3390/nano15020117

37. Kroese DP, Brereton T, Taimre T, *et al*. Why the Monte Carlo method is so important today. *Wiley Interdiscip Rev Comput Stat*. 2014;6(6):386-392.

doi: 10.1002/wics.1314

38. Gao H, He W, Zhao YB, Opris DM, Xu G, Wang J. Electret mechanisms and kinetics of electrospun nanofiber membranes and lifetime in filtration applications in comparison with corona charged membranes. *J Membr Sci*. 2020;600:117879.

doi: 10.1016/j.memsci.2020.117879

39. Tong HW, Wang M. Electrospinning of fibrous polymer scaffolds using positive voltage or negative voltage: A comparative study. *Biomed Mater*. 2010;5(5):054110.

doi: 10.1088/1748-6041/5/5/054110

40. Liao Y, Wang R, Tian M, Qiu C, Fane AG. Fabrication of polyvinylidene fluoride (PVDF) nanofiber membranes by electro spinning for direct contact membrane distillation. *J Membr Sci*. 2013;425:30-39.

doi: 10.1016/j.memsci.2012.09.023

41. Mi HY, Jing X, Jacques BR, Turng LS, Peng XF. Characterization and properties of electrospun thermoplastic polyurethane blend fibers: Effect of solution rheological properties on fiber formation. *J Mater Res*. 2013;28(17):2339-2350.

doi: 10.1016/j.memsci.2012.09.023

42. Lem KW, Haw JR, Curran S, *et al*. Effect of hard segment molecular weight on dilute solution properties of ether based thermoplastic polyurethanes. *Spectroscopy*. 2013;1:11-18.

doi: 10.13189/nn.2013.01030

43. Awad M, Khanna R. Support vector regression. In: *Efficient Learning Machines: Theories, Concepts, and Applications for Engineers and System Designers*. Springer; 2015.

doi: 10.1007/978-1-4302-5990-9

ACCSCIENCE PUBLISHING

International Journal of AI for Materials and Design

ORIGINAL RESEARCH ARTICLE

Structural health monitoring of metal structures using an improved carbon nanotube bucky paper sensor and LSTM neural network

Faeez Masurkar*

Department of Engineering, Faculty of Engineering and IT, The British University in Dubai, Dubai International Academic City, Dubai, United Arab Emirates

Abstract

In this paper, an improved fabrication method is presented for fabricating carbon nanotube (CNT) based multi-functional bucky paper (CNT-BP) sensors that will be primarily used for adaptive sensing in structural health monitoring applications. A large number of BPs were fabricated using multi-walled CNTs with varying methanol-CNT compositions, sonication times, temperatures, curing durations, membrane thicknesses, and electrode placements to determine the optimal configuration for large-scale production. The obtained optimal configuration of the ingredients that yields an adequate sensitivity and ductility of the CNT-BP was then employed for measuring the crack propagation behavior in the fatigued samples. Further, a long short-term memory (LSTM)-based neural network was proposed for prognosis in a metallic plate with fatigue crack propagation. The actual crack lengths of the fatigue crack obtained by the high-speed digital camera were correlated with that predicted by the CNT-BP-based model and LSTM, showing good agreement. Thus, the present study demonstrates that the proposed improved method of CNT-BP is highly efficient in the diagnosis and prognosis of fatigue cracks in metallic structures.

Keywords: Carbon nanotube; Bucky paper; Adaptive sensing; Piezo-resistivity; Fabrication; Structural health monitoring; Metallic structures

***Corresponding author:**
Faeez Masurkar
(faeez.masurkar@buid.ac.ae)

Citation: Masurkar F. Structural health monitoring of metal structures using an improved carbon nanotube bucky paper sensor and LSTM neural network. *Int J AI Mater Design*. 2025;2(3):78-87. doi: 10.36922/IJAMD025310028

Received: July 29, 2025

Revised: September 2, 2025

Accepted: September 8, 2025

Published online: September 23, 2025

1. Introduction

Metallic structures undergo a variety of degradation mechanisms, such as fatigue cracks, notches, and corrosion. These cracks under the action of loads can propagate further and result in the breakage of the structure. Therefore, it is extremely important to investigate the health status of these structures from time to time to ensure their structural integrity is above the required limit and avoid potential mishaps.[1-3] These can be achieved in several ways by employing different types of sensors. One of the sensors that facilitate self-sensing of the material changes is the use of a carbon nanotube (CNT)-based bucky paper (BP) sensor for measuring the crack propagation in specimen. This type of sensor also can be used in numerous other applications as found in literature.

Luo *et al.*[4] developed an *in situ* structural health monitoring system for polymer matrix composites using BP embedded between the laminas. The BP-based testing is widely used for damage and load sensing in aerospace and defense applications due to

its low density, high electrical conductivity, and significant load sensitivity. Wang *et al.*[5] correlated the electrical resistance of BP sensor with the strain for monitoring the health of composite structures. It can be seen that the BP sensor has very high strain sensitivity in the static tensile test. Lu *et al.*[6] employed an omnidirectional, nanomaterial-based sensor for impact damage detection in composite structures. The influence of both tensile and low-velocity impact on the BP sensors was also further investigated. Lu *et al.*[7] proposed a real-time monitoring of resin infiltration process in vacuum-assisted molding of composites with CNT-BP sensors. Her *et al.*[8] employed CNT-BP sensor on a complex surface for monitoring the strain and temperature at the critical areas of the sample. Yee *et al.*[9] developed an improved fabrication process for enhancing the sensitivity of the BP sensor for strain monitoring applications. Yang *et al.*[10] proposed a flexible, lightweight, and low-thickness BP sensor for high-performance electromagnetic interference shielding materials for catering to the demand for smart and wearable electronic devices. De Paula Santos *et al.*[11] investigated the effect of incorporating CNT-BP on the interlaminar fracture toughness by testing under cyclic loading in Mode I and II. Ahmed *et al.*[12] investigated the efficiency of a CNT sensor to detect and monitor fatigue crack initiation and propagation in metal structures. The sensor consisted of a non-woven carrier fabric with a thin film of CNT that is superglued to the structure's surface using an epoxy adhesive. Jiang *et al.*[13] employed CNT-BP sensors to monitor the structural health status of composite structures subjected to ambient vibration condition. Hehr *et al.*[14] employed CNT thread in unidirectional glass fiber composites to identify the onset of track crack growth, matrix cracking, and differentiate between crack breathing and closing states. This information is obtained by analyzing the resistance response of the thread with a simple Wheatstone bridge circuit and a low-speed data acquisition system. Ribeiro *et al.*[15] reviewed the general characteristics, physical properties, and processing conditions of CNT-BP and its polymer composites. Wan *et al.*[16] investigate the *in situ* monitoring of Mode I interlaminar crack propagation behavior in woven glass fiber-reinforced epoxy (WGF/epoxy) composite laminates. Lecompte *et al.*[17] employed two different optical measurement techniques for the detection of cracks at the surface of a concrete beam being subjected to flexural loading. The primary aim of the study was to examine which of the two methods appears to be the most suitable for crack detection. Moreover, it was shown that it is possible to detect the appearance and evolution of cracks, even before the cracks become visually detectable. Ashrafi *et al.*[18] focused on the application of epoxy nanocomposite thin film sensors for continuous monitoring of crack evolution in metallic structures. The primary aim was to monitor the resistance change in these nanocomposite films, as cracks develop and propagate in the metallic host structure. Bian *et al.*[19] proposed a facile technique to enhance performance of carbon fiber composites through interlaminar insertion of aligned CNT sheets. The inserted CNT sheets also provide electrical conductivity in the composites even at a low CNT loading below the electrical percolation threshold established for CNT-filled composites. Lin *et al.*[20] presented a flexible CNT-based strain sensor that has a significant potential for applications in human motion monitoring systems and electronic skins in water. Olson *et al.*[21] investigated a CNT-based sensor to detect crack propagation in aluminum structures underneath composite patching. Initial tests were conducted to determine the correct procedure and materials to properly fabricate a highly sensitive CNT-based sensor.

The present work proposes an improved fabrication process for the CNT-BP for measuring the fatigue crack propagation in a metallic specimen under uniaxial loading. First, an optimal composition for different ingredients required for fabricating CNT-BP was obtained and further optimized for its sensing architectures. This includes the CNT-BP sensor size, sensing locations, and number of sensing points, and the silver ink electrode placement. It is found that the fabricated CNT-BP sensor has enhanced sensitivity and has adequate ductility so that it can be easily superglued to the test structure. Moreover, a strong correlation was observed among the actual crack lengths measured by a high-speed optical camera, the crack estimates based on CNT-BP resistance, and the predictions from the long short-term memory (LSTM) neural network. This shows that CNT-BP has promising potential for fatigue crack prognosis and diagnosis without the need for complex equipment, signal processing, and measurement units.

The rest of the paper is organized as follows. The theoretical model for prediction of crack length is presented in Section 2, while the CNT-BP fabrication process is detailed in Section 3. Section 4 discusses the LSTM neural network for prognosis of a metallic plate with fatigue crack propagation, and the experimental study is discussed in Section 5. The results obtained are discussed in Section 6, and lastly, the concluding remarks and future study are given in Section 7. The following section discusses the theoretical model for crack length prediction based on the measurement of resistance change of CNT-BP as a function of fatigue cycles.

2. Theoretical model for prediction of crack length

A measurement model to correlate between the fatigue crack at any instant of time and the electrical resistance

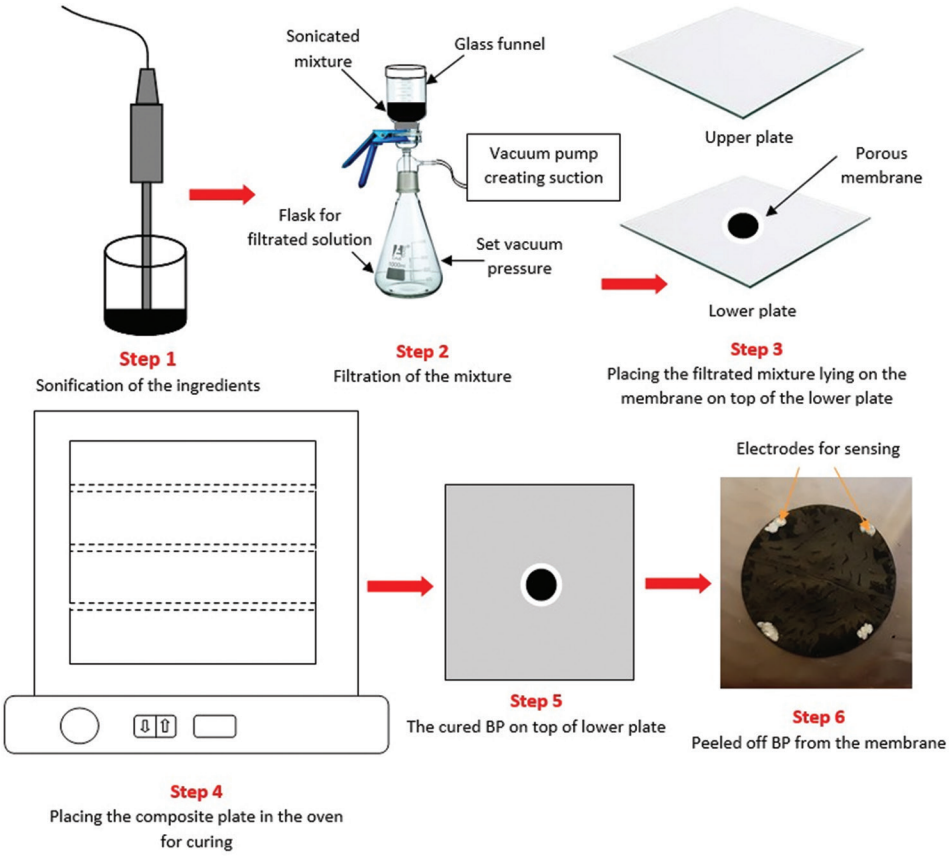

Figure 1. Schematic of the complete setup employed for fabrication of CNT-BP.
Abbreviations: BP: Bucky paper; CNT: Carbon nanotube.

of the CNT-BP specimen is required. This model must consider the dimensions of the CNT-BP specimen, positioning of the silver ink electrode, baseline resistance, and subsequent changes in the resistivity due to fatigue loading. Since the loading is purely uniaxial and with Mode I, the crack growth is perpendicular to the direction of the uniaxial loading. The relation between the resistance of the BP and crack length can be established as follows,

$$R = \frac{\rho d}{t(D - \hat{a})} \quad \text{(I)}$$

which can be re-written as:

$$\hat{a} = D - \left(\frac{\rho d}{Rt}\right) \quad \text{(II)}$$

In the above equations, R is the measured electrical resistance of the CNT-BP, ρ is the resistivity of embedded CNT-BP, d is the length of CNT-BP between electrodes, t is the thickness of CNT-BP, D is the diameter of omnidirectional CNT-BP specimen, and $\hat{a}$ is the estimated fatigue crack length.

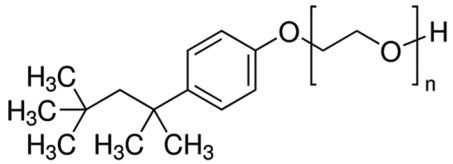

Figure 2. Chemical structure of Triton X-100

3. Fabrication process of the CNT-BP membrane

The improved fabrication process used to prepare the BP membranes is shown schematically in Figure 1. The key ingredients used were multi-walled CNTs (MWCNTs), Triton X-100 (t-octylphenoxypolyethoxyethanol, polyethylene glycol tert-octylphenyl ether), methanol, nitric acid solution, and distilled water. Triton X-100 was procured through Sigma-Aldrich (USA), and its chemical structure is shown Figure 2. The MWCNT used were obtained from US Research Nanomaterials (Houston, Texas, USA). These CNTs have an average outer diameter of 10–30 nm with an average length of 15–30 μm and purity of 90% as per the specifications given by supplier.

The properties of CNTs are as follows: density of 2100 kg/cu.m, specific surface area of $200\ m^2/g$, and conductivity $>10^4 S/m$. The experimental setup for fabricating the CNT-BP consists of a sonicator, a filtering setup equipped with vacuum pump that creates the controlled and pre-determined vacuum for sucking the liquid, metallic plates that house the CNT-BP, a vacuum oven that is used to cure the CNT-BP, and the CNTs. The filter membrane is Deschem with an outer diameter (OD) of 150 mm and a membrane of cellulose acetate with thickness of 45 μm.

For the fabrication procedure, 300 mg of MWCNT were mixed in 30 mL of methanol solution and 3 mL of Triton X-100, followed by 30 mL of distilled water. This high-concentration mixture was thoroughly ultrasonicated with a tip sonicator. The sonification time was set to roughly 30 mins. The process also assists in evaporation of methanol solvent and yields a highly viscous slurry for further process. Before transferring the slurry to the filtration process, a glass rod was used to stir the mixture to improve the overall homogeneity. Once the CNT-BP membrane is cured in the oven, it is peeled off from the membrane and is ready to use for testing purposes.

The major contribution of this paper is the development of improved fabrication process of CNT-BP, which was achieved by obtaining an optimal configuration of ingredients by conducting a significant number of trials. The use of Triton X-100 facilitates the production of a highly ductile and sensitive CNT-BP. The excess amount of Triton X-100 after curing was then washed off with nitric acid. Validated in our laboratory for multiple times, this procedure yields a CNT-BP that has significant potential for structural health monitoring applications of isotropic or anisotropic materials.

4. LSTM neural network

The LSTM neural network was employed in this study for prognosis of the metallic plate under fatigue loading. This type of neural network accurately predicts the time-series data with information fusion capabilities exhibiting multiple-input multiple-output (MIMO) and left/right cracks under propagation. It also facilitates the alleviation of the gradient vanishing problem in recurrent neural network by incorporating LSTM unit, thereby having enhanced prediction accuracy.[22-25] A schematic illustration of the LSTM model is shown in Figure 3. Crack propagation under increasing fatigue cycles is a complicated process; therefore, surrogate models based on machine learning are gaining attention for predicting crack length. It also facilitates automatic damage-sensitive feature extraction through the data pattern analysis in the measured experimental data.

Figure 3 shows the repeating module of an LSTM and how the information flows across the sequential time steps. In the figure, x_t is the input at time t, y_{t-1} is the hidden state from the previous step, y_t is the hidden state at the current time step (output of the LSTM). There are four interacting layers in LSTM controlling the information flow. The forget gate, whose operation is given as:

$$f_t = \rho(W_f \cdot [y_{t-1}, x_t] + b_f) \quad \text{(III)}$$

where W_f and b_f are the weight and bias parameters, respectively, and ρ is the sigmoid activation function. The function decides what portion of the previous cell state should be forgotten. The input gate is given as,

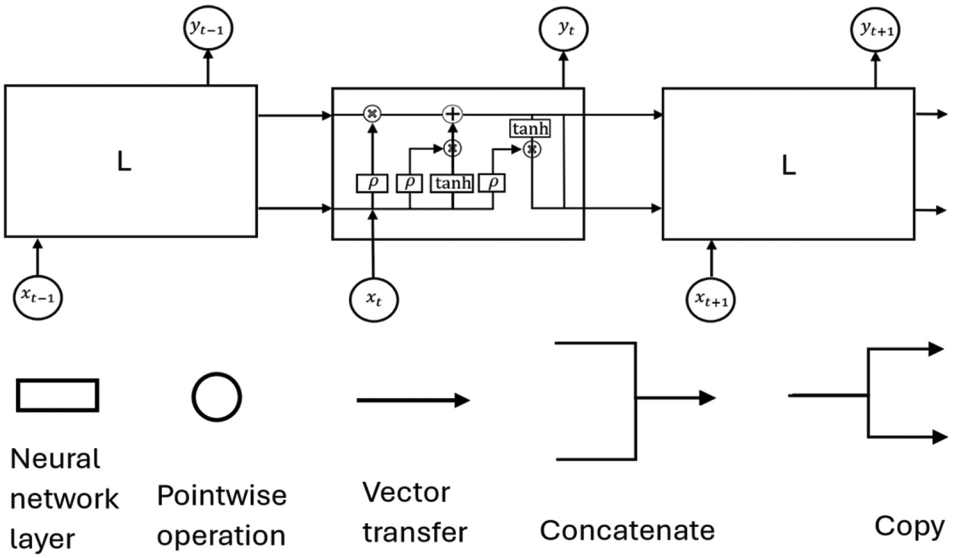

Figure 3. Schematic illustration of the long short-term memory (LSTM) model encompassing the repeating module and four interacting layers.[26]

$$i_t = \rho(W_i \cdot [y_{t-1}, x_t] + b_i) \quad \text{(IV)}$$

The input gate decides how much of the new information should be added to the cell state. The candidate cell state can be given as:

$$C_t = \tanh(W_c \cdot [y_{t-1}, x_t] + b_c) \quad \text{(V)}$$

The cell state decides what part of the new candidate values potentially be added to the cell state. The output gate is given as:

$$o_t = \rho(W_0 \cdot [y_{t-1}, x_t] + b_0) \quad \text{(VI)}$$

The output gate decides what part of the cell state will be the output at the hidden state h_t. The cell state is updated in two steps:

$$C_t = f_t \cdot C_{t-1} + i_t \cdot \widehat{C_t} \quad \text{(VII)}$$

The forget gate controls what to keep or discard from the past, and the input gate and candidate state add new information. Finally, the hidden state or the output of the LSTM cell is computed as:

$$h_t = o_t \cdot \tanh(C_t) \quad \text{(IX)}$$

This ensures that the hidden state is regulated and is not just the raw memory value. The experimental study is discussed in the following section.

5. Experimental study

In this section, the details of the experimental study related to the metallic plate testing with CNT-BP are given. The details of the testing scheme and experimental setup are given in the following subsection.

5.1. Experimental setup for testing

The loading mechanism applied to the test samples is shown in Table 1. Three types of fatigue tests were conducted, and test 1 shows the total life of the sample which resulted in its breakage. The samples were fatigued with the help of an accelerated fatigue machine (MTS 370) with a load capacity 25 kN. The specimens were fatigued under tension-tension stress-controlled condition with stress ratio of 0.1. Further, the complete components used in the experimental study are shown in Figure 4. A customized attachment holding the specimen within the upper and lower jaws of the MTS 370 was fabricated. A small hole was created with two notches on its periphery in horizontal direction to increase stress concentration and facilitate crack initiation and stable propagation with an increase of fatigue cycles.[27-29]

Two CNT-BPs of same shape and size were superglued near these notch locations, as shown in Figure 4. The outer periphery of CNT-BP was well aligned with the location of the notch, where crack is about to initiate. Moreover, an optical camera was employed to measure the actual crack length from the backside of the sample as a function of fatigue cycles. The purpose of fatigue test 1 is to determine the life of specimen. Tests 2 and 3 were employed for measuring resistance change of CNT-BP as a function of fatigue cycles. For brevity, only the results from test 3 are shown herein. Nevertheless, the nature of the results of CNT-BP resistance change measurement and crack length prediction is almost similar. The results and discussions of the study are presented in the following section.

Table 1. The loading mechanism for the fatigue test

Loading conditions	Fatigue test 1	Fatigue test 2	Fatigue test 3
Load	1–10 kN; R=0.1	1.5–15 kN; R=0.1	1.5–15 kN; R=0.1
Loading frequency	10 Hz	10 Hz	10 Hz
Fatigue life	Test aborted at 760,000 cycles resulting in breakage	115,087 cycles	119,652 cycles

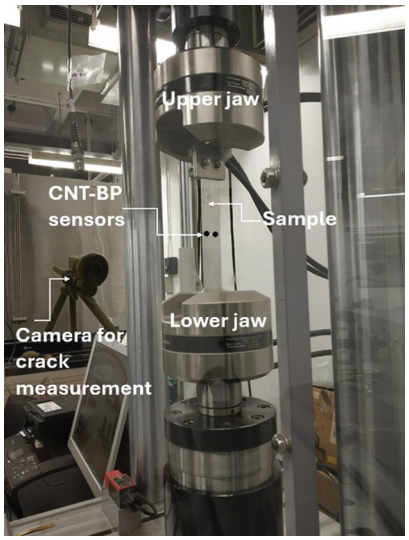

Figure 4. Experimental arrangement for fatigue crack propagation measurement using an optical camera and CNT-BP sensors
Abbreviations: BP: Bucky paper; CNT: Carbon nanotube

6. Results and discussion

The dimensions and intrinsic resistance of each BP were measured using a multimeter before being affixed to the specimen with superglue. These resistance values of the BP serve as the baseline measurements, providing a reference for all future measurements. The dimensions between each of the silver ink electrodes were also measured, forming a part of the theoretical model and accounted by parameter d in Equations I and II. It is worth noting that before affixing the CNT-BP to test specimen, the intrinsic values of the BP

serving as the baseline measurements were measured at five different times and with different multimeters. However, a single stable value was noted in each case, confirming that the baseline measurements are reproducible. Several fatigue tests were conducted on different Al 7075 specimens as detailed in Table 1. The stable resistance of the CNT-BP affixed on the left of the hole is 5.6 Ω, whereas that on the right is 5.8 Ω, as shown in Figure 5A and B. Only the baseline value measured from CNT-BP placed near the right hole is shown for demonstration purposes. The specimens were loaded to different fatigue cycles, and the resistance values of the BP were obtained simultaneously. However, the values were recorded at regular intervals. These resistance values were further used in Equations I and II to determine the correlated fatigue crack length, which is shown in Figures 6A and B for the left and right cracks, respectively.

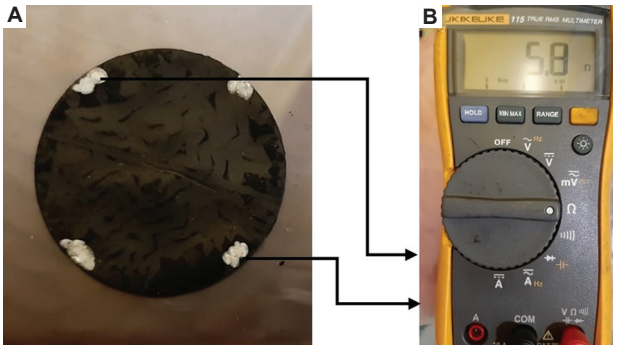

Figure 5. The improved bucky paper (A) and its measured resistance (B)

It can be seen that the error on the right crack measurement is less than that on the left crack. It could be because the initial resistance of right BP is slightly higher than that of the left BP, demonstrating a slightly higher sensitivity. Furthermore, the trend of the crack size for different fatigue cycles is captured accurately. Nevertheless, the variation of resistance for different fatigue cycles is also shown in Figure 7A and B, and the trend of this variation is in line with those obtained in related literature. Finally, the

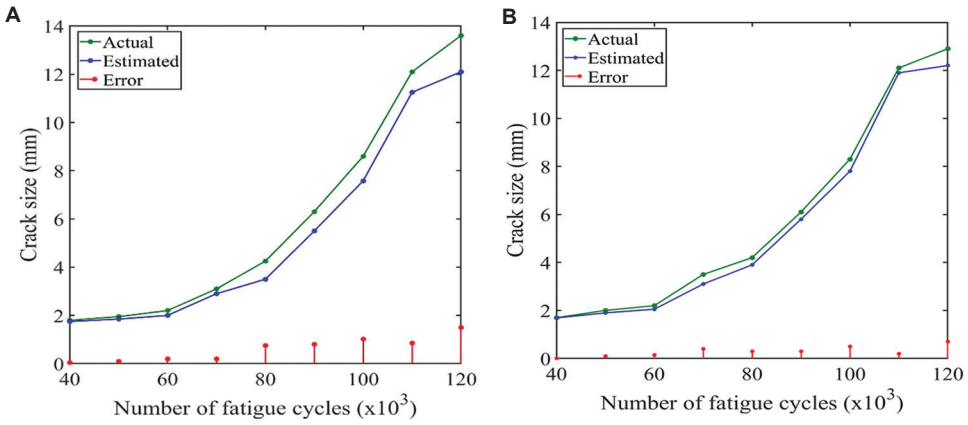

Figure 6. The propagation of crack size versus thousands of cycles: (A) Left crack, and (B) right crack.

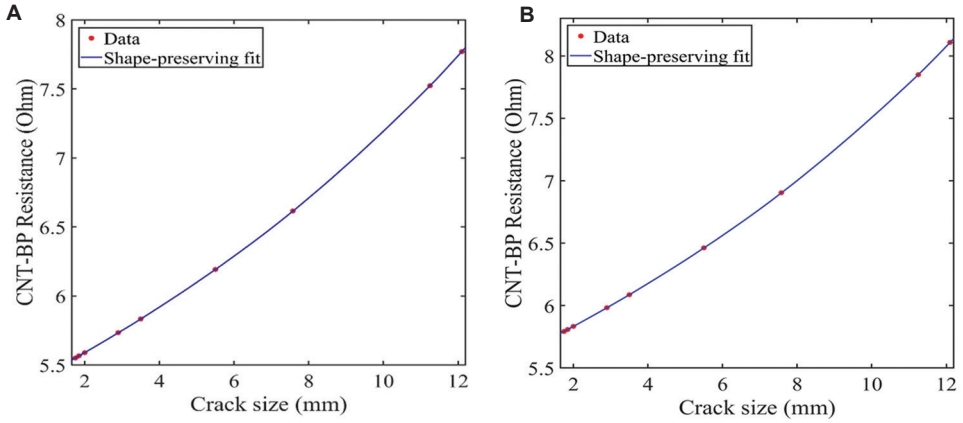

Figure 7. Variation of CNT-BP resistance with the propagation of crack: (A) Left crack, and (B) right crack
Abbreviations: BP: Bucky paper; CNT: Carbon nanotube.

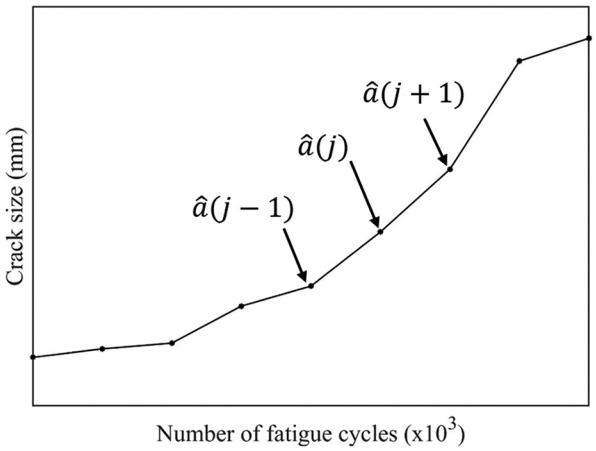

Figure 8. Crack size propagation as a function of fatigue cycles

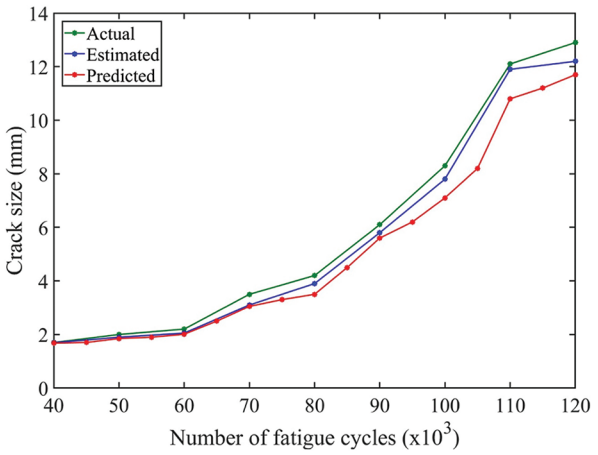

Figure 9. The variation of actual, estimated and predicted crack size versus the fatigue cycles

trend appears to increase approximately linearly with the number of cycles, suggesting a linear correlation between crack size and fatigue cycles. It can also be seen that for lower fatigue cycles, the crack size is not that noticeable and so is the change of resistance of CNT-BP demonstrating an approximate flat line with marginal error. This is seen for both the CNT-BPs placed on the left and right side of the hole.

The prognosis of the metallic plate with an increasing fatigue crack was obtained with the LSTM neural network. An illustrative relationship between crack size and increasing fatigue cycles is shown in Figure 8. Further, it is evident that the time transient crack size propagation is dependent on the previous crack size, fatigue cycle, and the rate at which the crack propagates with respect to fatigue cycle is shown in Table 2, and mathematically, this can be represented by Equation X:[30-32]

$$\hat{a}(j+1) = f\left(\ldots, \hat{a}(j), N(j), \frac{d\hat{a}}{dN(j)}\right) \quad \text{(X)}$$

The estimated values of the crack size based on the change in resistance measurement were used for training the LSTM model. The actual values obtained from the optical camera were only used as a reference for those obtained from measuring the change of resistances in CNT-BP as a function of fatigue cycles. Therefore, they were not used for training the LSTM model. The trained LSTM model was then used to predict the crack size as a function of fatigue cycles. The results, shown in Figure 9, demonstrate not only high prediction accuracy but also a strong alignment with the overall trend of crack growth over fatigue cycles. The concluding remarks and future studies are discussed in the following section.

Table 2. Time series data for crack propagation as a function of fatigue cycles

Time step	…	$j-1$	J	$j+1$	…
$\hat{a}$	⋯		$\hat{a}(j)$	$\hat{a}(j+1)$	⋯
N	…	$N(j-1)$	$N(j)$	$N(j+1)$	…
$\frac{d\hat{a}}{dN}$	⋯	$\frac{d\hat{a}}{dN(j-1)}$	$\frac{d\hat{a}}{dN(j)}$	$\frac{d\hat{a}}{dN(j+1)}$	⋯

7. Concluding remarks and future study

The present study focuses on the development of an improved method for the fabrication of CNT-BP membranes that can be used as self-sensing material with an application for structural health monitoring of metallic plate structures which are subjected to fatigue loading. A significant number of trials were conducted to determine the optimal configuration of the ingredients to fabricate the CNT-BP that has adequate ductility and enhanced sensitivity. The optimized CNT-BPs were superglued to the fatigued test specimens to measure the change in resistance values of the CNT-BP as a function of fatigue cycles. The measured resistance values were then used to calculate the fatigue crack sizes. Moreover, a high-speed optical camera was employed to measure the actual size of the fatigue crack. A good correlation was observed between the actual size of the crack measured by the optical camera and the one calculated using the established theoretical model based on the change in resistance of the CNT-BP and that predicted from the LSTM model. Thus, the obtained results demonstrated the promising potential of CNT-BP for health monitoring applications. The major findings and outcomes from the present study are outlined below:

(i) The ductility of the fabricated CNT-BP is enhanced with the improved fabrication process. This is paramount because if the CNT-BP is brittle, it can be difficult to handle and may break while being glued to the test specimen. Furthermore, it may be relatively easy to superglue the ductile CNT-BP to the test specimen by tapping to ensure a uniform attachment of CNT-BP to the specimen, avoiding any voids formation at the interface.
(ii) The sensitivity of the fabricated BP is enhanced with the improved fabrication process, as demonstrated by the marginal error between the actual and predicted results of fatigue crack. The piezoresistivity is improved up to 5.8 Ω compared to the earlier reported values between 4 Ω and 5 Ω.
(iii) The error analysis shows the potential of CNT-BP in crack length estimation with enhanced accuracy and sensitivity.
(iv) For higher crack length estimation, an approximate linear relationship seems to exist, indicating that the LSTM model can predict the trend with higher accuracy.
(v) The use of CNT-BP as a self-sensing material eliminates the need for sophisticated equipment and sensors, complex signal processing, and high computational resources. Further, CNT-BP can be easily affixed to the test structure, and changes in its electrical resistance can be readily measured.
(vi) The omnidirectional shape of the CNT-BP can facilitate the detection of cracks in different directions with higher sensitivity.

In contrast, the current work identified several limitations that could be explored in future studies. The limitations are as follows:

(i) Limited BP size due to the filter membrane size.

To yield CNT-BP with larger sizes, a flask with a bigger funnel width, membrane, and pore sizes must be employed during the fabrication process. This could also facilitate mass fabrication since smaller pieces with equal sizes and shapes can be cut out of the large BP, thereby reducing the fabrication time. The fabrication of BP into different shapes and sizes for future testing may lead to further overall optimization of the sensing architecture.

(ii) Different crack directions.

In this work, only the crack propagating perpendicular to the loading direction was considered. The CNT-BP must be tested for different crack directions to further investigate and confirm the reliability of its sensing efficiency and use in prognosis and diagnosis of fatigued specimens.

(iii) Different electrode arrangements for damage detection and quantification.

The electrode arrangements must be varied according to the location and direction of the crack propagation. This would give further insights for optimizing the sensing architecture for a specific application.

(iv) Obtaining readings at different load levels and directions.

In the present study, the load was tension-tension controlled at a specific loading frequency. In future work, both the loading amplitude and direction—ranging from tension to compression—and the loading frequency can be varied to further evaluate the reliability of CNT-BP in the prognosis and diagnosis of fatigue in specimens.

Acknowledgments

None.

Funding

None.

Conflict of interest

Faeez Masurkar is the Youth Editorial Board Member of this journal, but was not in any way involved in the editorial and peer-review process conducted for this paper, directly or indirectly.

Author contributions

This is a single-authored article.

Ethics approval and consent to participate

Not applicable.

Consent for publication

Not applicable.

Availability of data

The data presented in this study are available from the corresponding author on request.

References

1. Masurkar F, Tse PW, Yelve NP. Theoretical and experimental measurement of intrinsic and fatigue induced material nonlinearities using Lamb wave based nonlinearity parameters. *Measurement*. 2020;151:107148.

   doi: 10.1016/j.measurement.2019.107148

2. Tse P, Masurkar F, Yelve NP. Estimation of remaining useful life of fatigued plate specimens using Lamb wave-based nonlinearity parameters. *Struct Control Health Monit.* 2020;27(4):e2486.

   doi: 10.1002/stc.2486

3. Yelve NP, Masurkar F, Tse PW. Application of rayleigh wave-based nonlinearity parameter to estimate the remnant useful life of fatigued thick aluminum plates. *ISSS J Micro Smart Syst.* 2021;10(2):161-178.

doi: 10.1007/s41683-021-00074-5

4. Luo W, Liu Y, Saha M. CNT Bucky Paper Enhanced Sandwich Composites for In-Situ Load Sensing. In: *Proceedings of the ASME International Mechanical Engineering Congress and Exposition*. Vol. 58493. 2017. p. V014T11A044.

doi: 10.1115/IMECE2017-71550

5. Wang X, An B, Lu S, Ma K, Zhang L, Xu T. Electrical response of carbon nanotube buckypaper sensor subjected to monotonic tension, cycle tension and temperature. *Micro Nano Lett.* 2018;13(6):862-867.

doi: 10.1049/mnl.2017.0914

6. Lu S, Du K, Wang X, *et al*. Real-time monitoring of low-velocity impact damage for composite structures with the omnidirection carbon nanotubes' buckypaper sensors. *Struct Health Monit.* 2019;18(2):454-465.

doi: 10.1177/1475921718757937

7. Lu S, Yang X, Zhang L, *et al*. Real-time monitoring of resin infiltration process in vacuum assisted molding (VARI) of composites with carbon nanotube buckypaper sensor. *Mater Res Express.* 2019;6(11):115628.

doi: 10.1088/2053-1591/ab507b

8. Her SC, Hsu WC. Strain and temperature sensitivities along with mechanical properties of CNT buckypaper sensors. *Sensors (Basel)*. 2020;20(11):3067.

doi: 10.3390/s20113067

9. Yee MJ, Mubarak NM, Khalid M, Abdullah EC, Jagadish P. Synthesis of polyvinyl alcohol (PVA) infiltrated MWCNTs buckypaper for strain sensing application. *Sci Rep.* 2018;8(1):17295.

doi: 10.1038/s41598-018-35638-3

10. Yang R, Gui X, Yao L, *et al*. Ultrathin, lightweight, and flexible CNT buckypaper enhanced using MXenes for electromagnetic interference shielding. *Nanomicro Lett.* 2021;13:66.

doi: 10.1007/s40820-021-00597-4

11. De Paula Santos LF, Monticeli FM, Ribeiro B, Costa ML, Alderliesten R, Botelho EC. Effect of carbon nanotube buckypapers on interlaminar fracture toughness of thermoplastic composites subjected to fatigue tests. *Int J Fatigue*. 2025;195:108868.

doi: 10.1016/j.ijfatigue.2025.108868

12. Ahmed S, Schumacher T, Thostenson ET, McConnell J. Performance evaluation of a carbon nanotube sensor for fatigue crack monitoring of metal structures. *Sensors (Basel)*. 2020;20(16):4383.

doi: 10.3390/s20164383

13. Jiang XW, Wang Z, Lu SW, *et al*. Vibration monitoring for composite structures using buckypaper sensors arrayed by flexible printed circuit. *Int J Smart Nano Mater.* 2021;12(2):198-217.

doi: 10.1080/19475411.2021.1910874

14. Hehr A, Schulz M, Shanov V, Song Y. Micro-crack detection and assessment with embedded carbon nanotube thread in composite materials. *Struct Health Monit.* 2014;13(5):512-524.

doi: 10.1177/1475921714532987

15. Ribeiro B, Botelho EC, Costa ML, Bandeira CF. Carbon nanotube buckypaper reinforced polymer composites: A review. *Polímeros*. 2017;27(3):247-255.

doi: 10.1590/0104-1428.03916

16. Wan Y, Yang H, Tian Z, *et al*. Mode I interlaminar crack length prediction by the resistance signal of the integrated MWCNT sensor in WGF/epoxy composites during DCB test. *J Mater Res Technol.* 2020;9(3):5922-5933.

doi: 10.1016/j.jmrt.2020.03.119

17. Lecompte D, Vantomme J, Sol H. Crack detection in a concrete beam using two different camera techniques. *Struct Health Monit.* 2006;5(1):59-68.

doi: 10.1177/1475921706057982

18. Ashrafi B, Johnson L, Martinez-Rubi Y, Martinez M, Mrad N. Single-walled carbon nanotube-modified epoxy thin films for continuous crack monitoring of metallic structures. *Struct Health Monit.* 2012;11(5):589-601.

doi: 10.1177/1475921712449509

19. Bian N, Ren Y, Shrivastava A, *et al*. Enhancing the interlaminar adhesion of carbon fiber composites via carbon nanotube sheets. *Acad Mater Sci*. 2024;1(2).:1-11.

doi: 10.20935/AcadMatSci6206

20. Lin H, Zhang C, Liao N, Zhang M. Microcracked strain sensor based on carbon nanotubes/copper composite film with high performance and waterproof property for underwater motion detection. *Compos Part B Eng.* 2023;254:110574.

doi: 10.1016/j.compositesb.2023.110574

21. Olson TM, Kwon YW, Hart DC, Loup DC, Rasmussen EA. Carbon nanotube based sensor to monitor crack growth in cracked aluminum structures underneath composite patching. *Appl Compos Mater.* 2015;22(5):457-473.

doi: 10.1007/s10443-014-9417-0

22. Abbasi A, Nazari F, Nataraj C. Application of long short-term memory neural network to crack propagation prognostics. In: *Proceedings of the 2020 IEEE International Conference on Prognostics and Health Management*

(ICPHM); 2020. p. 1-6.

doi: 10.1109/ICPHM49022.2020.9187033

23. Pan Y, Khodaei ZS, Aliabadi FM. In-service fatigue crack monitoring through baseline-free automated detection and physics-informed neural network quantification. *NDT E Int.* 2025;153:103360.

doi: 10.1016/j.ndteint.2025.103360

24. Shin H, Yoon T, Yoon S. Fatigue life predictor: Predicting fatigue life of metallic material using LSTM with a contextual attention model. *RSC Adv.* 2025;15(20):15781-15795.

doi: 10.1039/d5ra01578b

25. Giannella V, Bardozzo F, Postiglione A, Tagliaferri R, Sepe R, Armentani E. Neural networks for fatigue crack propagation predictions in real-time under uncertainty. *Comput Struct.* 2023;288:107157.

doi: 10.1016/j.compstruc.2023.107157

26. Colah. *Understanding LSTMs*; 2015. Available from: https://colah.github.io/posts/2015-08-Understanding-LSTMs/ [Last accessed on 2025 Sep 19].

27. Masurkar F, Tse P. Theoretical and experimental evaluation of the health status of a 1018 steel I-beam using nonlinear rayleigh waves: Application to evaluating localized plastic damage due to impact loading. *Ultrasonics*. 2020;108:106036.

doi: 10.1016/j.ultras.2019.106036

28. Yelve NP, Tse PW, Masurkar F. Theoretical and experimental evaluation of material nonlinearity in metal plates using Lamb waves. *Struct Control Health Monit.* 2018;25(6):e2164.

doi: 10.1002/stc.2164

29. Masurkar F, Tse P, Yelve NP. Evaluation of inherent and dislocation induced material nonlinearity in metallic plates using Lamb waves. *Appl Acoust.* 2018;136:76-85.

doi: 10.1016/j.apacoust.2018.02.011

30. Xu N, Fu Z, Wang Y, Shen X. Study on the short fatigue crack initiation and propagation behavior of 42CrMo. *Adv Mech Eng.* 2022;14(9):1-9.

doi: 10.1177/16878132221119928

31. Ibrahim MFE, Miller KJ. Determination of fatigue crack initiation life. *Fatigue Fract Eng Mater Struct.* 1979;2(4):351-360.

doi: 10.1111/j.1460-2695.1979.tb01093.x

32. Wang H, Liu X, Wang X, Wang Y. Numerical method for estimating fatigue crack initiation size using elastic-plastic fracture mechanics method. *Appl Math Model.* 2019;73:365-377.

doi: 10.1016/j.apm.2019.04.010

Our Journals

Tumor Discovery is a peer-reviewed and open-access journal that aims to present new cancer research with strong emphasis on fundamental and translational studies. *Tumor Discovery* covers topics, including but not limited to the following:

- Etiology and pathogenesis of cancer
- Mechanisms and molecular pathways underlying cancer initiation and progression
- Tumor metastasis
- Tumor evolution and heterogeneity
- Tumor microenvironment and tumor-host interactions
- Cancer genetics and genomics
- Cancer characterization using omics approaches
- Discovery and validation of cancer biomarker
- Discovery of new therapeutic targets
- New approaches of diagnostic and treatment modalities
- Statistical methods in cancer research

Global Translational Medicine is a quarterly journal that focuses on medicine, biological sciences, and biomaterials engineering. The goal of *Global Translational Medicine* is to provide a platform to researchers for showcasing their latest research works in translational medicine so as to advance the field towards the betterment of human health. Despite the advancement of omics and new technologies, the process of transforming these technologies and scientific research results into effective therapies and putting them into clinical use still has a long way to go. *Global Translational Medicine* provides a platform to fill the gaps in preclinical and inter-disciplinary research, to promote clinical translation of scientific research results, and to contribute to the conception of new and improved preventive measures as well as diagnostic and therapeutic techniques of diseases.

Global Translational Medicine covers the following themes: cardiovascular disease, metabolism/diabetes/obesity, neuroscience/neurology, cancer, biomaterials and their applications in medicine, proteomics/metabolomics, pharmacogenomics, biomarkers, bioinformatics and data mining, animal and clinical research, and medical methods arising from interdisciplinary crossover.

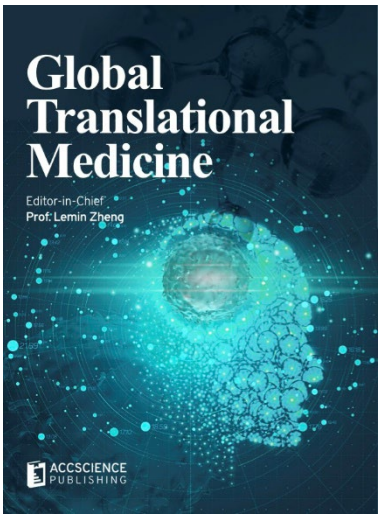

Start a new journal

Write to us via email if you are interested to start a new journal with AccScience Publishing. Please attach your CV, professional profile page and a brief pitch proposal in your email. We shall inform you of our decision whether we are interested to collaborate in starting a new journal.

Contact: info@accscience.com

https://accscience.com/journal/IJAMD

Contact

www.accscience.com

9 Raffles Place, Republic Plaza 1 #06-00 Singapore 048619

E-mail: editorial@accscience.com

Phone: +65 8182 1586